Dude, Where's My Car? Cellular Navigation for Autonomous Driving

Whiton, Russ

2024

Total number of authors:
1

LUND UNIVERSITY

PO Box 117
221 00 Lund
+46 46-222 00 00

Dude, Where's My Car? Cellular Navigation for Autonomous Vehicles

RUSS WHITON
DEPARTMENT OF ELECTRICAL AND INFORMATION TECHNOLOGY |
FACULTY OF ENGINEERING | LTH | LUND UNIVERSITY
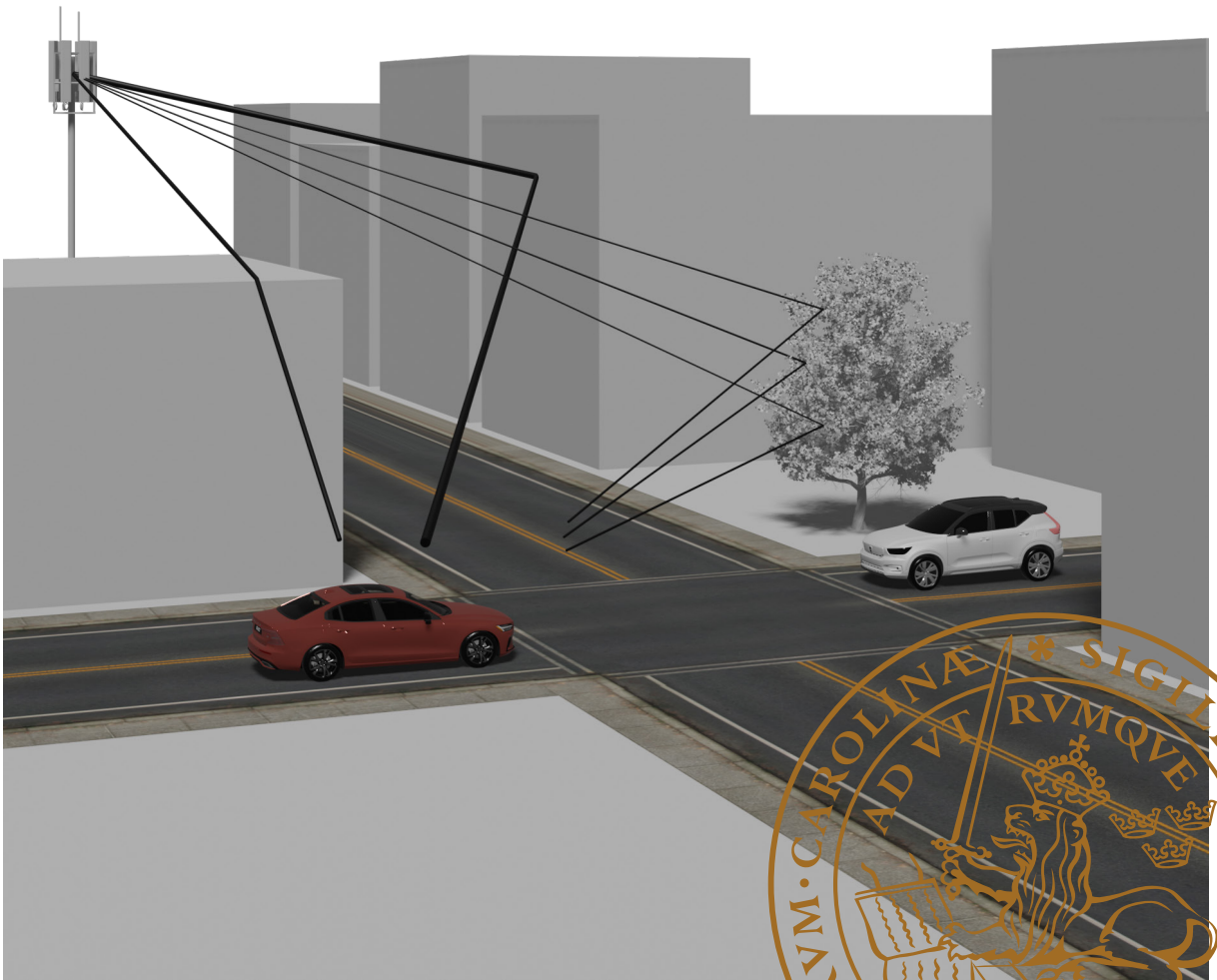
Dude, Where's My Car?
Cellular Navigation for
Autonomous Vehicles

Doctoral Thesis

Russ Whiton

LUND
UNIVERSITY

Department of Electrical and
Information Technology
Lund, March 2024

Organization: LUND UNIVERSITY Department of Electrical and Information Technology Ole Römers Väg 3 223 63 Lund Sweden	Document Type: DOCTORAL THESIS
	Date of Issue: 13 March 2024
Author: Russ Whiton	Sponsoring Organisation(s): Volvo Car Corporation (VCC) Swedish Innovation Agency (Vinnova)

Title: Dude, Where's My Car? Cellular Navigation for Autonomous Vehicles

Abstract:

Position and direction estimation is useful for numerous engineering applications for commercial, scientific, and military purposes. Technology that fuses observations of signals broadcast by Global Navigational Satellite Systems (GNSS) with inertial measurements is standard for electronic devices, but this requires at least a periodically unobstructed view of the sky to perform reliably. This has motivated the use of terrestrial radio signals as navigation references to complement or as an alternative to satellite systems, but environments with obstructions, specular reflectors, and scatterers of electromagnetic waves create challenges for any wireless navigation system.

This thesis is about how wireless signals other than those transmitted by GNSS might be used for navigation in complex propagation environments, particularly for safety-critical systems, and conversely how position and orientation information can be used to better understand electromagnetic wave propagation. The thesis is split into introductory chapters that provide broad background on the researched subjects, and five papers published in or submitted to scientific conferences and journals.

The first paper offers a broad analysis of the requirements for a cellular navigation system to meet the unique and particularly challenging operating requirements of an autonomous vehicle. Aspects of the problem that are not frequently addressed in literature on terrestrial positioning, particularly requirements for safety-critical operation, are included in the analysis.

The second, third, and fourth papers propose methods for position estimation for a passenger vehicle operating in a dense urban canyon environment, tested with a specially-designed measurement system that makes passive (opportunistic), high-resolution observations of down-link synchronization signals transmitted by commercial cellular base stations that are paired with highly accurate pose estimates. Inspired by the prominence and success of Artificial Neural Networks (ANNs) in computer vision, ANNs are used for wireless navigation. The results show that meter-level position estimates and accurate heading estimation can be achieved simultaneously when receiving only reflected and scattered signals from a single transmitter that is never within line-of-sight of the receiving antenna array, relying entirely on multipath propagation.

Finally, in the fifth paper, the link between geometry and multipath propagation is explored from a different perspective. Known navigation states are used to study and characterize multipath propagation. A method for multipath component clustering for statistical channel modeling is proposed, where knowledge about the receiver position is used to gain insight into channel statistics. The algorithm is shown to provide consistent results and to be scalable to large data sets.

Keywords: Machine Learning, Massive MIMO, Radio-based localization.

Signature: *Russell & m*   Date: 8 March 2024

Dude, Where's My Car? Cellular Navigation for Autonomous Vehicles

Doctoral Thesis

Russ Whiton

Frontispiece: Electromagnetic waves transmitted by a base station arriving at a vehicle through various propagation mechanisms. Rendering by Max Boerboom.

To Barb, From Russ

Abstract

ᴘosɪᴛɪᴏɴ and direction estimation is useful for numerous engineering applications for commercial, scientific, and military purposes. Technology that fuses observations of signals broadcast by Global Navigational Satellite Systems (GNSS) with inertial measurements is standard for electronic devices, but this requires at least a periodically unobstructed view of the sky to perform reliably. This has motivated the use of terrestrial radio signals as navigation references to complement or as an alternative to satellite systems, but environments with obstructions, specular reflectors, and scatterers of electromagnetic waves create challenges for any wireless navigation system.

This thesis is about how wireless signals other than those transmitted by GNSS might be used for navigation in complex propagation environments, particularly for safety-critical systems, and conversely how position and orientation information can be used to better understand electromagnetic wave propagation. The thesis is split into introductory chapters that provide broad background on the researched subjects, and five papers published in or submitted to scientific conferences and journals.

The first paper offers a broad analysis of the requirements for a cellular navigation system to meet the unique and particularly challenging operating requirements of an autonomous vehicle. Aspects of the problem that are not frequently addressed in literature on terrestrial positioning, particularly requirements for safety-critical operation, are included in the analysis.

The second, third, and fourth papers propose methods for position estimation for a passenger vehicle operating in a dense urban canyon environment,

tested with a specially-designed measurement system that makes passive (opportunistic), high-resolution observations of down-link synchronization signals transmitted by commercial cellular base stations that are paired with highly accurate pose estimates. Inspired by the prominence and success of Artificial Neural Networks (ANNs) in computer vision, ANNs are used for wireless navigation. The results show that meter-level position estimates and accurate heading estimation can be achieved simultaneously when receiving only reflected and scattered signals from a single transmitter that is never within line-of-sight of the receiving antenna array, relying entirely on multi-path propagation.

Finally, in the fifth paper, the link between geometry and multipath propagation is explored from a different perspective. Known navigation states are used to study and characterize multipath propagation. A method for multipath component clustering for statistical channel modeling is proposed, where knowledge about the receiver position is used to gain insight into channel statistics. The algorithm is shown to provide consistent results and to be scalable to large data sets.

Popular Science Summary

FIGURING out where one is and what direction one is facing, the science of navigation, is an ancient problem. The genus *homo* spread through six of the seven continents long before the agricultural revolution or the advent of written language, in large part thanks to innovation in navigating through varied environments. The sun, stars, and topographically prominent landmarks on Earth guided our way for most of human history, until the mid 20th century when humans began launching artificial satellites.

The most famous and ubiquitously used of these artificial satellite systems is the United States Department of Defense's Global Positioning System (GPS), which employs a constellation of satellites orbiting Earth and transmitting wireless signals that serve as our modern position landmarks. GPS receivers in electronic devices are so common that "GPS" is widely used as a metonym for navigation system. Navigators need not use a sextant, chronometer, and nautical almanac to determine their position by sighting the sun or stars, anyone with a smartwatch and a view of the sky can now determine their position within a few meters and time with an accuracy of around one microsecond.

In spite of this incredible leap in navigation capabilities, the forward march of technology has resulted in a demand for technologies that can perform similarly in the environments where we spend much of our time: indoors or in proximity to buildings that obstruct the sky. New applications like autonomous driving systems also seem to demand navigation technologies that operate well in other environments as well. A naturally appealing solution is to use our wireless communication systems as navigation references,

particularly mobile networks for cellular communication. The innovations that have led cellular networks to offer better data rates, including intelligent focusing of energy through antenna arrays, utilization of signal bounces, and frequent transmission of synchronization signals, increase their potential for navigation as well.

This thesis is a case study in using cellular signals for navigation for a passenger vehicle in environments where GPS is most likely to be unsatisfactory. It touches on many of the important aspects of the problem, starting with how such a navigation technology might be integrated into vehicular electronic systems for advanced use cases like autonomous driving and what challenges need to be overcome if cellular navigation is to work in the environments where satellite navigation also struggles.

The way that wireless signals interact with the environment can resemble a hall of convex and concave mirrors in a circus. One particular family of machine learning (pattern matching) methods is used to see whether the hall of mirrors effect can be turned from a detriment to navigation to a benefit. Even without knowing the locations of the transmitting infrastructure, yesterday's received signals usually closely resemble today's received signals at the same point in space, and it is possible to build up an understanding of how signals look by surveying and matching.

The problem is then flipped on its head, and information about the vehicle location and orientation is then used to study how the signals propagate. This understanding has always been necessary for building data communication and wireless navigation systems, and the two are starting to merge together as geometry information is used for the former as well.

In aggregate, the thesis describes how understanding radio wave propagation is critical for navigating, if we wish to use wireless navigation systems in the places where we spend most of our time.

Acknowledgments

RATHER than waxing poetic about the nature of a Ph.D. I will uncere-moniously list people and organizations to whom I feel I owe a debt of gratitude, and punctuate the list with a few inside jokes.

It is humbling that *Volvo Car Corporation* and the *Swedish Innovation Agency Vinnova* (in the MIMO-PAD project) collectively made a big investment in me in the apparent belief that my fiddling around on things without immediate and obvious commercial value was in the interests of those they represent, from shareholders in Santiago and Hong Kong to taxpayers in Höllviken and Övre Soppero.

To my closest collaborator for this work, *Junshi Chen*, it has been a great pleasure to develop ideas with you, to troubleshoot problems, and to uncon-ditionally offer and receive assistance. Outside of our many conversations about navigation, wireless communications, machine learning and signal processing, it has been enlightening to discuss economics, history, geopolitics, science, and family.

A special thanks to dear friends. To *Mitra (also listed under the subheadings: advisors, family, frisörer), Seb, Casper-Joon (näää, **min** kompis!!)* and *Caira*. To *Guillaume, Anita* and *Eliza*, if only the French had a word for "camaraderie"! To *Shea* and *Christina*. To *Peter, Helena, Elliott* and *Olivia*. To *Max* and *Galini*. To *Linus* and *Diana*. To *Ryan* and *Melinda*. To *Julie* and *James*. To the entire *Let's Climb!åååå* group, particularly *"Herr Efterdoktor" Elias, Jakob, Elena, Stefan (oh hey, you're here?! in the acknowledgments?), Fanny, Ville, Sarah, Jana, David, Lukasz, Marc* and *Johanna*. From Sogndalfjorden to Leonidío it has meant a lot to celebrate first sends, newborns, birthdays, and weddings. To paddle, to skate, to camp, to basta, and to gripe about the slow service at Foxes.

Thanks to mentors, formal and informal, who have demonstrated how complicated engineering problems can be decomposed with great clarity of

Lund, March 2024

Contents

Preface

THIS doctoral thesis is the culmination of work done from November 2018 through December 2023 while I was employed as a Senior Hardware Engineer in the Safe Vehicle Automation department at Volvo Car Corporation in Gothenburg, Sweden. Through Volvo's Industrial PhD Program (VIPP), I was simultaneously enrolled as a student in the Communications group at Lund University in Lund, Sweden. The academic work was supervised by Professor *Fredrik Tufvesson* at Lund University and Dr. *Mikael Nilsson* at Volvo Car Corporation.

STRUCTURE OF THE THESIS

The thesis consists of an introduction section and five papers. The introduction opens with a description of the problem to be addressed and the research objectives for the thesis. The following chapters offer exposition to provide a broad basis in the relevant scientific and engineering disciplines, and the final chapter of the introduction concludes with a list of contributions for the papers and how the state-of-the-art has been advanced through the research, together with an outlook for the future. Five conference and journal papers by the author and collaborators follow, which are published in or submitted to scientific journals and conference proceedings and re-printed with permission from the publishers. Those publications mostly follow a standard "IMRaD" (Introduction, Methods, Results, and Discussion) structure in which a few concise paragraphs are considered sufficient to set the stage for material that necessarily seems esoteric to a broader audience. The introduction section in this thesis provides significantly longer exposition than is typically desirable for those publications, and can either be read in isolation or as a more in-depth primer for the included papers. It also serves the purpose of logically

weaving together a coherent narrative for the collection of included papers, which might otherwise seem disparate at first glance.

- **INTRODUCTION**

  This thesis is primarily a treatise on the inter-play between wireless channels and navigation, and the resulting consequences for modern autonomous systems. Chapter 1 provides background to the thesis and gives an overview of the major research questions, limitations of this work, and the structure of the remainder of the introduction. The exposition in Chapter 2 introduces the science of navigation and the necessary terminology. Chapter 3 gives an introduction to modern wireless navigation systems, and particularly more information about electromagnetic wave propagation and the methods and challenges for performing navigation with wireless signals. Chapter 4 discusses automotive-specific navigation including the sensor suite used for automotive navigation, as the motivation for the thesis project was the particularly challenging problem of navigation for an autonomous vehicle. Chapter 5 provides a brief primer on machine learning, and its use within navigation using wireless signals, important for several of the included papers. Chapter 6 spells out the research contributions of the attached papers as well as my personal speculation about the outlook for such systems, technologically and commercially, together with suggestions for future research. Appendix A offers a more detailed description of the measurement system used for Papers II-V than was possible to include in the scientific publications.

- **PAPERS**

  Five papers are included in their entirety in the thesis. They are listed as follows, with a brief description of my contributions to each:

Paper I: R. WHITON, "Cellular Localization for Autonomous Driving: A Function Pull Approach to Safety-Critical Wireless Localization", *IEEE Vehicular Technology Magazine*, vol. 17, no. 4, pp. 28-37, Dec. 2022, doi: 10.1109/MVT.2022.3208392.

▶ *This was an independent project that I initiated early-on after starting the Ph.D., after a series of conversations with my colleague Harsh Tataria at Lund University. To paraphrase, the suggestion from Harsh was something along the lines of, "Russ, there isn't much in the communications literature about concepts like navigation integrity. It would be useful for you to write about some of these things from your vantage point of doing practical implementation." The paper was my attempt to build a bridge between the practical challenges we at Volvo and Zenseact faced at that time when working*

on commercial development of localization systems for autonomous driving to the novel proposals from academia for cellular localization. I developed the framing for the paper, conducted interviews with numerous colleagues and peers in industry, performed the academic literature search, created the figures (with CAD help for the 3-D rendering), wrote the paper, and corresponded with the journal through to publication in VTM's Special Issue on Recent Advances in Automated Driving Technologies.

Paper II: R. WHITON, J. CHEN, T. JOHANSSON, AND F. TUFVESSON, "Urban Navigation with LTE using a Large Antenna Array and Machine Learning", *2022 IEEE 95th Vehicular Technology Conference: (VTC2022-Spring), Helsinki, Finland*, pp. 1-5, Jun. 2022, doi: 10.1109/VTC2022-Spring54318.2022.9860844.

▶ *This was the first article based on channel estimation results from the novel measurement system developed primarily by my colleague Junshi Chen (more details in Appendix A). We jointly planned and performed the data collection and post-processing. The idea of augmenting fingerprints with external state information was mine. The implementation for generating the positioning results and figures was mine, and I wrote the paper and integrated comments from the co-authors and eventually the reviewers.*

Paper III: R. WHITON, J. CHEN, AND F. TUFVESSON, "LTE NLOS Navigation and Channel Characterization", *Proceedings of the 35th International Technical Meeting of the Satellite Division of The Institute of Navigation (ION GNSS+ 2022), Denver, Colorado*, pp. 2398-2408. Sept 2022. doi: 10.33012/2022.18386

▶ *This paper followed shortly after Paper II, and coincided with my trip to ION GNSS+ to chair an industry panel. The positioning results from the first paper seemed unsatisfactory given the resolution of the measurement aperture, and my preliminary testing of the matched filter indicated that it performed much better than discrete estimates. I also thought it would be interesting to characterize biases in a heavy multipath environment as a parameter of interest for a classical navigation audience (ION). The positioning method and implementation was mine. I performed the analysis, generated the figures, and wrote the paper with comments from the co-authors and reviewers.*

Paper IV: R. WHITON, J. CHEN, AND F. TUFVESSON, "Wiometrics: Comparative Performance of Artificial Neural Networks for Wireless Navigation", *Originally submitted to: IEEE Transactions on Vehicular Technology, Aug 2023. Resubmitted after Major Revision Mar 2024.*

▶ *This was the final paper regarding navigation with neural networks. It is a journal-length extension of Papers II and III that incorporates the*

matched-filter method from Paper II but establishes a much more comprehensive benchmark against other methods proposed in literature, and includes different training/testing splits as well as the additional base station that was visible for sections of the test route. I generated the results and figures and wrote the paper, with comments from the co-authors and reviewers.

Paper V: R. WHITON, J. CHEN, AND F. TUFVESSON, "Flexible Density-based Multipath Component Clustering Utilizing Ground Truth Pose", *2023 IEEE 98th Vehicular Technology Conference (VTC2023-Fall), Hong Kong, Hong Kong, 2023, pp. 1-6, doi: 10.1109/VTC2023-Fall60731.2023.10333453.*

▶ *This paper was the result of my visualization efforts after our measurement campaigns. My colleague Junshi Chen's work (see Related Work, below) entailed solving a difficult data association problem with a long data series of noisy channel estimates, and it was useful to have a method for rapid and intuitive visualization of results. The data association methods for channel modeling and positioning in literature were cumbersome to implement and did not lend themselves to rapid iteration, so I wanted to propose a method that would be useful for colleagues and other researchers. The idea for the method was mine, I tested and tuned it, generated the figures, and wrote the paper, integrating comments from my co-authors and the reviewers.*

RELATED WORK

As is customary, a list of scientific publications to which I made contributions during the time of work on the thesis, but which are not included in thesis itself, are also listed below:

CONFERENCE CONTRIBUTIONS

Paper vi: L. DING, G. SECO-GRANADOS, H. KIM, R. WHITON, E.G. STRÖM, J. SJÖBERG, AND H. WYMEERSCH, "Bayesian Integrity Monitoring for Cellular Positioning–A Simplified Case Study", *2023 IEEE International Conference on Communications Workshops (ICC Workshops)*, Jun. 2023.

Paper vii: J. CHEN, R. WHITON, X. LI, AND F. TUFVESSON, "High-Resolution Channel Sounding and Parameter Estimation in Multi-Site Cellular Networks", *2023 Joint European Conference on Networks and Communications & 6G Summit (EuCNC/6G Summit)*, Jun. 2023.

Paper viii: J. CHEN, R. WHITON, AND F. TUFVESSON, "Extended FastSLAM Using Cellular Multipath Component Delays and Angular Information", *2023 IEEE 97th Vehicular Technology Conference: (VTC2023-Spring), Florence, Italy*, Jun. 2023.

Paper ix: J. Chen, R. Whiton, and F. Tufvesson, "SLAM Using Cellular Multipath Component Delays and Angular Information with JPDA Approximation", *2023 8th International Conference on Signal and Image Processing (ICSIP)*, Jul. 2023.

Acronyms and Symbols

Here, important acronyms, abbreviations, and symbols are listed, which are recurring throughout the thesis. Some parameters, which only occur in a narrow context, are intentionally omitted; some parameters are used in more than one way, but the context is always explicitly clarified in the corresponding text. Some (compound) units are provided with prefixes to reflect the most commonly encountered notations in the literature.

GLOSSARY

3G Third Generation

3GPP Third Generation Partnership Project

4G Fourth Generation

5G Fifth Generation

5GAA 5G Automotive Association

6DOF 6 Degrees of Freedom

6G Sixth Generation

AGC Automatic Gain Control

ANN Artificial Neural Network

C2C-CC CAR 2 CAR Communication Consortium

CNN Convolutional Neural Network

CRS Cell-specific Reference Signals

CSI Channel State Information

DARPA Defense Advanced Research Projects Agency

DOA Direction of Arrival

GNSS Global Navigational Satellite Systems

GPS Global Positioning System

GSCM Geometry-based Stochastic Channel Model

IEC International Eletrotechnical Commission

ILS Instrument Landing Systems

IMU Inertial Measurement Unit

INS Inertial Navigation System

IoT Internet of Things

LEO Low Earth Orbit

LOS Line-of-Sight

LTE Long-Term Evolution

MEMS Micro-Electromechanical Systems

MEO Medium Earth Orbit

MIMO Multiple-Input Multiple-Output

ML Machine Learning

MPC Multipath Component

OFDM Orthogonal Frequency Division Multiplexing

PNT Positioning, Navigation and Timing

PRS Positioning Reference Signal

PSS Primary Synchronization Signal

RAIM Receiver Autonomous Integrity Monitoring

RFID Radio-Frequency Identification

RSS Received Signal Strength

RSSI Received Signal Strength Indicator

RTOF Round-trip Time-of-Flight

SAE Society of Automotive Engineers

SDR Software-Defined Radio

SGD Stochastic Gradient Descent

SLAM Simultaneous Location and Mapping

SSS Secondary Synchronization Signal

SUCA Stacked Uniform Circular Array

TDOA Time-Difference of Arrival

TOA Time of Arrival

TOF Time-of-Flight

UE User Equipment

UTC Coordinated Universal Time

UWB Ultra-Wideband

VLF Very Low Frequency

INTRODUCTION

1

Background and Objectives

If there is a lesson to be learned from this fragmentary history, it is that the pressure of navigational requirements has always demanded more than our knowledge of the facts of radio wave propagation could supply.

Pierce, J. A., & Woodward, R. H.
NAVIGATION: Journal of the Institute of Navigation 18.1 (1971) [1]

1.1 BACKGROUND

The Defense Advanced Research Projects Agency (DARPA) Grand Challenge was launched in 2003, a competition that offered a $1M USD cash prize to the team capable of fielding an unmanned vehicle which could win a race on a course in the Mojave desert up to 175 miles (280 km) long with a time limit of 10 hours. No team finished the inaugural race in 2004, but the following year 5 teams completed the track, including the winner, Stanley, a Volkswagen Tuareg pick-up truck retrofitted with an impressive array of hardware and software developed by a Stanford University-led team [2]. This event amplified nascent enthusiasm for automated driving technologies, and inspired visions of widespread commercial deployment when the innovative technology employed by Stanley inevitably reached a level of maturity such that it could be used on public roads. Two decades after the first DARPA Grand Challenge, ambitious visions for commercial deployment have not yet come to fruition. Deploying safety-critical systems at scale is always difficult, and the transition from a system running in the desert with a DARPA employee diligently following behind with the finger on a remote kill switch to systems operating on public roads by anyone with (or perhaps without) a driver's license has proven enormously challenging.

Stanley's innovative architecture provided a rough template upon which many subsequent designs have been based, but each of the modules described in Stanley's architecture requires significant development to be suitable for operation without a safety driver. The *positioning sensor group* module is no exception. It consisted of several Global Positioning System (GPS) receivers and an Inertial Measurement Unit (IMU) for position and velocity estimation. GPS receivers operate by receiving signals broadcast by satellites orbiting Earth at an elevation of around 20,000 km, and in the open landscape of the Mojave desert the Grand Challenge vehicles had very reliable signal reception. For autonomous systems operating in environments with higher population density, the prevalence of man-made structures occluding the view of the sky means that reliable reception is far from guaranteed [3]. The reason for this is that the electromagnetic waves transmitted by GPS satellites, and observed by the receiver and used to estimate distances, interact with objects (and the atmosphere) as a function of their shape and material properties.

The problem of modeling radio wave propagation on a large scale, as understood by Pierce and Woodward half a century ago per the quotation at the beginning of this chapter, has been studied continuously since then. Pierce and Woodward were describing how developers of what eventually became the LORAN system investigated skywave propagation (radio waves sent from the ground reflected or refracted by the ionosphere) at different frequencies, but even more ominously for those aspiring to solve precise geometry problems with radio waves, these sorts of interactions happen with all manner of objects.

Figure 1.1 illustrates some of these propagation mechanisms at work; signals transmitted by a cellular base station arrive at a car through different physical paths, more commonly known as Multipath Components (MPCs). In the foreground, rooftop diffraction gives rise to several MPCs. Specular reflection from a large building results in a powerful MPC, while many weak MPCs stem from diffuse reflections from a tree. This is an example of a dreaded non-Line-of-Sight (LOS) scenario, where the direct path between sender and receiver has too little power to be detected. Looking at the various propagation mechanisms, one can see how challenging it might be to estimate the physical relationship between the transmitter and receiver in the absence of a direct path. Using the distances will not work, because even the shortest path traveled has excess length compared to the true separation. The angles measured at the sender or receiver are not quite right to use angulation, either, even the signals refracted over the roof depart and arrive at a different angle than a direct path would follow.

Navigating accurately and reliably in such environments is a focus of significant attention by researchers and in industry as advanced applications,
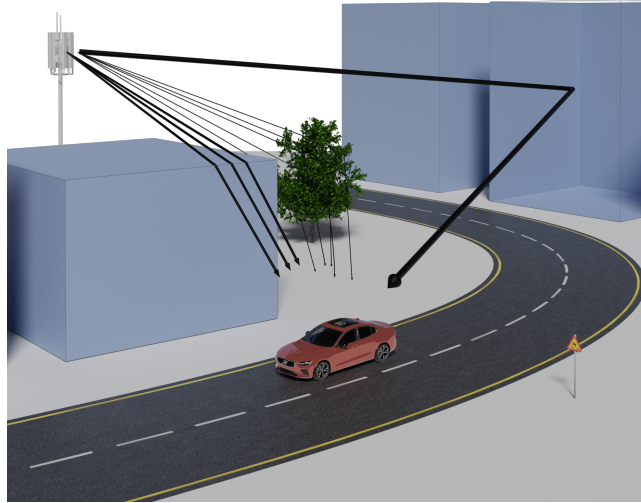
Figure 1.1: A transmitted wave from a base station takes multiple paths and undergoes different propagation phenomena including reflection, diffraction, and scattering before arriving at a receiving antenna on a Volvo S60. Other vehicle makes and models are also subject to the laws of physics as described by Maxwell's equations. Rendering created by Max Boerboom.

particularly those in autonomous systems, demand ubiquitous navigation capabilities. The IEEE recently launched a new journal [4], the *IEEE Journal of Indoor and Seamless Positioning and Navigation*, precisely for this reason. This thesis explores the relationship between the paths that signals take from transmitter to receiver (the wireless channel) and navigation. The first paper is application-focused, understanding what safety-critical autonomous systems require from a wireless navigation system and how they might operate in the presence of MPCs. Papers two, three and four evaluate and expand a particular method for navigation in multipath environments called fingerprinting, through the use of Artificial Neural Networks (ANNs). Finally, the fifth paper is an inversion of the navigation-multipath problem, where known navigation states are used to make insights about the wireless channel.

The remaining sections in this chapter describe the central research questions and limitations of the thesis. They may seem somewhat inaccessible to the uninitiated reader. If so, reading Chapters 2-5 first should provide more context.

1.2 RESEARCH QUESTIONS

Making contributions to scientific literature is difficult, particularly the first few contributions for an aspiring researcher. It takes a certain level of confidence to waltz into a worldwide network of highly motivated, intelligent and prolific researchers who have made careers in a scientific discipline and claim, "I have now contributed something novel and interesting!" Combining this with the inherent unpredictability of research (if the results were predictable, it wouldn't be much of a research question), the investigative direction usually evolves over the course of a project. The scarlet thread* connecting the articles in compilation theses can seem far-fetched when the author stitches together contributions in Ainu language syntax, a retrospective on the stability of the Biafran pound, and the epidemiology of adenoviruses in reptiles into a single tome. In this thesis, the author has tried to investigate a problem that should be of both academic and industrial interest, and the research questions are heavily influenced by the author having had a day job in the automotive industry in parallel with the research being conducted.

For autonomous vehicles to operate safely in environments with buildings or other "electrically large" (large relative to the wavelength) obstacles, localization capabilities are desirable beyond those which can be provided by wireless systems today. Given these limitations, it is worthwhile to investigate the role of wireless localization technologies other than satellite navigation, how to formulate and deploy alternative measurement models that take into account channel behavior, and how to learn more about wireless channels based on confident localization estimates. Approximately restated in list form, the central research questions of this thesis include:

RQ1: What role do wireless navigation technologies, other than satellite navigation, have in an autonomous drive system?

RQ2: How can and should the wireless channel be represented for data-driven (ANN-based) navigation techniques?

RQ3: What impact does ANN architecture have for data-driven navigation techniques?

RQ4: In what manner should the inputs and outputs be structured when using ANNs for fingerprint-style navigation?

RQ5: How can confident estimates of pose contribute to a better, geometry-based understanding of the wireless channel?

It is not the intention of the author to lead the reader to believe that there is limited prior work on using terrestrial wireless or even cellular systems specifically for navigation. Dedicated cellular signals have been used

---

*Translating *röd tråd* into *red thread* is a surefire way to out oneself as a Swede.

for decades to localize users, primarily to assist emergency responders [5]. Alternative wireless signals are broadly used to augment navigation in mobile phones, even if the companies doing this are deliberately opaque about the exact signals and methods used [6]. Additionally, the *opportunistic* use (defined in Chapter 3) of down-link cellular signals has been proposed, tested, and analyzed [7, Chapter 38], and even the idea of using the richness of the wireless channel to augment positioning has been investigated for decades, either through pattern matching [8] or more recently through channel super-resolution [9] (also defined in Chapter 3). This is the body of work to which this thesis aims to make a contribution.

1.3 LIMITATIONS

Every engineering company has eternal internal strife between sales people and the engineering organization. For companies in the business of selling navigation systems, customers typically want a single, magical scalar value called *accuracy* without any nuance for the operating conditions. Reading a data sheet for a satellite navigation receiver, one can typically find microscopic text at the bottom that reads, "Under open sky conditions". This serves in part as a hedge against inevitable customer complaints, but also placates the internal developers who demanded four pages of text describing ionospheric storms and antenna axial ratios. This work is free, so the author can elaborate on limitations in the same font size as the rest of the manuscript.

Critically, the experimental work (at least for the published papers) was based on a single measurement campaign in a particular environment, at a specific carrier frequency and bandwidth and an antenna array with a gain pattern favorable for channel sounding but impractical for deployment at scale. The environment was particularly rich with geometrically-diverse multipath[†], which intuitively ought to be favorable for the proposed methods. It is not easy to state with confidence what the results might look like if the same methods were tested under different conditions, but some of the primary factors impacting performance are intuitive. Larger channel bandwidth and the subsequent improvement in timing resolution should improve performance, for example, while a reduction in the antenna aperture should result in worse performance.

On a related note, three of the included papers employ ANNs as estimation tools. Data-driven techniques do not lend themselves well to the analytical lower-bounding of estimation theory, particularly the Cramér-Rao Bound [10]. Numerous parameters determine the predictive performance including

---

[†]That is to say, reflected and scattered signals all around the vehicle.

the data splits among testing, validation, and training sets; the network dimensions and form; and the learning rates, optimizers, and number of training epochs. Freezing exactly one of these parameters while exploring all the others systematically means that the time and resource-consuming process of Stochastic Gradient Descent (SGD) needs to be run anew, where even SGD itself actually comprises an ever-growing family of methods. The works employing ANN in this thesis have probed of all of these parameters, but cannot claim global optimality.

For Papers I and V, there is nothing resembling a lower bound at which to aim. Paper I discusses autonomous systems, but there are numerous technologies and engineering practices which can realize complicated goals. Humans set foot on the moon using 1960s technology, after all. Paper V proposes a method for clustering, but data clustering itself necessarily entails a degree of subjectivity [11].

Finally, the author is adamant that clock drift should never be given short shrift in a discussion of wireless positioning, and numerous references on the subject are offered (see, e.g., [7, Chapter 38.3] and [12, Chapter 5]), even if the papers do not have specific proposals for addressing clock drift.

1.4 THESIS OUTLINE

The remainder of these introductory chapters are dedicated to providing technical and historical background for the five included papers and to place to answer both the *why* and *what* for the research questions.

Chapter 2 discusses the science of navigation, including the ancient history, and reviews the basic terminology necessary for understanding navigation problems. Chapter 3 covers aspects of wireless positioning and communication systems, including the basic methods for estimating position and orientation with wireless signals. Chapter 4 gives a lengthier primer on automotive systems to help place Paper I in its proper context. Chapter 5 is about machine learning with a focus on wireless channels as inputs. Chapter 6 summarizes contributions and lessons from the work, and offers suggestions for future research.

2

The Science of Navigation

For example, when a foreigner asks him for directions, the idiot will reply idiomatically, rather than refer to a shared coordinate system.

Matthew Crawford
The Case for Working with Your Hands [13, Page 98]

HIS chapter provides an introduction to the science of navigation. Some of the fundamental technical concepts are introduced, and the central questions of the thesis are placed into their historical context.

2.1 THE NAVIGATION PROBLEM

Those of us who have lived our formative years in the age of commodity GPS receivers do not spend much time thinking about the sensory inputs our navigation devices use for navigation. Equipped with a smartphone, we are rarely at risk of getting truly lost, even if we might have a few personal anecdotes about struggling to find our way in an unfamiliar city or missing trail markers while hiking and getting turned around in the forest. We are accustomed to employing navigation apps, which can even be miniaturized to run on a wrist watch, to simultaneously solve numerous problems, each of which is challenging in isolation:

Problem 1: Determining position in three dimensions: North-South, East-West, Up-Down or Latitude, Longitude, and Elevation.

Problem 2: Determining orientation: heading, pitch and roll.

Problem 3: Maintaining a geospatial database (a map) with a target destination and the network of paths to follow and obstacles to avoid.

Problem 4: Plotting and maintaining a course to the desired destination.

Problem 5: Determining time.

This thesis deals primarily with the first two items. The "Science of Navigation" [14] entails estimating where one is, what orientation one has, and possibly the associated translational/rotational velocities and accelerations.

We have evolved to accomplish this naturally as a fusion of external sensing (primarily our vision; other mammals like bats use their olfactory sense in an analogous manner) and internal sensing (the vestibular system of the inner ear). If we are in familiar territory, a cursory glance at known landmarks is sufficient for confident estimates, and we can even navigate by touch sometimes, such as stumbling around one's apartment in the dark. Recent advances in brain imaging have enabled research demonstrating that our spatial navigation skills are inherently multi-sensory, flexible, and adaptable [15]. Birds are hypothesized to navigate with one or more of celestial cues, infrasound, olfactory sensing, or magnetic sensing [16]. Theories of collective navigation (including emergent sensing) for animal migration have been studied [17]. Entertainingly enough for the casual navigation enthusiast, even arthropod navigation is a subject of intensive study [18].

The goals of the engineer or geodesist working with navigation are to develop and employ sensors from which navigation information can be inferred, and to create methods to transform sensor readings into plausible guesses about position and orientation, just as our sensory system and brains have evolved to do. In the parlance of estimation theory (a branch of statistics [10]), we make physical observations (measurements of distances or angles) to estimate the values of parameters (our location and orientation).

2.2 A BRIEF HISTORY OF NAVIGATION

Navigation history is frequently taught as a history of marine navigation, but there are numerous fascinating historical navigational concepts documented in anthropological studies of terrestrial navigation, such as navigation by the Aboriginal peoples of Australia's Western Desert Region [19]. An observer on the surface of Earth typically wishes to estimate, in degrees, North-South position (latitude) and East-West position (longitude), together with the altitude in meters.

Finding reference landmarks on Earth's surface that allow one to determine latitude and longitude over a wide geographical area rapidly runs into practical limitations. An observer taking readings at a height of 2 meters can only see about 5 kilometers until the curvature of the Earth blocks sight, and even a generous observation height of 15 meters still results in a modest

14 kilometers to the horizon. This means that navigation references available ubiquitously for users on Earth need to be placed at a towering height, or be observable without physical sight, or be placed ubiquitously in moderate proximity to wherever users intend to navigate. Historically, the method of choice has been to utilize celestial objects observable over large geographical areas, i.e., the stars and the sun.

Determination of latitude has been performed reliably for thousands of years through observation of celestial objects. The star Polaris lines up fairly well with Earth's axis of rotation, so it serves as a brilliant marker of latitude for an observer in the Northern hemisphere when the sky is dark. Polaris will always be found approximately overhead at the North pole*, and can be found at the horizon around the equator. Other stars observed in the night sky appear to rotate around Polaris. The Southern Cross (crux) performs an analogous role in the Southern Hemisphere.

Islands in the South Pacific were discovered and inhabited by humans over the course of the last 4000 years. Discovering these islands, including Hawaii and Easter Island, entailed journeys of thousands of kilometers of open ocean in outrigger canoes, far from the sight of landmarks. This required numerous innovations in navigation, famously the Polynesian star compass built on the reliable declination of specific stars, offering navigation references every cloudless night [20].

The voyaging season for the Vikings was during the Northern hemisphere's summer months, which meant few opportunities for sightings of stars at Northern latitudes. The sun served a similar function, and even if the movement of the sun through the sky has the additional complication of seasonal variation, it provides an easily-used reference for determining latitude if one knows what day of the year it is. The sun will be directly overhead at local noon on the June solstice at the latitude of the Tropic of Cancer, for example.

Using celestial observations to determine longitude is much more difficult because of the rotation of the Earth. Distant objects like stars and quasars maintain their declination as the Earth spins, but appear to move continuously through the sky from East to West at a rate of about 15° per hour for an observer spinning with the Earth. The missing ingredient in tracking changes in longitude was precise timekeeping to compare relative time between celestial events (local noon or, more rarely, an eclipse) at a starting point compared to later in the journey. The major breakthrough for precise timekeeping came

---

*Learned astronomer types talk about "axial precession," but what they mean to say is that the Earth's axis of rotation is a mite bit wobbly, wobbling on a 26,000-year cycle. As a consequence, anyone reading this dissertation 1,000+ years after publication might be confused about which star the author means; *Alpha Ursae Minoris* is the "North Star" at the time of writing. Sorry for the confusion, future person.

just a few centuries ago stemming from, somewhat bizarrely, a succession conflict on the Iberian Peninsula at the dawn of the 18th century in which the British Royal Navy experienced a series of maritime disasters owing to insufficient navigational tools. The British government established the Board of Longitude in 1714, which was authorized to give out cash prizes for reliable determination of longitude. Most of the prize money was eventually (after decades of petty squabbling and personal vendettas delayed the payout) awarded to the clock-maker John Harrison for his brilliant engineering feat of designing a clock that was long-term stable [21], or more precisely, with low Allan variance for long sampling times [22]. To put this in a more relatable manner, it was like a wrist watch left in a drawer for years having kept the time remarkably well without adjustment. If local noon is 6 hours after noon at a reference location, then one can infer that one is a quarter of the way around the world to the West of the reference location (a delta of $-90°$ of longitude).

The 20th century and the advent of radio technology led to major innovations in the science of navigation. Hyperbolic navigation systems [1] including the British GEE system, American LORAN and LORAN-C systems, and Russian CHAYKA system were all constructed and rolled out primarily for military aircraft and ship navigation, but found application for civilian use as well. In 1957, the Soviet Union launched the first artificial satellite into orbit and mankind entered the space age[†]. Almost immediately, scientists and engineers realized that observations of the transmitted signal's Doppler frequency allowed for estimation of a satellite's position in its orbit, and so the inverse could be utilized as well, i.e., a satellite with a known trajectory could provide observations enabling estimation of position for a user on Earth. The United States Navy initiated several programs to support ground user navigation and precise timekeeping from satellites in orbit, creating the TRANSIT satellite system[‡] and the TIMATION programs, eventually amalgamated with the US Air Force's 621B program to create GPS, which launched its first satellite in 1978. The GPS constellation became fully operational in 1980. The Soviet Union (and subsequently the Russian Federation) followed suit with GLONASS in the 1980s, but the development stagnated in Russia's turbulent 1990s (see [12, Chapter 8.1.1]). BeiDou-3 and Galileo are the other global constellations that have come online since then. The overwhelming majority of navigation systems on Earth today use Global Navigational Satellite Systems (GNSS), typically all four constellations (GPS, GLONASS, BeiDou-3 and

---

[†]Curiously, this also prompted the United States to launch the DARPA program, mentioned in Chapter 1.

[‡]The Soviet Union's Tsikada system used essentially the same operating principle.

Galileo) together, as the primary reference for determination of position and time.

2.3 NAVIGATION TERMINOLOGY AND CONCEPTS

This thesis is a work at the intersection of several scientific disciplines and industrial developments, each of which have their own naming conventions, and the same words are used to describe slightly different ideas in different disciplines. The author has tried to follow the conventions laid out by Dr. Paul Groves in his invaluable book *Principles of GNSS, Inertial, and Multisensor Integrated Navigation Systems* [14]. The term *navigation* is used here in the classical sense, as in the *Institute of Navigation* or *Henry the Navigator* or *We, the Navigators* [20]. In the field of Robotics, and subsequently inherited by those working with autonomous vehicles, *localization* is the equivalent term of art [23]. In the wireless communications discipline, one typically speaks of *positioning* and frequently problems are formulated as a network tracking a User Equipment (UE) rather than the operator of a "UE" estimating his or her own position. Confusingly, *navigation* in the automotive sector frequently refers to routing in the map, as in, *"Why is my worthless navigation system telling me to drive directly through this nuclear waste storage facility to get to Starbucks?!"*

2.3.1 COORDINATE SYSTEMS

For most of us, if we ask for directions, we expect that they will be translated into our own reference frame, e.g., *"continue straight for 500 meters and turn left"* or, *"the fasteners are 4 aisles behind you"*. The Guugu Yimithirr are an Australian Aboriginal people who have a famously excellent sense of direction. Equivalent directions in the Guugu Yimithirr language would likely be stated in cardinal directions, *"continue East for 500 meters and turn South"* or *"the fasteners are 4 aisles to the Northwest"* [24]. One might suspect that this mechanism of language would reinforce our orientation skills, though all of us switch dynamically between egocentric and external (allocentric) systems [15].

Landmarks in the world are defined by their latitude (North-South), longitude (East-West), and altitude (Up-down) given an ellipsoidal representation of the globe. Running along a line of constant longitude from my apartment in Gothenburg, Sweden would land me in Svalbard (North) or along the coast of Namibia (South). The same exercise along a line of latitude would land me around Juneau, Alaska (West) or on the banks of the Volga river in Yaroslavl (East). Ascending in altitude might put me on a collision course with a Starlink satellite or a GLONASS satellite; Gothenburg is too close to the North Pole to collide with the International Space Station or a GPS satellite. Even if

the grocery store is just a few hundred meters away, smartphone navigation uses coordinates defined in this global frame for the user location and the store location.

Most of the time we are interested in navigating in a global reference frame, and even though we do not typically think of it this way, when navigating outdoors with a smartphone we are using several reference frames, each of which is centered at the center of Earth; one reference frame rotates with Earth and one that does not [14, Chapter 2.1]. Dealing with a globe is unwieldy and we typically are content to use a 2-D projection, characterized by the qualities that it preserves for our application, whether those be distances, angles, or some other compromise of properties [25]. In a small enough area, there are many acceptable projections that will work well. Even smaller areas like indoor environments typically lend themselves well to Cartesian representation, and reference frames can be arbitrarily defined in terms of the zero points and orientation.

2.3.2 POSITION FIXING AND DEAD RECKONING

Estimating position in a defined reference frame is known as *position fixing* or *absolute positioning*. In parametric positioning, this is done through observations of distance and/or angles. Measuring three distances (lateration), two angles (angulation), or one combined measurement of distance and angle is sufficient to perform a position fix. These are illustrated in Section 3.2.

Differential navigation, or *dead reckoning*§ is the method of estimating and adding a change in distance and orientation to a previous estimate, rather than making an independent observation of position and orientation in the external frame (position fixing). This combination of relative changes and anchoring in the external frame reflects how our own biological orientation systems work, mostly through the vestibular system and vision [27].

Typically differential observations come at a higher rate than observations in the external frame; this was true when observations of latitude and longitude were only feasible once per day on a calm sea in the absence of clouds, and it is applicable now with high-rate observations from IMUs fused with less frequent satellite observations from GNSS receivers. The particular sensors used in autonomous driving are discussed in Chapter 4, but typically Inertial Navigation Systems (INSs), based on IMU observations, are the most commonly-deployed sensors. Cameras, lidar, wheel odometry, or multiple other sensors can and are used for differential navigation as well.

---

§A term with uncertain provenance. It may refer to *dead shot* (an accurate shot) or *deduced* reckoning [26].

Figure 2.1 illustrates the advantages of using complementary high-rate observations from an INS and fusing those observations with the occasional, possibly noisy but unbiased estimates from a position fixing system. The error grows exponentially for the stand-alone INS system, but with occasional corrections from the position fixing system the maximum error of the fused system is kept to a much lower value, yet retains the high observation rate of the INS.
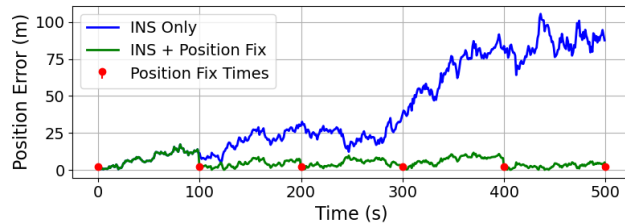
Figure 2.1: A purely inertial (INS) system with unconstrained error growth (blue), compared with the same outputs with occasional position fixing observations on a 100-second interval. Each position fix reduces both the absolute error and values of the IMU biases.

One particular problem formulation that incorporates elements of both position fixing and differential navigation is Simultaneous Location and Mapping (SLAM). This is essentially differential navigation with the additional feature of "loop closure", in which compounding errors can be bounded within a surveyed area [28]. While this problem formulation has a long history in robotics, autonomous driving tends to be a problem where *a priori* maps are used and position fixing is essential [29], rather than relying on loop closure to build an understanding of a fresh world. As Hassani et al. phrase it, *"However, SLAM is insufficient in safety-critical ADS navigation applications because localization errors drift over distance and loop closures are trajectory-constraining"* [30]. Not only trajectory-constraining, but even legal mandates can require that the function only be operated, or that operation be disabled, within certain geographic bounds. This is discussed further in Chapter 4.

2.3.3 FEATURE MATCHING

Borrowing again from the definitions laid out in [14, Chapter 13], feature matching entails making observations other than explicit range and bearing calculations to known, discrete landmarks. The examples given span from conventional map matching (discussed further in Section 4.2) to more obscure methods like gravity gradiometry.

An alternative form of feature matching is the use of machine learning. Rather than maintaining an explicit database of features which are geo-referenced, some alternative model of weights is created for associating observations, typically in a higher-dimensional space, with points in space. This is discussed in more detail in Chapter 5. Wireless signals lend themselves well to such methods, especially at lower frequencies and where overlapping signals from different sources can be observed simultaneously.

3

Wireless Systems for Navigation

Marconi is a good fellow. Let him continue. He is using seventeen of my patents.

Nikola Tesla

UGLIELMO Marconi shared the 1909 Nobel Prize in Physics *"in recognition of [his] contributions to the development of wireless telegraphy,"* and is commonly known as the inventor of radio. This designation seems to irk some prominent researchers in the field. Professor Andreas Molisch, who literally wrote the book on Wireless Communications [31], opens his authoritative treatise on the discipline with (well-deserved) praise for James Maxwell, Heinrich Hertz, and Nikola Tesla, but attributes Marconi's success to having had "better public relations" and adds a footnote explaining that Marconi's patents were eventually overturned. However, the dissenting opinion from Justice Rutledge in the five-to-three Supreme Court decision makes a plausible defense of Marconi: *"Until now law has united with almost universal repute in acknowledging Marconi as the first to establish wireless on a commercial basis. He won by the test of results. No one disputes this. His invention had immediate and vast success, where all that had been done before, including his own work, gave but narrow limited utility"* [32].

Regardless of how the credit for the early history should be allocated (no damages were awarded in the 1943 Supreme Court case), wireless technology is pervasive in modern industrial society at a level that likely exceeds the wildest expectations of all the early pioneers with the probable exception of Tesla, who was an undeniable genius but prone to a certain grandiosity [33]. Telling a complete story of the early history of wireless communications would be a massive undertaking, but one way to understand is to separate the discoverers and inventors [34].

3.1 HISTORY OF WIRELESS NAVIGATION SYSTEMS

Even if much of the early history of wireless in the late 19th and early 20th centuries was concentrated on wireless telegraphy, the early inventors including Marconi realized that there was potential to use the systems for geometry estimation problems as well. Marconi filed a patent application in 1900 for a system that could perform Direction of Arrival (DOA) estimation, and Fessenden was fast on his heels with a 1904 patent that used Received Signal Strength (RSS) as a proxy for distance.

The lead-up to the Second World War saw multiple militaries making investments in "hyperbolic" radio ranging for the navigation of ships and airplanes. The Time-Difference of Arrival (TDOA) principle was familiar to engineers, with its origins based in acoustic ranging from the First World War, where microphones distributed across the battlefield were used to estimate the position of enemy artillery [35].

The October 1957 launch by the Soviet Union of mankind's first artificial satellite, poetically named "Earth's Traveling Companion," *Sputnik Zemlyi*, set off a series of events that led to the modern era of satellite navigation. The first generations of satellite navigation systems operated using observations of Doppler shift [36] from a single satellite, but innovations in atomic clocks eventually led to a Time of Arrival (TOA) model based on *pseudoranges*. Readers are referred to [37] for a first-hand history of events from the launch of *Sputnik Zemlyi* to the development and launch of GPS.

Satellite signals are not always available, and even since the advent of satellite navigation systems, new forms of terrestrial systems for radio signal navigation and tracking have been developed as well. TDOA systems have been developed for emergency responders [5] within the Third Generation Partnership Project (3GPP) consortium, and an entirely new family of TOA methods based on the Round-trip Time-of-Flight (RTOF) principle have also been developed to handle the issue of ranging without atomic clocks.

Some milestones are provided in Table 3.1 to establish a coarse timeline. Note that this list of milestones omits important developments outside the English-speaking world which were frequently pacing and occasionally preceding the technological developments of Table 3.1, but for which historical documentation in English is sparse. The Soviet Tsikada system was a satellite constellation operating using Doppler observations. The GLONASS, BeiDou (third-generation), and Galileo systems are very similar in principle and operation to GPS. The interested reader is refered to [12, Part B] for a history and technical description of the other major constellations, including smaller regional constellations used for GNSS augmentation.

Table 3.1: Milestones in wireless positioning

Year	Milestone	Method	Reference
1900	Marconi patent application for navigational system measuring direction	DOA	[38]
1904	Patent filed by Fessenden for measuring distance based on received signal strength	RSS	[38]
1941	First proof-of-concept of commercial DECCA navigation system	TDOA	[38]
1941	Trials of what became the LORAN navigation system	TDOA	[1]
1942	British GEE system brought into operation	TDOA	[1]
1964	First position fix of TRANSIT receiver using transmitters in orbit	Doppler	[37]
1978	First GPS satellite launched	TOA	[37]
2000	3GPP Release 99 specifies several positioning methods	TDOA	[5]
2002	Permission granted for unlicensed operation of Ultra-Wideband (UWB) devices	TOA	[39]
2009	3GPP Release 9 defines Positioning Reference Signal (PRS)	TDOA	[5]
2016	802.11mc standard ratified	TOA	[40]
2020	3GPP Release 16 defines multiple positioning signals	DOA & TOA	[41]

The history of radar is omitted, because it is not considered a navigation technology within the context of this work. Radar is an example of monostatic sensing [23], where sensing is done in the coordinate frame of the ego-user, rather than a user trying to localize himself or herself in an external frame. Pairing radar with a map of radar-detectable static objects can perform this function in a manner analogous to lidar or cameras; see Chapter 4. However, a history of radar is largely parallel to innovations with wireless localization technologies. The early inventors including Marconi foresaw the use of the technology for monostatic sensing, but the primary development into practical systems occurred in parallel among the major powers during the interwar period [42].

3.2 FUNDAMENTALS OF WIRELESS POSITIONING SYSTEMS

There are numerous tutorials on radio localization and sensing that include overviews of the fundamental methods. Readers are referred to [43] for an accessible tutorial on the subject. A more concise and mathematical tutorial can be found in [23]. The most common methods are described briefly in the following subsections.

3.2.1 MULTILATERATION

Multilateration, sometimes called trilateration or simply "lateration" entails making measurements of distances from at least three references to find the point of overlap, illustrated with three satellites as transmitting references in Figure 3.1. The location of the references in the external coordinate system needs to be known to plot the origins of the circles (or spheres, for a three-dimensional problem).
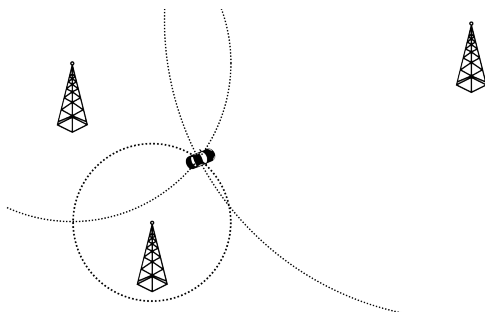
Figure 3.1: An illustration of multilateration. Distance measurements are made to three references and the point of overlap corresponds with the user location. In three dimensions, each distance measurement is represented as a sphere from the source. Clock offsets between transmitters and the receiver need to be specifically handled for most methods.

Alternatively, the distance estimates themselves can be biased so long as the bias values are equivalent for each transmitter, which is useful because it is typically easier to ensure time synchronization (used for distance measurements as explained below) among transmitters than between the transmitters and the mobile receiver. Rather than each range defining a circle or sphere from the point of origin, each pair of ranges defines a hyperbola in two dimensions or a hyperboloid for problems in three dimensions, and the user can infer his or her location to be somewhere on that line or surface if the measurements are correct.

There are numerous ways to estimate distance based on radio signals. The observed power of electromagnetic waves decreases as the square of distance (the *"inverse-square law"*) because the transmitted power is spread out over a larger area the farther the waves propagate from a point source. If the transmitted and received powers are known, and the antenna gains are compensated for (Friis transmission formula), then the distance can be calculated exactly. Practically speaking, this approximation is rarely useful because most environments of interest have other propagation mechanisms, as shown in Figure 1.1, which make waves spreading out in a vacuum into

a poor approximation. Additionally, when the signals are weak (and they usually are in radio systems, thanks to the pesky inverse-square law), the measurement precision for small differences in received power is generally low.

The second, and most ubiquitous, manner of making distance observations is multiplying the estimated propagation time, or Time-of-Flight (TOF), by the speed at which the waves propagate. Radio waves travel at the speed of light, 299,792,458 m/s. If the clocks are synchronized* and the geometrical problem set-up is of overlapping spheres, this method is called positioning by TOA. If there is a single systematic bias in the measurements, then TDOA is used.

A third method for estimating ranges is possible, which addresses the issue of absolute clock synchronization in a rather ingenious manner. With RTOF ranging, rather than requiring absolute synchronization, two-way communication is used. One side of the link initiates, requesting a response to be sent after a specific waiting period, and the range is estimated based on half the difference of the reception time and transmission time, minus the waiting period. This means that only the *stability* of each node's frequency reference is the limiting factor, rather than the synchronization between the two. Such measurements are still subject to positive range biasing from multipath or excess delay [45]. As always, timing precision is inversely proportional to channel bandwidth, which is why UWB is an attractive RTOF technology.

The requirement of two-way communication limits scalability, because each exchange requires the channel to be monopolized for the particular link, and not just for one transmission, but usually multiple exchanges (say, eight) are performed for a single range estimate [40]. For this reason RTOF is almost universally considered for short-range links with limited power.

As a final note on multilateration, estimating the orientation of the receiver is not possible with multilateration techniques in isolation. Orientation information may be inferred in other ways; for example, a car is highly constrained in the direction it can move (at least without a probable insurance claim), so sequential position estimates based on multilateration can be used to estimate the orientation of a car by assuming alignment with the direction of travel, and then forward-backward ambiguity can be solved by using gear lever position or odometry. Magnetometers can also be used to estimate

---

*In practice, even tiny time synchronization mismatches are consequential for TOA. One nanosecond corresponds to about 30 cm of distance at the speed of light. GNSS satellites employ multiple atomic clocks on-board, and they broadcast models of their current estimated clock drift in their data message [12]. For precise GNSS operation, even more frequent satellite clock drifts are estimated by a network of terrestrial stations and sent to the user [44].

orientation in tandem with multilateration for position estimates, but have their own limitations for operating environment and bias drift.

3.2.2 TRIANGULATION

A receiver with multiple antennas can make inferences about the direction of arrival of signals based on the phase differences experienced at multiple antennas, which is even more powerful when directional antennas are employed that have gain patterns with minimal overlap [31]. This is largely associated with radar systems (out of scope for this work), but with the advent of millimeter-wave systems signals, defined signals for angular measurements are now implemented for Fifth Generation (5G) systems as well [41]. Each angular measurement defines a line, and two intersecting lines to different references will intersect at only one point. Alternatively, one measurement each of angle and range is sufficient to estimate position. These two alternatives are shown in Figure 3.2.
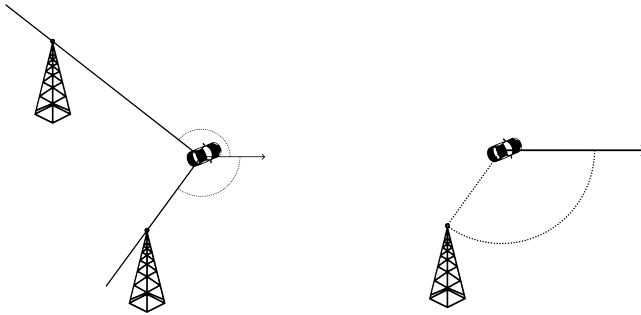
Figure 3.2: An illustration of triangulation (left) with two angle measurements, as well as a combined range and bearing measurement (right).

3.2.3 PROXIMITY

Proximity is a form of localization, though typically formulated as a detection problem rather than as an estimation problem. The most ubiquitous technology for proximity is Radio-Frequency Identification (RFID), used for identity badges, key tags, public transit payment, and numerous other applications. For simplicity in the design for the mobile unit, and because minimal range is desirable for security in most applications, backscattered energy is typically used [46].

3.2.4 FINGERPRINTING

Positioning techniques like multilateration and triangulation work brilliantly in LOS scenarios, but electromagnetic waves interact with objects as a function of the wavelength and the material's electrical conductivity and geometry as described by Maxwell's equations. Typically a fraction of the power is reflected; some of the power passes through and some is scattered. Environments with numerous objects to interact with will cause interesting and complicated patterns of waves. Rather than explicitly estimating individual paths, or working to identify and discard non-LOS measurements, one technique is to conduct a survey where a series of received wireless signals are associated with the physical location where they were measured. When this is complete, a model is created to associate locations and signals but without explicit calculation of bearings or ranges, or necessarily even knowledge of the transmitter locations. This model is subsequently applied at run-time, and new channel measurements are fed into the model to estimate position.
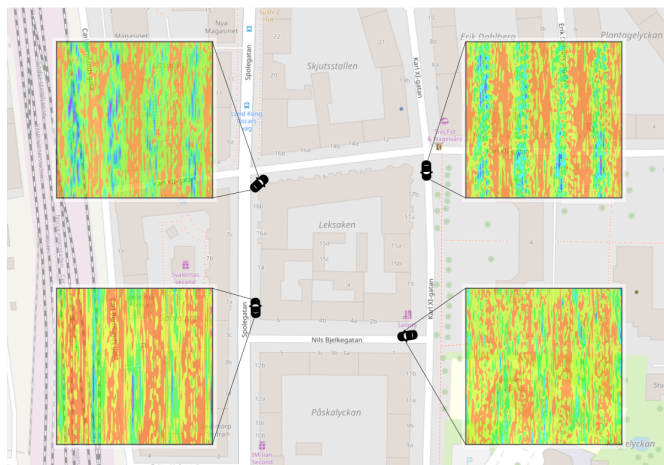
Figure 3.3: An example of the surveying phase for wireless fingerprinting. At different locations, channel measurements and their associated positions are taken and either stored in a database or used to train a model to associate position and channel measurement. At run-time, new channel measurements are taken to estimate position.

Fingerprinting is the name applied in the wireless domain[†], which is analogous to Feature Matching as described in Section 2.3.3, though *scene understanding* is used sometimes in the wireless world as well [43]. An example of the surveying phase is shown in Figure 3.3. Channel measurements and positions are used to build a model, which is later employed to estimate new positions. The representation shown in the figure is arbitrary, and can take numerous forms, as described in more detail in Section 5.3.

3.3 WIRELESS CHANNEL MODELING

In data communication, when the receiver sees multiple copies of the original transmitted signal in short succession with differences in arrival time and power[‡] corresponding to different MPCs, it presents a challenge for the receiver. For Orthogonal Frequency Division Multiplexing (OFDM) systems, which are heavily relied on for data communication, reference symbols or *pilot symbols* known *a priori* to the receiver are interleaved with the data. The receiver can estimate a frequency-dependent value of channel gain and phase to ultimately equalize the impact of the channel response [47, Chapter 3]. As long as the impact of the channel is negated in this way, the physical mechanisms giving rise to that frequency-dependent response are not highly consequential.

However, when designing and operating wireless systems, it is essential to understand the operating environment and how signals will propagate. How frequently equalization needs to be done might change if a system is intended to support users with high velocities on a train, for example, or if other environmental considerations otherwise require special consideration. Wi-Fi or cellular signals that usually work fine in most scenarios might not manage the echoing chasm of an open copper pit mine [48], or in the example from Chapter 1, a long-range navigation system range might be limited in the early morning hours before the sun ionizes particles in the upper atmosphere to prevent signals from escaping into space [1].

[†]"Fingerprinting" is also begrudgingly accepted in these introductory chapters as the accepted term-of-art, rather than "wiometrics" as proposed in Paper IV, Section II.B. lest the author sound like he is proselytizing.

[‡]Power differences span many orders of magnitude for most communications systems. Understood analogously in terms of sound intensity, the received energy that can be decoded by a receiver spans in range from a faint whisper to a Motörhead concert.

3.3.1 PHYSICAL CHANNEL MODELS

When evaluation of candidate technologies was being done for Third Generation (3G) systems, standardized propagation models were developed to examine delay dispersion of wireless channels, and eventually also the spatial properties in target environments of interest [34]. These models aim to capture the large-scale effects visible over longer distances, typically from large objects (relative to a wavelength) as well as the small-scale fluctuation that happens over the course of a wavelength.

For approximating propagation in specific environments, simulation through ray tracing is frequently employed. In ray tracing, a map of the environment is enriched with some assumptions about material properties to approximate the major paths that the signals might take through the environment. The simplifications employed to generate computationally feasible scenarios, both in terms of the map fidelity and quality of models for wave interaction with objects, tend to limit the applicability of such models for small-scale fading, especially for higher frequencies as details necessarily must become more precise [49]. There is also a general dearth of data for scenarios where both ray tracing and empirical studies have been performed to verify the performance [50].

A more widely-employed method for studies of channel models is to treat the temporal and geometrical channel behavior as stochastic phenomena for environments of interest by employing Geometry-based Stochastic Channel Models (GSCMs). These models are generated through lengthy and difficult measurement campaigns using dedicated wireless channel sounding systems, and have evolved from simple path loss exponents to models with numerous parameters for the "birth" and "death" of individual MPCs [51], which tend to appear in clusters.

In a measurement campaign, pilot sequences are transmitted at the desired frequency and bandwidth so the receiver can generate a high-fidelity estimate of the channel impulse response in an environment of interest. The receiver usually moves through the environment capturing a discrete number of impulse responses called snapshots. For each snapshot, channel estimation is applied to create a more compact representation of the channel, usually as a number of MPCs with defined angles, delays, and complex gain. Once this is done for the set of snapshots, data association is performed to decide which MPCs have similar parameters and are likely derived from the same physical objects interacting with the transmitted signals.

3.3.2 CHANNEL ESTIMATION ALGORITHMS

Numerous problems in both acoustics [52] and electromagnetics have benefited from research in array signal processing. Discrete incoming signals contributing to the impulse response are "resolved" and characterized by their angles, delays, Doppler values, and magnitudes with well-established super-resolution algorithms like ESPRIT and MUSIC and their various extensions [53].

In propagation modeling studies the typical workflow is to record the time-domain samples of the receiver and perform channel estimation and subsequent data association in post-processing, removing the necessity for highly efficient channel estimation. The norm for the past few decades has been to employ channel estimation algorithms based on expectation maximization, SAGE [54]. One ancillary benefit of SAGE is that it is well-suited to expand the dimensionality for the parameterization of the incoming signals for parameters like polarization as well.

A valuable extension of SAGE was the inclusion of "dense" multipath, described in Andreas Richter's highly readable dissertation where the RIMAX algorithm was described [55]. In addition to estimation of plane waves, a time domain signal contributing energy to the impulse response is parameterized, understood physically as the result of many small reflections arriving in short succession with random phase. Numerous extensions of the dense multipath concept have been developed in the decades since RIMAX was first proposed [56].

3.3.3 CLUSTERING

After channel estimation is performed, for modern GSCMs the next step is to perform data association among the MPCs estimated over the entire time series, to determine which are derived from the same, or similar sources that can be distinguished by the measurement aperture. Similar to RIMAX for channel estimation, Nikolai Czink's dissertation developed the Random Cluster Model, which has been highly influential in clustering for channel modeling [11].

Understanding the channel in terms of clusters corresponding to inherently geometric phenomena that can be characterized stochastically has led to an increasingly sophisticated understanding of wireless channels, permitting more intelligent design of wireless systems.

3.4 MULTIPATH-AIDED POSITIONING

For wireless positioning systems, the intention is not to equalize the channel to transfer data, but rather to use the pilot symbols transmitted to estimate geometry. Positioning systems built upon multilateration including GNSS, UWB or 802.11mc usually do not employ antenna arrays and do not perform channel estimation in the manner described by the array processing techniques of the previous section. The channel is frequently modeled as a single LOS component[§] between the transmitter and receiver antenna phase centers. Sometimes methods are employed to estimate multipath for their exclusion from the positioning algorithm, such as multipath-estimating loops [57] or synthetic aperture-like techniques [58]. Angular techniques are similar; the angles of the incoming signals are treated as representative of the true geometry without explicit estimation of multipath [59].

Explicit inclusion of discrete MPCs in order to enhance positioning performance has been widely explored in wireless communications literature [9] where communications experts saw radio waves as an obvious choice for an alternative "front end" technology [28], even if it has not seen commercialization. Using the angles, delays, and phases of incoming signals allows for precise tracking of movement [60]. However, virtually all of these papers are formulated as problems of differential navigation, rather than problems of estimating position in an external reference frame defined *a priori*.

3.5 OPPORTUNISTIC POSITIONING

It is significantly easier to solve a detection or estimation problem when one knows what to look for. Civilian signals for GNSS use repeating sequences that are unique per-satellite and intentionally designed to be simply replicated by a receiver[¶] [12, Chapter 4]. The pilot symbols used in OFDM for network acquisition and coherent data modulation are promising precisely because they are known and unencrypted [7]. Channel sounding signals are designed to maximize the resolvability of MPCs when performing channel estimation.

In all of these examples, communication is one-way. The transmitter is oblivious to whether anyone is taking advantage of the transmitted pilot signals. This can be contrasted with two-way communication approaches, like the RTOF method used in UWB or 802.11mc, which are sometimes classified as "network-based". Opportunistic positioning offers superior scalability because the medium can be shared by any number of users, but when it

---

[§]The model for signals from space is a bit more complicated, as described in Section 4.1.

[¶]This also makes GNSS signals susceptible to spoofing by malicious actors [61].

comes to opportunistic cellular positioning, there are some headwinds for use in future systems. A trend toward "ultra-lean" design makes clear the antagonistic nature of pilot symbols in their use for data communication and for navigation [62]. For a system intended for maximizing data throughput, pilot symbols are overhead, but for a positioning system like GNSS the pilot symbols are the primary function, and the small quantities of data that need to be transmitted are multiplexed.

For this reason, work is ongoing on "cognitive" sensing, where little to no information is available about the signal structure [63]. This is likely to be a necessary approach for navigation with data communication system signals in the future.

4

Autonomous Vehicle Navigation

You can't get there from here.

New England proverb

OST of the major technological innovations of the past millennium in navigation and cartography have their origins in maritime exploration, but the 20th century witnessed a dramatic expansion in methods of transit and the inventive solutions to meet those application requirements. As early as the decade after the Wright Flyer was trialed at Kitty Hawk, Instrument Landing Systems (ILS) were developed for landing in conditions of limited visibility [64]. Today, autonomous vehicles operate in a tremendously diverse set of environments. Unmanned sea probes navigate the depths of the ocean by utilizing acoustic waves [65]. Even more spectacularly, NASA successfully navigated a 1026-kg rover 470 million km through our solar system into the Jezero Crater on Mars, with remarkable agreement between pre-flight simulations and the eventual landing trajectory [66].

The DARPA Grand Challenges described in Chapter 1 continued to evolve towards trickier environments, too, including an urban challenge and a subterranean challenge. Numerous car manufacturers offer commercial systems meeting the criteria for level 2 automation, as defined by the Society of Automotive Engineers (SAE) and their now widely-adopted J3016 taxonomy for automation levels, but the definitions and methods for implementing level 3 and above remain controversial [67]. However, since the legacy of Stanley and the 2004 challenge, a particular set of sensors is typically understood to hold promise for perception and localization, with variation among practitioners [68]. This chapter provides a brief overview of the primary sensors used for the localization module, and introduces some of the concepts for localization in safety-critical systems.

4.1 THE SENSOR TOOLKIT

All sensors used for navigation have limitations in their operation, which is almost certainly why animals have evolved complementary sensing modalities. Our vision system is of minimal utility in low-light conditions and can be impacted by cataracts or other impairments; our vestibular systems can be disturbed by vertigo or other forms of dizziness; and our sense of touch by hypoesthesia. The sensing suite of autonomous vehicles has no singular fail-safe sensor either. A brief summary of the primary sensors used, together with their strengths and weaknesses, is given in Table 4.1. While there are numerous tutorials in literature specific to autonomous vehicle operation [69], each is discussed briefly in the following sub-sections as it relates to the central themes of this thesis.

Table 4.1: Sensor Strengths and Weaknesses

Sensor	Strengths	Weaknesses
GNSS	• Global estimation of position • Commodity hardware	• Sky-view limitation, range biasing • Difficulty to estimate physical errors without external augmentation • Susceptibility to spoofing/jamming
IMU	• Rapid observation rate and continuous availability • Commodity hardware in Micro-Electromechanical Systems (MEMS) packages	• Requires systematic handling of numerous calibration errors • Unbounded errors without periodic drift bias correction
Wheel Encoder	• High-rate observations that scale with speed • Provides independent estimate of yaw rate	• Systematic biases for wheel circumferences • Wheel slip, discretization errors
Camera	• Reliable angular measurements at long range • Powerful computer vision base to draw upon	• Physical occlusion, bloom lights • Limited depth estimation
Lidar	• Highly precise angle and range measurements • Operation in dark environments	• Power consumption and range tradeoff • Occlusion
Radar	• Range and angular measurements • Cost	• Resolution • Difficult data association

4.1.1 GNSS

GNSS is the workhorse for worldwide Positioning, Navigation and Timing (PNT) applications. Obvious and familiar applications include automotive and pedestrian navigation, but GNSS is also used to establish timing for cellular networks and power grids, for scientific applications and, because most GNSS constellations are military projects, tactical and strategic considerations are fundamental for the system's operation and development.

All GNSS systems operate on the principle of multilateration, as described in Chapter 3.2. A constellation of ≥ 24 Medium Earth Orbit (MEO) satellites in a Walker constellation [12, Figure 1.9] acts as time-synchronized transmitting references, each with unique pilot sequences that are continuously repeated and multiplexed with low-rate information of other system parameters including orbital trajectories.

Ranges are estimated to satellites by TOA, but when the user clock runs too quickly, ranges are underestimated. When the user clock lags the system time base[*], the satellites appear farther away. To handle this perennial clock synchronization problem, a fourth satellite is used to solve for clock offset simultaneously with position in three dimensions. For this reason, the range estimates are referred to as *pseudoranges*, because they all include a bias parameter for the current clock offset.

Most consumer electronic devices with GNSS receivers, as well as vehicles, have either a dedicated receiver chip or have the receiver packaged in the same chip as other wireless technologies including cellular communication. After decades of development and user segment device volumes in the billions, they are well optimized for performance with minimal requirements for power consumption. High-end receivers for surveying or scientific applications offer superior performance with the trade-off of larger size and power use. Regardless, all receivers, even those with the most sophisticated signal processing, are limited by physical obstructions between the receiving antenna and the satellites, as well as the multipath mechanisms illustrated in Figure 1.1. Virtually all literature on alternative wireless localization emphasizes this problem as the single critical factor that justifies use of wireless technologies other than GNSS as a replacement or complement.

There are a few other physical error sources that contribute to position error estimation in GNSS even in the absence of multipath. A few of these error sources are illustrated in Figure 4.1. Even with several atomic clocks on-board the satellites, each satellite experiences stochastic deviations from system time. Nor are orbits easily modeled and predictable long in advance.

---

[*]Each of the global constellations has its own timescale [12, Chapter 5.6], with specific requirements on allowable deviation from Coordinated Universal Time (UTC).

Both the ionosphere and the troposphere are mediums that introduce signal delays that vary across time and space. These and several other sources of errors are explained in [70].
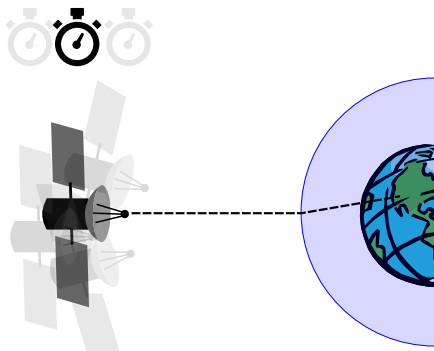
Figure 4.1: The major GNSS error sources, illustrated. Satellite orbital parameters and clock drift differ slightly from the satellite's own navigation message broadcast. Time and space-varying atmospheric parameters also induce consequential signal delays for a receiver on the ground. Multipath also causes positive range biasing, as shown in Figure 1.1.

For nominal operation by a standalone receiver, simple models are used to mitigate or estimate these error sources. For precise operation, two main families for handling of these sources of error have been developed in parallel for different applications. In *observed space representation*, the errors are double-differenced out by calculating a differential position from a well-surveyed proximate static point. In *state-space representation*, the physical errors (primarily those of Figure 4.1) are modeled by a worldwide network of stations and transmitted to the user to compensate for them in a highly-accurate manner. Typically when these advanced error models are applied, the observable parameter of the signal used for the precise position calculation is the high-frequency carrier signal phase, rather than the pseudoranges that are derived from down-converting the pilot symbols and looking for a correlation peak.

4.1.2 PROPRIOCEPTION

The British neurophysiologist Charles Sherrington coined the term proprioception [71], which covers a range of sensory neurons related to body movement and position that are fed into motor control in the brain. These neurons encode things like muscle length and rate of contraction or extension,

and tension. While the comparison to vehicular sensors may be a bit tortured, vehicles have multiple sensors that can be used for differential navigation without external inputs from the environment.

IMUs provide observations of acceleration and turn-rates on three mutually orthogonal axes, which can be used for highly precise differential navigation when integrated [14, Chapter 5]. The integration of these observations into position and orientation estimates forms an INS. As with GNSS, careful error modeling is required to attain reasonable performance by compensating for errors including cross-coupling of the axes and time-varying drift. The time-varying drift performance is typically what governs the underlying technology and subsequent price [72, Table 1]. The integration of low-cost but effective IMUs into electronic devices has made them attractive for many applications. Integration with cellular (or cellular-like) signals has been demonstrated for SLAM for both pseudoranges [73] and multipath-aided positioning [74].

Wheel odometry is also frequently employed for measuring differential movement in vehicular navigation systems. The wheel circumference multiplied by the number of measured rotations forms an effective proxy for distance traveled. The differential spin rate also gives information about changes in heading [75]. Wheel odometry is subject to systematic biases that need to be modeled, such as the individual wheel circumferences, and can provide faulty observations when friction is lost on any tire.

Ambient air pressure varies as a function of elevation, but also as a function of temperature and other weather considerations. Barometric pressure sensors can be used for absolute altitude estimation [14, Chapter 10.2] but are more frequently employed to observe relative changes in elevation.

The complementary properties of proprioception sensors and position fixing make them well-suited to pair together, as was shown in Figure 2.1. GNSS position estimates come in a global reference frame, but at a much lower rate than proprioception and frequently yield noisy estimates. Proprioception sensors, on the other hand, provide high-rate observations that are subject to slowly-changing biases.

4.1.3 EXTEROCEPTION

Charles Sherrington defined exteroception, the sensing of external stimuli, in contrast to proprioception. The primary sensors used for probing the environment immediately around the vehicle are vision (cameras), radar, and lidar. Stanley employed all three technologies [2], but the extent to which these should be depended upon and the merits of each are the subject of intense debate in and around the industry and in academia [76]. The author does

not feel qualified to offer an authoritative opinion, but will briefly summarize these sensors in this section.

The most important exteroceptive modality for humans is vision, and most autonomous vehicle localization and perception systems from Stanley onward have also depended most heavily on cameras for tasks like lane detection and object classification. Entire textbooks are written on the subject of computer vision for autonomous driving [77].

Lidar operates on the principle of emitting lasers and observing reflected energy to generate "point clouds". The 2007 Urban DARPA challenge, 3 years after Stanley's success, was a watershed moment for lidar in autonomous driving, and the top teams all benefited from a particular 360-degree rotating lidar from Velodyne [78].

Automotive radars emit modulated signals at either 24 GHz or 76-81 GHz and interpret the returning received energy from reflection or other propagation mechanisms. Mass-produced automotive radar systems are currently transitioning from horizontal plane only to more advanced, 3-dimensional "imaging radar" [79].

Each of these three sensors has its relative merits regarding range, resolution, susceptibility to interference and occlusions, power consumption, price, and the ease with which integration is possible into mass-production vehicles. For the sake of navigation in the context of this thesis, all three of these act as essentially monostatic sensors [23] probing the immediate environment. They can be employed for relative positioning by taking successive measurements and comparing differences, or with a database of features detectable with the various sensors and performing data association with measurements (the subject of the following section).

Ad hoc radio communication between vehicles and infrastructure, called vehicle-to-vehicle and vehicle-to-infrastructure, respectively, is sometimes considered an additional form of external sensing. The preferred radio standard for widescale commercial deployment is a subject of its own, frequently rather acrimonious debate. The two major contenders are based on either 3GPP standards (C-V2X) or Wi-Fi based standards such as IEEE 802.11p and its successor 802.11bd [80].

4.2 MAPS AND MAP-MATCHING

A standard commercial automotive navigation system providing route-level guidance fuses absolute localization estimates from GNSS, proprioception from IMUs, and wheel odometry, and then applies a map-matching algorithm to show the user their estimated position and heading on the display. There

are dozens of methods for performing map-matching on road-level networks [81].

Since around 2010, significantly more detailed "high-definition" maps have been developed, with the intention of augmenting both perception and path planning for autonomous driving [29]. The expansion of standard definition maps to include more semantic information, lane geometry models, and localization models makes the map a more powerful "sensor" for using the exteroception sensors that provide estimates in a global frame[†]. For standard definition maps used for route guidance, meter-level precision of the localization solution is perfectly fine. However, if HD Maps are to be used as priors for path planning, then centimeter or decimeter-level precision is necessary [82].

4.3 SAFETY-CRITICAL OPERATION

One of the most challenging aspects of developing safety-critical systems is specifying a design methodology for the systematic assessment of risks. In 1985, an ambitious task group was set up by the International Eletrotechnical Commission (IEC) to develop a standard that would offer definitions, normative recommendations, and examples. Eventually, this led to the standard IEC 61508 - Functional Safety of Electrical/Electronic/Programmable Electronic Safety-related Systems [83]. The standard was intended to be adapted to different domains and has been tailored for nuclear power, avionics, rail transport and, among other applications, the automotive domain through the ISO 26262 standard [84].

The avionics industry has been working on the problem of safety-critical localization for 40 years [85], with GNSS receivers developed and certified according to recommendations from avionics derivatives of the IEC 61508 standard [86]. Among the methods developed is the "self-contained" Receiver Autonomous Integrity Monitoring (RAIM) method where redundant measurements are compared to search for outliers [87]. However, the denser and more electromagnetically-complicated a propagation environment becomes, the more difficult establishing integrity becomes owing to multipath [3], which was never a major consideration for aviation[‡]. Mitigation strategies for error flagging in automotive environments have included cross-checks with camera data [88] and "shadow matching" using 3-D maps [89]. Stochastic

---

[†]An important caveat discussed in the next section is that using map data for safety-critical operation requires performing a comprehensive functional safety analysis.

[‡]Committees were established for interference and antennas by the aviation working groups, but none explicitly for multipath [85, Figure 2].

treatment of how frequently multipath is encountered as an input for fault trees has also been suggested [90], similar to some channel modeling methods. RAIM has been adapted for cellular pseudorange estimates [91], as well as for simulated 5G signals with errors inducted according to 3GPP channel models [92]. The worst-case scenario for GNSS multipath of the low-elevation satellite in the presence of specular reflectors [93] is the standard set-up for many interesting terrestrial beacon scenarios.

Directly porting aviation localization safety concepts to the automotive use case is difficult. Procedurally, the ISO 26262 and ISO PAS 21448 standards prescribe analysis over the entire lifecycle. For aviation, the integrity concepts developed are applicable to certain stages of flight (with approach being the most challenging), but an entirely new analysis would need to be done for the driving domain. The likely outcome of such an analysis is that bounds confining uncertainty in an external frame to a lane width [94] can be used as a unit-level measure, but will not be sufficient in isolation to assert the absence of "unreasonable risks" for an entire function or even for a localization block, considering the inevitability of map errors.

5
Machine Learning for Navigation

The pervasive use of machine learning, both ahead [of] and during the race, made Stanley robust and precise. We believe that those techniques, along with the extensive testing that took place, contributed significantly to Stanley's success in this race.

Thrun et al. [2]

NAVIGATION problems are problems of geometry. As explained in Chapter 3.2, observations of distances and bearings to landmarks provide the opportunity to easily calculate position and orientation in an external reference frame. However, there are numerous ways to infer navigation information without explicit calculation of ranges and bearings to surveyed landmarks, but rather with pattern recognition.

One of the most remarkable methods of feature matching by humans for navigation was employed by Marshall Islanders in Eastern Micronesia. These navigators were intimately familiar with the impact that ocean swells and currents have on an outrigger canoe, and could effectively estimate their own position in what climatologists would call a wave field based entirely on feel [95]. This has been demonstrated by a Micronesian navigator who was blindfolded and taken out of sight of land; he was able to lie down in a canoe and infer his position based purely on the movement of his canoe, stemming from the refractive pattern that the dominant ocean swells create around the islands [96].

Pattern matching is well-suited to problems that are high-dimensional and extremely difficult to come up with parametric models for. Examples of this include diagnosis based on medical imaging, estimation of real-estate price values, making the best move in chess, and next word prediction in text editors. Pattern matching today with ANNs exceeds human performance on

all of these tasks. While there are a variety of methods for pattern matching including Kernel-based methods, Gaussian process-based methods, and tree-based methods, the best-performing methods for most such problems in recent years are ANNs. These other solutions are normally introduced in literature as an obligatory prelude to a broader discussion of ANNs; see [97, Section V-A] or [98, Section VIII-A] for relevant examples in the wireless localization domain.

5.1 ARTIFICIAL NEURAL NETWORKS

ANNs constitute a family of learning structures for solving pattern recognition problems. The typical explanation of the taxonomy is that ANNs are a form of Machine Learning (ML) and ML falls within the field of artificial intelligence, but as always with taxonomy, there is no universal consensus. Multi-layer ANNs are "deep" neural networks, and there are numerous ANN variations, such as Convolutional Neural Networks (CNNs) that perform convolution operations with the benefit of "weight sharing", or recurrent neural networks which include internal feedback mechanisms. The author of a recently-published dissertation described ANNs as follows:

A DNN [Deep Neural Network] is a data-driven method that constructs a chain of layered computations, where each layer consists of a set of nodes (also known as neurons) that receives a weighted sum of inputs from the previous layer and combines the sum with a non-linear activation function.

Jens Henriksson [99]

In more accessible (but less precise) language, the flow for making an ANN is approximately as follows:

Step 1: Numerical inputs based on sample data are collected, whether they be chess moves, vectorized text, or images. For supervised learning problems, of interest in this thesis, a label is also associated with that numerical input, either a categorical label (yes/no, for example, or maybe cat/dog/orangutan) or a numeric value for regression problems (latitude/longitude).

Step 2: The fixed structure (network architecture) is decided, dimensioned based on input size, output size, computational needs and knowledge of underlying data structure. In this structure, numerical inputs are multiplied by random numbers (weights), and then the resulting products are transformed in a somewhat arbitrary manner (an activation

function). Deep learning has several sequential such operations before the final layer, which has the same dimensionality as the categorical or numerical prediction.

Step 3: A cost function is defined to quantify the quality predictions and the correct labels, together with a learning rate to decide how malleable the network weight values should be.

Step 4: Test samples are fed into the input and propagated through the structure to see the result. If the output at the final layer was satisfactory (matching the label), the random numbers are modified only slightly. If the output was unsatisfactory, the random numbers (weights) undergo a larger step change (SGD).

Step 5: New data (presented to the network in batches, typically) is run through the network and weights are updated according to the cost function and learning rate.

Once the weights have been adjusted with many training samples, new inputs can be applied where the label is unknown in the hope that the weight adjustment from training data will prove to be useful for unlabeled data. Repeating this process many times on large and representative data sets has worked brilliantly for many problems, but unlike parametric models, it is frequently not easy to understand when or why the model fails to effectively predict using new data. For example, vision networks trained in only daylight are likely to perform poorly at night, but it might be less obvious that seasonal changes in vegetation could be problematic in computer vision [100].

An example CNN of the sort typical for Papers II-IV is illustrated in Figure 5.1. A representation of the wireless channel is input to predict an output (label) that includes position and heading. Several layers of convolutions are followed by several fully-connected layers before the final output.

In end-to-end learning, the input data in as raw a form as possible is fed into a neural network, under the assumption that human manipulation of such features will only serve to corrupt features that could effectively be learned by a sufficiently large network with enough weights in a favorable architecture. For the network of Figure 5.1, this might be raw samples in the time domain, or Channel State Information (CSI).

5.2 APPLICATION IN AUTONOMOUS SYSTEMS

In computer vision, parametric methods for robust keypoint identification to extract features for localization problems have a long history [102]. End-to-end learning with CNNs has also been established as a viable option to provide full 6 Degrees of Freedom (6DOF) pose estimates directly from input
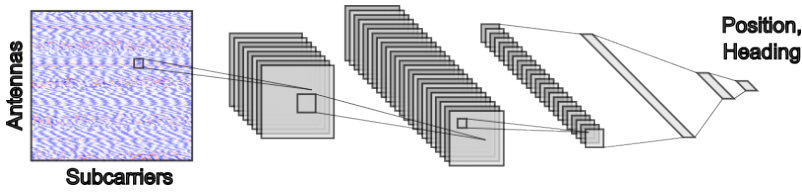
Figure 5.1: CNN accepting CSI as input and estimating position and heading. ANN graphic based on Alexander LeNail's NN-SVG tool [101].

images with no feature engineering. Pre-trained networks generated on public data sets are available from which transfer learning can be applied for new environments [103]. Lidar is also a natural choice for pose estimation with ANNs [82].

For Stanley and most other robotics applications, computer vision has been widely used for both perception and localization per the quote at the start of this chapter. End-to-end autonomous driving has even been proposed, in which raw sensor data leads to actuation decision without creating any kind of modular architecture with perception or control modules, see [69, Section III-3].

5.3 WIRELESS CHANNEL AS INPUTS

The idea of using wireless channels as the basis for position estimation without any explicit calculation of angles and ranges can be found in literature from more than 30 years ago* [8].

Adoption of pattern matching for navigation using wireless networks has tended to go hand-in-hand with the roll-out of data networks, which can now be found essentially wherever there is human settlement in an industrialized society. It is so natural to think of wireless fingerprinting for indoor localization that in a survey of indoor localization systems, wireless technologies like Wi-Fi and Bluetooth are the primary examples and other forms of localization are almost an afterthought [104]. Low-frequency signals spanning from Very Low Frequency (VLF) [105] to sub-6 GHz cellular are typically used for fingerprinting, when resolution in both angular and delay domains tends to be small. Higher frequency signals lend themselves more to parametric estimation on the wavelength scale of most navigation problems.

---

*For more detailed exposition on the history, Paper IV includes a longer discussion in Sections II.A and B.

5.3.1 SIGNAL STRENGTH AND CHANNEL STATE INFORMATION

The physics of wave propagation are a function of Maxwell's equations, and while modeling complexity quickly escalates beyond practical limits for most localization problems to calculate received power analytically, with anything other than spherical cow[†] problem formulations, there is nothing inherently mysterious about the received power in a wireless link. The received power can be detected and quantized for display in different manners to provide a Received Signal Strength Indicator (RSSI), whether with dedicated circuitry or through signal processing. For commodity hardware, different manufacturers and even different transceiver models coming from the same manufacturer quantize differently to produce various ranges of RSSI[‡]. Given the heavy use of RSSI for navigation, for which these considerations are important, numerous analyses have been conducted with RSSI treated as a stochastic parameter [106].

An obvious limitation with the scalar signal strength parameter is that one typically wishes to estimate a multi-dimensional state vector. Signal strength is typically a lackluster proxy even for distance, as described in Chapter 3.2, so it is unlikely to perform better for a multi-dimensional estimation problem. For OFDM systems, the receiver produces complex-valued estimates per subcarrier after performing downconversion and a Fourier Transform. This frequency-dependent channel gain, CSI, provides more insight into the channel than a scalar RSSI value. The frequency-dependent channel gain for several antenna ports, using the measurement system described in Appendix A, is shown for one snapshot in Figure 5.2.

5.3.2 IMPULSE RESPONSE

The impulse response, sampled at the Nyquist rate, is an equivalent representation to CSI [97, Footnote 8], and a representation which lends itself reasonably well to intuition. Figure 5.3 shows the same data as Figure 5.2 as an impulse response; the latter is a Fourier Transform of the former. There are several easily distinguishable peaks that correspond with dispersion in the delay domain. Only the relatively early-arriving components contain significant power, which might hold promise for enabling similar performance as CSI even after discarding later-arriving components.

[†]An old physics joke about model simplifications rendering them useless for real problems. Alternatively formulated as "assume a can opener" in economics.

[‡]See [106, Table III].
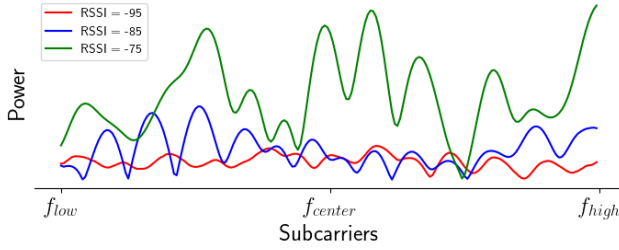
Figure 5.2: The frequency response and scalar value of signal strength for several antenna ports for one snapshot. The directionality and polarization differences of the antennas result in antennas on the same array experiencing channels that differ significantly in their absolute strength and in their frequency and phase responses.
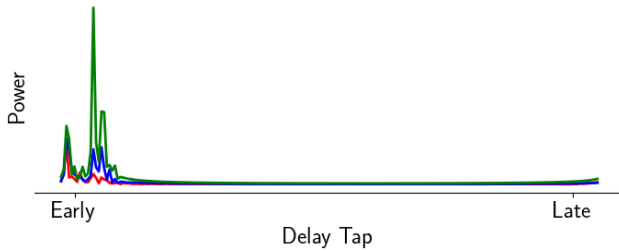
Figure 5.3: The impulse response representation of the same three measurements shown in Figure 5.2.

5.3.3 ANGLE-DELAY DOMAIN

The angle-delay representation of the channel was suggested in [107]. It can be formulated either in the beamspace domain, or using the complete radiation pattern of the antenna. Figure 5.4 shows a response representative of many non-LOS environments. Incoming signals arrive with varying degrees of dispersion from a range of azimuthal angles with different delays. Note that the directions are indicated in an egocentric coordinate system. They could be expressed equivalently in an allocentric system or in an antenna-centric system if there is an offset between the antenna coordinate system and the egocentric system of interest.
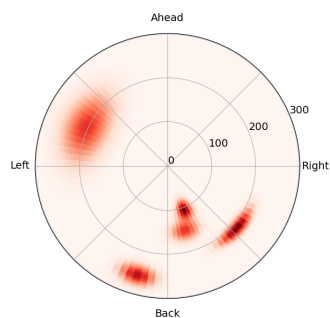
Figure 5.4: A simulated angle-delay representation. Strong, presumably specular components arrive from the back with different angles and delays. Weaker, dispersive power is also observed in the front left.

6

Contributions and Outlook

It's difficult to make predictions, especially about the future.

Danish proverb

IXTH-generation wireless systems are being defined at the time of this writing [108]. The convergence of wireless communication and localization technologies into future cellular standards seems inevitable, because not only are there application demands for positioning, but cellular networks themselves can operate more intelligently and efficiently with user location information, or with at least effective proxies for user location [109]. This summarizing chapter describes the research contributions of the included papers and lessons from the project more generally, and speculates about future directions for wireless positioning systems.

6.1 RESEARCH CONTRIBUTIONS

Peer reviewers are typically asked to assign articles a novelty score as part of the grading criteria for acceptance for publication. Not every submission can be the next special relativity, but the state-of-the-art should be advanced in a manner that can be clearly articulated. The author's assessment of what he and his collaborators have done to accomplish this for the included papers follows in this section.

Paper I: Cellular Localization for Autonomous Driving: A Function Pull Approach to Safety-Critical Wireless Localization

The excitement about autonomous systems has led to efforts to quantify performance requirements for various automotive use cases, including autonomous driving. Multiple industry consortia including 3GPP, 5G Automo-

tive Association (5GAA), and the CAR 2 CAR Communication Consortium (C2C-CC) have tried to formulate performance requirements for collaborative applications [110], with accuracy requirements of 1σ to 3σ and reliability of 99.9%. The manner in which these are derived is somewhat opaque. For example, a Coordinated, Co-operative Driving Maneuver [110, Table I] is said to require a 3σ accuracy of 1.5 meters. But at the frequency with which driving maneuvers transpire, this is a paltry level of confidence. Does one assume that other sensors will pick up the slack when the error exceeds the 3σ specification? Is it predicated on all users having a common understanding of where lanes and road edges are? It is difficult to formulate requirements without systematically breaking down the entire use case. Absolute position accuracy requirements that do not carefully account for tail error represent an unacceptable tolerance for either risk, if used for actuation, or tolerance for false alarms, if used for driver warnings.

The author has the impression that there are several branches of literature that exist in silos and would do well to borrow more from each other; that they will do so eventually seems inevitable. The first branch is classical navigation literature, in which three separate families of positioning integrity systems have their origins [85]. Some of these systems have been applied directly to the road use case [94], and even to cellular signals with the important understanding that flagging bad measurements is necessary for safety-critical operation [91]. However, as articulated in this paper, safety-engineering practice is likely to lead to conclusions other than that an absolute positioning system must have a continuously-converged protection level that bounds the vehicle within a lane.

The second branch is communication literature, in which the amazing success of Multiple-Input Multiple-Output (MIMO) has led to work on how multi-antenna systems can improve geometrical understanding of the channel. A mathematically appealing problem formulation for such problems is multipath-SLAM, but navigation applications like autonomous driving stand to benefit most from novel forms of position fixing, which are well within reach using similar methods. Integrity concepts from navigation are starting to enter the lexicon [111, 112], but to this point are still given only a cursory mention even in Sixth Generation (6G) literature where autonomous systems are discussed [98].

Paper I builds a bridge between concepts familiar in navigation literature including over-bounding, position fixing, and awareness of multi-sensor fusion and the advanced understanding of electromagnetic signal propagation and wireless positioning from the communications world. This is woven into a coherent analysis also seen through the lens of safety engineering

principles [84] specific to the automotive domain, in a format highly accessible to those working in the various disciplines.

Paper II: Urban Navigation with LTE using a Large Antenna Array and Machine Learning

While there is a massive body of literature on wireless fingerprinting [97], much of it is from the Internet of Things (IoT) domain, where electrically-small antennas necessitate omni-directionality, at least for the mobile user. Surprisingly, even though angular-delay domain representation was first suggested as a sparse representation for fingerprinting in 2017 in a frequently-cited paper that partially inspired the work in this dissertation [107], finger-prints based on either signal strength or CSI have been the norm for the overwhelming majority of fingerprinting papers based on measurements. To the author's best knowledge, this was the first work to attempt an angular-delay representation with measurement data, even if others had understood its merits and suggested various types of simulation. It was also, as far as the author could discern, the first attempt at augmenting fingerprints with other localization states (orientation).

Paper III: LTE NLOS Navigation and Channel Characterization

This was the first instance of using fingerprinting to perform joint heading and position estimation and the first instance of implementing the matched filter using the complex radiation pattern of the antenna for fingerprinting, even if it had been used behind the scenes for initialization of RIMAX in Paper II. This work also had an additional component of examining ranging and angular biases. Previous work had recognized the utility of modeling pseudorange bias errors by using statistical channel models [113], and another platform had been demonstrated for angle estimation of LTE signals [59], but this work joined the two together in a measured non-LOS scenario to show angular and delay biases for a challenging scenario.

Paper IV: Wiometrics: Comparative Performance of Artificial Neural Networks for Wireless Navigation

An extension of papers II and III, this is a more comprehensive examination of how the azimuthal-delay representation compares with other methods and provides a benchmark for feature engineering on an interesting data set. A similar analysis is offered for different neural network architectures, and one small contribution (or at least a methodological aspect) that the author hopes others will follow is to test how performance is affected by different training and test splits. This factor is frequently neglected in fingerprinting literature, where the input space of labels is frequently laid out as a rectangular grid. More than any other, this paper offers a compelling vision for how finger-printing should still be considered a viable alternative even with the advent of massive-MIMO systems.

Paper V: Flexible Density-based Multipath Component Clustering Utilizing Ground Truth Pose

For GSCMs, a geometry-based understanding of channels [114] is baked into the name itself, but despite this, there is limited work in literature where information about position informs channel modeling work aside from simple path-loss models. This paper offers a novel, easily implementable and intuitive method for data association that should be straightforward to build upon for anyone working with channel modeling, even with double-directional wireless channels or highly mobile channels.

6.2 GENERAL CONCLUSIONS

Rumors of the death of Sub-6 GHz frequencies are greatly exaggerated.

Millimeter-wave systems are all the rage in communications literature, although even those are starting to lose their coolness-factor in favor of "Terahertz" systems. Some of the selling points of mmWave like network densification [115] are actually antithetical to their commercial viability for autonomous systems, because in the end someone will need to pay for a dense network. What Papers II-IV show in aggregate is that there is a great deal of potential for achieving compelling performance in the blurry world of decimeter-scale wavelengths and limited-bandwidth signals without highly resolvable observables. This is especially interesting when the lessons from Paper I are taken into consideration, namely that for autonomous systems, having redundant sources of information may be more useful than maximizing accuracy for each system. An affordable system that can provide an integrity check against a map-matched localization solution derived from other sensors (a QM monitor, in the language of ISO 26262 [84]) might be more compelling than an expensive solution with better accuracy.

Not every problem is ready for end-to-end learning.

With the caveat that there is perhaps only a modest amount of training data in the publications (the author has spent so much time looking at 28,280 snapshots that he can just about re-create the data from memory), comparison of the networks using CSI versus the alternative representations shows that feature engineering provided compelling performance gains not only measurable in position error, but by requiring lower computational power for inference by reducing the size of the inputs, though manipulation of the inputs themselves takes some resources. It is reasonably intuitive to understand why performance gains are realized. If the antenna pattern is used prior to training, for example, the network need not learn the antenna pattern. If the CSI-based representations need to learn all the patterns of

small-scale fading, they will require heavy sampling and probably be less robust to changes in the configuration of reflecting and scattering objects.

Plane-wave estimation of MPCs is probably not well suited for mixing with CNNs.

While discrete channel estimation [116] has been used previously for fully-connected neural network representation, comparison of the results in Paper II to those of Papers III/IV showed that RIMAX was a step too far in feature engineering. It is both computationally demanding to generate discrete channel estimates and entails information loss for the network. There may be some situations in which a scaled-down version with simpler channel estimation (not based on expectation-maximization) could also benefit from computational savings by avoiding convolution operations, but it seems to have been a poor choice for this measurement set-up.

Visualization of MPCs in an external frame is critical for developing algorithms, whether for positioning or for channel characterization.

Understanding which physical objects give rise to multipath components provides a strong basis for developing intuition about why one sees the results that one sees with otherwise invisible electromagnetic waves. This requires measuring the fixed offsets between the antennas and receiver coordinate systems, and generating time-synchronized estimates of transmitter and receiver position and orientation in the external frame, and finally correlating these with a map. A high-grade GNSS-INS served this purpose fairly well for the measurements in this work, but camera or lidar-based photogrammetry are promising for indoor scenarios, which are uniquely challenging in both wireless communications and navigation.

The method proposed in Paper V has subsequently been tested by the author for higher-dimensional data sets including both angles of arrival and angles of departure on higher frequency data, with preliminary results indicating that it works effectively.

Localization integrity for automotive use cases requires a fresh analysis.

Numerous stakeholders contributed to the decades-long collaborative effort to develop a navigation safety concept for different stages of flight [85], but autonomous driving has been characterized by a race among competitors to establish a commercial offering, and this form of collaboration has not materialized. Unlike the aviation case, where the stages of flight are well understood, automotive use cases are much more variable and dynamic.

6.3 OUTLOOK AND FUTURE WORK

This work is filled with buzz words including machine learning, autonomous systems, and next-gen cellular communication. These trending topics have taken different trajectories over the course of the project, and opinion varies wildly about where they are on the Gartner hype cycle* [118]. However, these topics will continue to see significant attention in both academia and industry for the foreseeable future. The following subsections provide context for these trends and offer suggestions for future work.

6.3.1 CELLULAR NAVIGATION

The major GNSS constellations continue to be the backbone of navigation applications. New constellations are coming online for reasons of geopolitical strategy. Existing constellations are continuously being updated with new signals and new features like signal authentication. Correction data for GNSS observables is being broadcast both by satellite and private terrestrial networks, and the user equipment is becoming more sophisticated to take all of these inputs in small form factors for commercial applications as well [119]. However, transmitters in MEO will continue to have limited power as observed on the Earth's surface.

As large satellite constellations for data communication have been rolled out including Starlink, researchers and investors have shown enthusiasm for new generations of Low Earth Orbit (LEO) satellites[†] [120]. These lower-altitude and less expensive satellites can provide favorable geometries and coverage with polar orbits (see [36, Chapter 7]) and, even if signals are coming from the sky, they perhaps can penetrate buildings more effectively by virtue of having lower path loss [121, Section V. Part D.]. The business case and technical proof-of-concept for LEO-PNT are each a work in progress. Terrestrial wireless systems are still likely to play an important role for enabling resilient-PNT or assured-PNT, as it is sometimes called.

Cellular navigation faces some headwinds, technologically, commercially, and politically. Starting with the latter, if positioning methods such as trilateration and triangulation are to be used on a wide scale, the transmitter locations likely need to be anonymized. 5G base stations and telecom workers have been subjected to physical attacks by individuals who presumably have not engaged in a serious study of microbiology and assert that 5G is the progenitor (or perhaps vice-versa?) of SARS-CoV2 [122]. The author and his collaborators came to realize that the spectrum regulation authorities

---

*Just as various observers might place the author at different points on the Dunning-Kruger curve [117].

[†]The first satellite navigation systems, TRANSIT and Tsikada, operated in LEO.

and network operators were not keen to hand over lists of base stations for these reasons, and crowdsourced databases were frequently erroneous and otherwise imprecise. GNSS satellites broadcast their orbital parameters freely, but do not lend themselves well to physical sabotage by paranoid individuals.

Commercially, PRS have been defined since 3GPP Release-9 more than a decade ago, but few operators have deployed them because they have not been able to find customers willing to pay for the feature. The superior performance of 5G signals [41] might be more compelling, but operators need to be able to provide an attractive business case. Confined environments like factories, ports, or private networks like the 5G networks operated by some rail operators are more likely to see their first large-scale deployments of such technology rather than passenger vehicles which roam over huge geographical areas. Further work should focus on developing position fixing methods that more elegantly utilize multipath. Multi-sensor fusion and 3-D map aiding are very promising in this regard [89], and integration with cellular signals is an obvious start that provides synergies with the communications literature on multipath-SLAM.

6.3.2 FINGERPRINTING

As an alternative to the "network-based" positioning including defined 3GPP positioning signals or RTOF, opportunistic positioning might prove to be the more appealing solution for many applications. Opportunistic methods are already widely deployed for Android and iOS, even if implementation details are opaque [6]. And while modern cellular systems strive for ultra-lean design, with more selective and variable transmission of pilot symbols, various "blind" or partially-blind methods of estimation have been proposed and demonstrated [63].

Opportunistic observables lend themselves well to fingerprinting, and Papers II-IV show that significantly more can be "squeezed" out of every transmitter than is possible with existing fingerprinting methods, without two-way communication and without knowledge of transmitter position or orientation. More effective combination of information from multiple transmitters than was proposed in Paper IV is certainly possible, and given the overlapping coverage of various networks, this is an obvious place to reduce error distribution tails.

An obvious limitation of fingerprinting is that once the model is trained, it is subject to a range of errors from distribution shifts like seasonal variations to out-of-distribution samples stemming from hardware failures or any other unlikely events not captured in training. More intricate representations might encounter limitations when applied across different types of hardware,

analogous to issues with the differing light intensity and beams across models and manufacturers for lidar [82].

The burgeoning body of literature on ML safety is rich with ideas that can be used as inspiration for application in fingerprinting, including networks that simultaneously output a "do not trust" reject option [123] in addition to other outlier detection methods [99] or explainability as a safety mechanism [124]. More generally, the application of ML in safety-critical systems is a major topic of research [125], and numerous proposals for work flows to develop and deploy safety-critical ML systems have appeared in the past few years [126, 127]. In addition to the "unit-level" testing with techniques like outlier detection, these "system-level" safety concepts are also critical to consider for fingerprinting systems if they are to be used for autonomous systems.

6.3.3 CHANNEL MODELING

The trends discussed in this section and throughout the thesis indicate that channel modeling as a discipline will need to continue to expand its scope to new environments and to new frequencies. LEO satellites are being deployed for numerous new applications, including PNT. While wide geographic coverage will continue to be enabled by sub-6 GHz frequencies, the search for ever-higher data rates has led to consideration of ever-higher frequencies [128]. A more sophisticated understanding of geometric relationships continues to be key to improving system efficiencies. Employing even millimeter-wave technologies requires adaptive beemsteering to intelligently focus energy, owing to the quadratic increase in path loss with frequency [49], but lower frequency operation also benefits from an improved understanding of propagation effects as a function of environment and frequency.

The fidelity of site-specific models will improve as photogrammetry and cheaper computational power and memory enable more sophisticated simulation, but there will still be plenty of utility for physical channel sounding and GSCMs for both research and product development. As Larry Greenstein said, related by Tataria et al. [34], *"Every time a new system has been built in a new band, in a new environment, or for a new service, major questions have had to be answered about the nature of the radio propagation. It was true for Marconi's wireless telegraph; it is true for today's cellular systems; and it will be true for as long as people dream up new ways to use radio waves."* We will continue to carry on the legacy of Pierce and Woodward [1] as we fiddle with our channel sounders well into the 21st century to design and optimize our wireless navigation systems.

Bibliography

[1] J. Pierce and R. Woodward, "The development of long-range hyperbolic navigation in the United States," *NAVIGATION: Journal of the Institute of Navigation*, vol. 18, no. 1, pp. 51–62, 1971.

[2] S. Thrun, M. Montemerlo, H. Dahlkamp *et al.*, "Stanley: The robot that won the DARPA grand challenge," *Journal of Field Robotics*, vol. 23, no. 9, pp. 661–692, 2006.

[3] N. Zhu, J. Marais, D. Bétaille, and M. Berbineau, "GNSS Position Integrity in Urban Environments: A Review of Literature," *IEEE Transactions on Intelligent Transportation Systems*, vol. 19, no. 9, pp. 2762–2778, 2018.

[4] V. Renaudin and F. Potorti, "Editorial an important step for indoor and seamless positioning and navigation," *IEEE Journal of Indoor and Seamless Positioning and Navigation*, vol. 1, pp. iii–iii, 2023. doi: 10.1109/JISPIN.2023.3344291

[5] J. A. del Peral-Rosado, R. Raulefs, J. A. López-Salcedo, and G. Seco-Granados, "Survey of cellular mobile radio localization methods: From 1G to 5G," *IEEE Communications Surveys & Tutorials*, vol. 20, no. 2, pp. 1124–1148, 2017.

[6] F. Nedelkov, D.-K. Lee, D. Miralles, and D. Akos, "Accuracy and performance of the network location provider in android devices," in *Proceedings of the 33rd International Technical Meeting of the Satellite Division of The Institute of Navigation (ION GNSS+ 2020)*, 2020, pp. 2152–2165.

[7] Z. M. Kassas, "Navigation with cellular signals of opportunity," *Position, Navigation, and Timing Technologies in the 21st Century: Integrated Satellite Navigation, Sensor Systems, and Civil Applications*, vol. 2, pp. 1171–1223, 2020.

[8] Christ, Godwin, and Lavigne, "A prison guard duress alarm location system," in *1993 Proceedings of IEEE International Carnahan Conference on Security Technology*, 1993. doi: 10.1109/CCST.1993.386816 pp. 106–116.

[9] C. Gentner, T. Jost, W. Wang *et al.*, "Multipath assisted positioning with simultaneous localization and mapping," *IEEE Transactions on Wireless Communications*, vol. 15, no. 9, pp. 6104–6117, 2016.

[10] S. M. Kay, *Fundamentals of statistical signal processing: estimation theory*. Prentice-Hall, Inc., 1993.

[11] N. Czink, "The random-cluster model - a stochastic MIMO channel model for broadband wireless communication systems of the 3rd generation and beyond," Ph.D. dissertation, Vienna University of Technology, 12 2007.

[12] P. Teunissen and O. Montenbruck, *Springer Handbook of Global Navigation Satellite Systems*, ser. Springer Handbooks. Springer International Publishing, 2017. ISBN 9783319429281

[13] M. Crawford, *The Case for Working with Your Hands: Or why office work is bad for us and fixing things feels good*. Penguin UK, 2010.

[14] P. Groves, *Principles of GNSS, Inertial, and Multisensor Integrated Navigation Systems, Second Edition*. Artech House, 03 2013.

[15] T.-T. N. Do, C.-T. Lin, and K. Gramann, "Human brain dynamics in active spatial navigation," *Scientific Reports*, vol. 11, no. 1, p. 13036, 2021.

[16] R. Holland, "True navigation in birds: from quantum physics to global migration," *Journal of Zoology*, vol. 293, no. 1, pp. 1–15, 2014.

[17] A. M. Berdahl, A. B. Kao, A. Flack *et al.*, "Collective animal navigation and migratory culture: from theoretical models to empirical evidence," *Philosophical Transactions of the Royal Society B: Biological Sciences*, vol. 373, no. 1746, p. 20170009, 2018.

[18] R. I. Wilson, "Neural networks for navigation: From connections to computations," *Annual Review of Neuroscience*, vol. 46, pp. 403–423, 2023.

[19] D. Lewis, "Observations on route finding and spatial orientation among the aboriginal peoples of the western desert region of central australia," *Oceania*, vol. 46, no. 4, pp. 249–282, 1976.

[20] ——, *We, the navigators: The ancient art of landfinding in the Pacific*. University of Hawaii Press, 1994.

[21] D. Sobel, *Longitude: The true story of a lone genius who solved the greatest scientific problem of his time*.   Macmillan, 2005.

[22] D. W. Allan, "Statistics of atomic frequency standards," *Proceedings of the IEEE*, vol. 54, no. 2, pp. 221–230, 1966.

[23] H. Wymeersch and G. Seco-Granados, "Radio localization and sensing—Part I: Fundamentals," *IEEE Communications Letters*, vol. 26, no. 12, pp. 2816–2820, 2022.

[24] J. B. Haviland, "Guugu Yimithirr cardinal directions," *Ethos*, vol. 26, no. 1, pp. 25–47, 1998.

[25] F. C. Kessler, S. E. Battersby, M. P. Finn, and K. C. Clarke, "Map projections and the internet," *Choosing a Map Projection*, pp. 117–148, 2017.

[26] C. H. Cotter, "Early dead reckoning navigation," *The Journal of Navigation*, vol. 31, no. 1, pp. 20–28, 1978.

[27] B. K. Hulse and V. Jayaraman, "Mechanisms underlying the neural computation of head direction," *Annual review of neuroscience*, vol. 43, pp. 31–54, 2020.

[28] C. Cadena, L. Carlone, H. Carrillo *et al.*, "Past, present, and future of simultaneous localization and mapping: Toward the robust-perception age," *IEEE Transactions on robotics*, vol. 32, no. 6, pp. 1309–1332, 2016.

[29] R. Liu, J. Wang, and B. Zhang, "High definition map for automated driving: Overview and analysis," *The Journal of Navigation*, vol. 73, no. 2, pp. 324–341, 2020.

[30] A. Hassani and M. Joerger, "Analytical and empirical navigation safety evaluation of a tightly integrated Lidar/IMU using return-light intensity," *NAVIGATION: Journal of the Institute of Navigation*, vol. 70, no. 4, 2023.

[31] A. F. Molisch, *Wireless communications*.   John Wiley & Sons, 2012, vol. 34.

[32] R. H. Lochte, "Invention and innovation of early radio technology," *Journal of Radio Studies*, vol. 7, no. 1, pp. 93–115, 2000.

[33] M. J. Seifer, *Wizard: the life and times of Nikola Tesla: biography of a genius*. Citadel Press, 1996.

[34] H. Tataria, K. Haneda, A. F. Molisch, M. Shafi, and F. Tufvesson, "Standardization of propagation models for terrestrial cellular systems: A historical perspective," *International Journal of Wireless Information Networks*, vol. 28, pp. 20–44, 2021.

[35] R. Costley, "Battlefield acoustics in the first world war: artillery location," *Acoust. Today*, vol. 16, pp. 31–39, 2020.

[36] M. L. Psiaki, "Navigation using carrier doppler shift from a LEO constellation: TRANSIT on steroids," *Navigation*, vol. 68, no. 3, pp. 621–641, 2021.

[37] B. W. Parkinson, "Origins, evolution, and future of satellite navigation," *Journal of Guidance, Control, and Dynamics*, vol. 20, no. 1, pp. 11–25, 1997.

[38] W. Blanchard, "The genesis of the decca navigator system," *The Journal of Navigation*, vol. 68, no. 2, pp. 219–237, 2015.

[39] R. J. Fontana, "Recent system applications of short-pulse ultra-wideband (uwb) technology," *IEEE Transactions on microwave theory and techniques*, vol. 52, no. 9, pp. 2087–2104, 2004.

[40] F. Van Diggelen, R. Want, and W. Wang. (2018) How to achieve 1-meter accuracy in Android. [Online]. Available: https://www.gpsworld.com/how-to-achieve-1-meter-accuracy-in-android/

[41] S. Dwivedi, R. Shreevastav, F. Munier *et al.*, "Positioning in 5G Networks," *IEEE Communications Magazine*, vol. 59, no. 11, pp. 38–44, 2021.

[42] M. Guarnieri, "The early history of radar [historical]," *IEEE Industrial Electronics Magazine*, vol. 4, no. 3, pp. 36–42, 2010.

[43] H. Liu, H. Darabi, P. Banerjee, and J. Liu, "Survey of wireless indoor positioning techniques and systems," *IEEE Transactions on Systems, Man, and Cybernetics, Part C (Applications and Reviews)*, vol. 37, no. 6, pp. 1067–1080, 2007.

[44] P. Teunissen and A. Khodabandeh, "Review and principles of PPP-RTK methods," *Journal of Geodesy*, vol. 89, no. 3, pp. 217–240, 2015.

[45] D. Dardari, A. Conti, U. Ferner, A. Giorgetti, and M. Z. Win, "Ranging with ultrawide bandwidth signals in multipath environments," *Proceedings of the IEEE*, vol. 97, no. 2, pp. 404–426, 2009.

[46] M. Bolic, M. Rostamian, and P. M. Djuric, "Proximity detection with RFID: A step toward the internet of things," *IEEE Pervasive Computing*, vol. 14, no. 2, pp. 70–76, 2015.

[47] E. Dahlman, S. Parkvall, and J. Skold, *4G: LTE/LTE-advanced for mobile broadband*. Academic press, 2013.

[48] R. Nilsson and J. van de Beek, "Channel measurements in an open-pit mine using USRPs: 5G—expect the unexpected," in *2016 IEEE Wireless Communications and Networking Conference*. IEEE, 2016, pp. 1–6.

[49] M. Shafi, J. Zhang, H. Tataria *et al.*, "Microwave vs. millimeter-wave propagation channels: Key differences and impact on 5G cellular systems," *IEEE Communications Magazine*, vol. 56, no. 12, pp. 14–20, 2018.

[50] A. W. Mbugua, Y. Chen, L. Raschkowski *et al.*, "Review on ray tracing channel simulation accuracy in sub-6 GHz outdoor deployment scenarios," *IEEE Open Journal of Antennas and Propagation*, vol. 2, pp. 22–37, 2020.

[51] J. Flordelis, X. Li, O. Edfors, and F. Tufvesson, "Massive MIMO extensions to the COST 2100 channel model: Modeling and validation," *IEEE Transactions on Wireless Communications*, vol. 19, no. 1, pp. 380–394, 2019.

[52] I. McCowan, "Microphone arrays: A tutorial," *Queensland University, Australia*, pp. 1–38, 2001.

[53] H. Krim and M. Viberg, "Two decades of array signal processing research: the parametric approach," *IEEE signal processing magazine*, vol. 13, no. 4, pp. 67–94, 1996.

[54] B. H. Fleury, M. Tschudin, R. Heddergott, D. Dahlhaus, and K. I. Pedersen, "Channel parameter estimation in mobile radio environments using the SAGE algorithm," *IEEE Journal on selected areas in communications*, vol. 17, no. 3, pp. 434–450, 1999.

[55] A. Richter, "Estimation of radio channel parameters: Models and algorithms," Ph.D. dissertation, Technische Universität Ilmenau, Germany, 2005.

[56] S. Jiang, W. Wang, Y. Miao, W. Fan, and A. F. Molisch, "A survey of dense multipath and its impact on wireless systems," *IEEE Open Journal of Antennas and Propagation*, 2022.

[57] P. Wang and Y. J. Morton, "Multipath estimating delay lock loop for LTE signal TOA estimation in indoor and urban environments," *IEEE Transactions on Wireless Communications*, vol. 19, no. 8, pp. 5518–5530, 2020.

[58] R. Faragher, N. Couronneau, M. Powe *et al.*, "Supercorrelation: Enhancing the accuracy and sensitivity of consumer GNSS receivers with a DSP upgrade," in *Proceedings of the 31st International Technical Meeting of the Satellite Division of The Institute of Navigation (ION GNSS+ 2018)*, 2018, pp. 357–375.

[59] K. Shamaei and Z. M. Kassas, "A joint TOA and DOA acquisition and tracking approach for positioning with LTE signals," *IEEE Transactions on Signal Processing*, vol. 69, pp. 2689–2705, 2021.

[60] X. Li, E. Leitinger, M. Oskarsson, K. Åström, and F. Tufvesson, "Massive MIMO-based localization and mapping exploiting phase information of multipath components," *IEEE transactions on wireless communications*, vol. 18, no. 9, pp. 4254–4267, 2019.

[61] M. L. Psiaki and T. E. Humphreys, "GNSS spoofing and detection," *Proceedings of the IEEE*, vol. 104, no. 6, pp. 1258–1270, 2016.

[62] S. Parkvall, E. Dahlman, A. Furuskar, and M. Frenne, "NR: The new 5G radio access technology," *IEEE Communications Standards Magazine*, vol. 1, no. 4, pp. 24–30, 2017.

[63] M. Neinavaie, "Cognitive sensing and navigation with unknown terrestrial and LEO satellite signals," Ph.D. dissertation, The Ohio State University, 2023.

[64] L. Sanders and V. Fritch, "Instrument landing systems," *IEEE Transactions on Communications*, vol. 21, no. 5, pp. 435–454, 1973.

[65] T. Zhang, B. Liu, and Y. Liu, "Positioning systems for Jiaolong deep-sea manned submersible: sea trial and application," *IEEE Access*, vol. 6, pp. 71 644–71 650, 2018.

[66] D. W. Way, S. Dutta, C. Zumwalt, and D. Blette, "Assessment of the Mars 2020 entry, descent, and landing simulation," in *AIAA SciTech 2022 Forum*, 2022, p. 0421.

[67] T. Inagaki and T. B. Sheridan, "A critique of the SAE conditional driving automation definition, and analyses of options for improvement," *Cognition, technology & work*, vol. 21, pp. 569–578, 2019.

[68] S. Kuutti, S. Fallah, K. Katsaros *et al.*, "A survey of the state-of-the-art localization techniques and their potentials for autonomous vehicle applications," *IEEE Internet of Things Journal*, vol. 5, no. 2, pp. 829–846, 2018.

[69] E. Yurtsever, J. Lambert, A. Carballo, and K. Takeda, "A survey of autonomous driving: Common practices and emerging technologies," *IEEE access*, vol. 8, pp. 58 443–58 469, 2020.

[70] M. Karaim, M. Elsheikh, and A. Noureldin, "GNSS error sources," *Multifunctional Operation and Application of GPS*, pp. 69–85, 2018.

[71] J. C. Tuthill and E. Azim, "Proprioception," *Current Biology*, vol. 28, no. 5, pp. R194–R203, 2018.

[72] N. El-Sheimy and A. Youssef, "Inertial sensors technologies for navigation applications: State of the art and future trends," *Satellite Navigation*, vol. 1, no. 1, pp. 1–21, 2020.

[73] J. J. Morales and Z. M. Kassas, "Tightly coupled inertial navigation system with signals of opportunity aiding," *IEEE Transactions on Aerospace and Electronic Systems*, vol. 57, no. 3, pp. 1930–1948, 2021.

[74] C. Gentner, R. Pöhlmann, M. Ulmschneider *et al.*, "Positioning using terrestrial multipath signals and inertial sensors," *Mobile Information Systems*, vol. 2017.

[75] E. Stenborg and L. Hammarstrand, "Using a single band GNSS receiver to improve relative positioning in autonomous cars," in *2016 IEEE Intelligent Vehicles Symposium (IV)*. IEEE, 2016, pp. 921–926.

[76] P. Wang, "Research on comparison of LiDAR and camera in autonomous driving," in *Journal of Physics: Conference Series*, vol. 2093, no. 1. IOP Publishing, 2021, p. 012032.

[77] J. Janai, F. Güney, A. Behl, A. Geiger *et al.*, "Computer vision for autonomous vehicles: Problems, datasets and state of the art," *Foundations and Trends® in Computer Graphics and Vision*, vol. 12, no. 1–3, pp. 1–308, 2020.

[78] Y. Li and J. Ibanez-Guzman, "Lidar for autonomous driving: The principles, challenges, and trends for automotive lidar and perception systems," *IEEE Signal Processing Magazine*, vol. 37, no. 4, pp. 50–61, 2020.

[79] C. Waldschmidt, J. Hasch, and W. Menzel, "Automotive radar—from first efforts to future systems," *IEEE Journal of Microwaves*, vol. 1, no. 1, pp. 135–148, 2021.

[80] A. Bazzi, G. Cecchini, M. Menarini, B. M. Masini, and A. Zanella, "Survey and perspectives of vehicular Wi-Fi versus sidelink cellular-V2X in the 5G era," *Future Internet*, vol. 11, no. 6, p. 122, 2019.

[81] M. A. Quddus, W. Y. Ochieng, and R. B. Noland, "Current map-matching algorithms for transport applications: State-of-the art and future research directions," *Transportation research part c: Emerging technologies*, vol. 15, no. 5, pp. 312–328, 2007.

[82] I. A. Barsan, S. Wang, A. Pokrovsky, and R. Urtasun, "Learning to localize using a LiDAR intensity map," in *Proceedings of The 2nd Conference on Robot Learning*, ser. Proceedings of Machine Learning Research, A. Billard, A. Dragan, J. Peters, and J. Morimoto, Eds., vol. 87. PMLR, 29–31 Oct 2018, pp. 605–616. [Online]. Available: https://proceedings.mlr.press/v87/barsan18a.html

[83] R. Bell, "Introduction to IEC 61508," in *Acm international conference proceeding series*, vol. 162. Citeseer, 2006, pp. 3–12.

[84] O. Kirovskii and V. Gorelov, "Driver assistance systems: analysis, tests and the safety case. ISO 26262 and ISO PAS 21448," in *IOP Conference Series: Materials Science and Engineering*, vol. 534, no. 1. IOP Publishing, 2019, p. 012019.

[85] C. J. Hegarty, G. T. Ligler, K. Alexander *et al.*, "RTCA SC-159: 30 years of aviation GPS standards," in *Proceedings of the 28th International Technical Meeting of the Satellite Division of the Institute of Navigation (ION GNSS+ 2015)*, 2015, pp. 877–896.

[86] J. Ray, R. Nayak, S. KR, M. Shenoy *et al.*, "High integrity GPS-SBAS receiver using innovative correlator and software approach for avionics applications," in *Proceedings of the 17th International Technical Meeting of the Satellite Division of The Institute of Navigation (ION GNSS 2004)*, 2004, pp. 1539–1546.

[87] Y. C. Lee, "Analysis of range and position comparison methods as a means to provide GPS integrity in the user receiver," in *Proceedings of the 42nd Annual Meeting of The Institute of Navigation (1986)*, 1986, pp. 1–4.

[88] J. Marais, S. A. Kazim, Y. Cocheril, and C. Meurie, "Multipath and NLOS detection based on the combination of CN0 values and a fisheye camera," in *2020 European Navigation Conference (ENC)*. IEEE, 2020, pp. 1–13.

[89] Q. Zhong and P. D. Groves, "Multi-epoch 3D-mapping-aided positioning using bayesian filtering techniques," *NAVIGATION: Journal of the Institute of Navigation*, vol. 69, no. 2, 2022.

[90] S. Khanafseh, B. Kujur, M. Joerger *et al.*, "GNSS multipath error modeling for automotive applications," in *Proceedings of the 31st International Technical Meeting of the Satellite Division of The Institute of Navigation (ION GNSS+ 2018)*, 2018, pp. 1573–1589.

[91] M. Maaref and Z. M. Kassas, "Autonomous integrity monitoring for vehicular navigation with cellular signals of opportunity and an IMU," *IEEE Transactions on Intelligent Transportation Systems*, 2021.

[92] Y. Sun, L. Cao, S. Li, and Z. Deng, "G5GIM: Integrity monitoring for GNSS/5G integrated navigation of urban vehicles," *IEEE Transactions on Instrumentation and Measurement*, 2023.

[93] L. Lau, "GNSS multipath errors and mitigation techniques," in *GPS and GNSS Technology in Geosciences*. Elsevier, 2021, pp. 77–98.

[94] T. G. Reid, S. E. Houts, R. Cammarata *et al.*, "Localization requirements for autonomous vehicles," *SAE International Journal of Connected and Automated Vehicles*, vol. 2, no. 12-02-03-0012, 2019.

[95] J. Genz, J. Aucan, M. Merrifield *et al.*, "Wave navigation in the marshall islands: Comparing indigenous and western scientific knowledge of the ocean," *Oceanography*, vol. 22, no. 2, pp. 234–245, 2009.

[96] J. E. Huth, *The lost art of finding our way*. Harvard University Press, 2013.

[97] D. Burghal, A. T. Ravi, V. Rao, A. A. Alghafis, and A. F. Molisch, "A comprehensive survey of machine learning based localization with wireless signals," *arXiv preprint arXiv:2012.11171*, 2020.

[98] S. E. Trevlakis, A.-A. A. Boulogeorgos, D. Pliatsios *et al.*, "Localization as a key enabler of 6G wireless systems: A comprehensive survey and an outlook," *IEEE Open Journal of the Communications Society*, 2023.

[99] J. Henriksson, "Outlier detection as a safety measure for safety critical deep learning," Ph.D. dissertation, Chalmers University of Technology, 2023.

[100] T. Sattler, W. Maddern, C. Toft *et al.*, "Benchmarking 6dof outdoor visual localization in changing conditions," in *Proceedings of the IEEE conference on computer vision and pattern recognition*, 2018, pp. 8601–8610.

[101] A. LeNail, "NN-SVG: Publication-ready neural network architecture schematics," *Journal of Open Source Software*, vol. 4, no. 33, p. 747, 2019.

[102] D. G. Lowe, "Distinctive image features from scale-invariant keypoints," *International journal of computer vision*, vol. 60, pp. 91–110, 2004.

[103] A. Kendall, M. Grimes, and R. Cipolla, "Posenet: A convolutional network for real-time 6-dof camera relocalization," in *Proceedings of the IEEE international conference on computer vision*, 2015, pp. 2938–2946.

[104] P. Roy and C. Chowdhury, "A survey of machine learning techniques for indoor localization and navigation systems," *Journal of Intelligent & Robotic Systems*, vol. 101, no. 3, p. 63, 2021.

[105] J. A. I. a. Curro, "Navigation with artificial neural networks," Ph.D. dissertation, Air Force Institute of Technology (AFIT), 2018.

[106] K. Kaemarungsi and P. Krishnamurthy, "Analysis of WLAN's received signal strength indication for indoor location fingerprinting," *Pervasive and mobile computing*, vol. 8, no. 2, pp. 292–316, 2012.

[107] J. Vieira, E. Leitinger, M. Sarajlic, X. Li, and F. Tufvesson, "Deep convolutional neural networks for massive MIMO fingerprint-based positioning," in *2017 IEEE 28th Annual International Symposium on Personal, Indoor, and Mobile Radio Communications (PIMRC)*. IEEE, 2017, pp. 1–6.

[108] H. Tataria, M. Shafi, A. F. Molisch *et al.*, "6G wireless systems: Vision, requirements, challenges, insights, and opportunities," *Proceedings of the IEEE*, vol. 109, no. 7, pp. 1166–1199, 2021.

[109] C. Studer, S. Medjkouh, E. Gonultaş, T. Goldstein, and O. Tirkkonen, "Channel charting: Locating users within the radio environment using channel state information," *IEEE Access*, vol. 6, pp. 47 682–47 698, 2018.

[110] S. Bartoletti, H. Wymeersch, T. Mach *et al.*, "Positioning and sensing for vehicular safety applications in 5G and beyond," *IEEE Communications Magazine*, vol. 59, no. 11, pp. 15–21, 2021.

[111] 3GPP, "Study on NR Positioning Enhancements," 3rd Generation Partnership Project (3GPP), TS 38.857, Mar. 2021. [Online]. Available: https://portal.3gpp.org/desktopmodules/Specifications/ SpecificationDetails.aspx?specificationId=3732

[112] 5GAA, "Trustable Position Metrics for V2X Applications," 5G Automotive Alliance, TS , Sep. 2023. [Online]. Available: https://5gaa. org/content/uploads/2023/10/5gaa-a-220044-tpm4v2x-tr-1.pdf

[113] P. Müller, J. A. del Peral-Rosado, R. Piche, and G. Seco-Granados, "Statistical trilateration with skew-t distributed errors in LTE networks," *IEEE Transactions on Wireless Communications*, vol. 15, no. 10, pp. 7114–7127, 2016.

[114] A. F. Molisch, H. Asplund, R. Heddergott, M. Steinbauer, and T. Zwick, "The COST259 directional channel model-part I: Overview and methodology," *IEEE Transactions on Wireless Communications*, vol. 5, no. 12, pp. 3421–3433, 2006.

[115] H. Wymeersch, G. Seco-Granados, G. Destino, D. Dardari, and F. Tufvesson, "5G mmwave positioning for vehicular networks," *IEEE Wireless Communications*, vol. 24, no. 6, pp. 80–86, 2017.

[116] X. Ye, X. Yin, X. Cai, A. P. Yuste, and H. Xu, "Neural-network-assisted UE localization using radio-channel fingerprints in LTE networks," *IEEE Access*, vol. 5, pp. 12 071–12 087, 2017.

[117] D. Dunning, "The Dunning–Kruger effect: On being ignorant of one's own ignorance," in *Advances in experimental social psychology*. Elsevier, 2011, vol. 44, pp. 247–296.

[118] A. Linden and J. Fenn, "Understanding Gartner's hype cycles," *Strategic Analysis Report Nº R-20-1971. Gartner, Inc*, vol. 88, p. 1423, 2003.

[119] N. Joubert, T. G. Reid, and F. Noble, "Developments in modern GNSS and its impact on autonomous vehicle architectures," in *2020 IEEE Intelligent Vehicles Symposium (IV)*. IEEE, 2020, pp. 2029–2036.

[120] T. Reid, T. Walter, P. Enge *et al.*, "Position, navigation, and timing technologies in the 21st century," *Wiley-IEEE*, vol. 2, pp. 1359–1379, 2021.

[121] F. S. Prol, R. M. Ferre, Z. Saleem *et al.*, "Position, navigation, and timing (PNT) through low earth orbit (LEO) satellites: A survey on current status, challenges, and opportunities," *IEEE Access*, 2022.

[122] D. Jolley and J. L. Paterson, "Pylons ablaze: Examining the role of 5G COVID-19 conspiracy beliefs and support for violence," *British journal of social psychology*, vol. 59, no. 3, pp. 628–640, 2020.

[123] Y. Geifman and R. El-Yaniv, "Selectivenet: A deep neural network with an integrated reject option," in *International conference on machine learning*. PMLR, 2019, pp. 2151–2159.

[124] É. Zablocki, H. Ben-Younes, P. Pérez, and M. Cord, "Explainability of deep vision-based autonomous driving systems: Review and challenges," *International Journal of Computer Vision*, vol. 130, no. 10, pp. 2425–2452, 2022.

[125] S. Mohseni, H. Wang, C. Xiao *et al.*, "Taxonomy of machine learning safety: A survey and primer," *ACM Computing Surveys*, vol. 55, no. 8, pp. 1–38, 2022.

[126] R. Hawkins, C. Paterson, C. Picardi *et al.*, "Guidance on the assurance of machine learning in autonomous systems (AMLAS)," *arXiv preprint arXiv:2102.01564*, 2021.

[127] EASA and Daedalean, "Concepts of design assurance for neural networks (CoDANN) II," Tech. Rep., 5 2021.

[128] C. Han, Y. Wang, Y. Li *et al.*, "Terahertz wireless channels: A holistic survey on measurement, modeling, and analysis," *IEEE Communications Surveys & Tutorials*, vol. 24, no. 3, pp. 1670–1707, 2022.

[129] T. Izydorczyk, F. M. Tavares, G. Berardinelli, and P. Mogensen, "A USRP-based multi-antenna testbed for reception of multi-site cellular signals," *IEEE Access*, vol. 7, pp. 162 723–162 734, 2019.

[130] K. Vasudeva, O. Ozdemir, S. R. Chandar, F. Erden, and I. Guvenc, "Vehicular LTE connectivity analysis in urban and rural environments using USRP measurements," *Array*, vol. 8, p. 100045, 2020.

[131] N. Instruments, "LabVIEW communications LabVIEW LTE application framework," 2023, online; accessed 04-Dec-2023. [Online]. Available: https://www.ni.com/sv-se/shop/software/products/labview-communications-lte-application-framework.html

[132] S. R. Systems, "Rubidium frequency standard - fs725," 2020, online; accessed 20-Dec-2023. [Online]. Available: https://www.thinksrs.com/products/fs725.html

[133] O. T. S. Ltd, "RT3000 v3," 2020, online; accessed 20-Dec-2023. [Online]. Available: https://www.oxts.com/products/rt3000/#

[134] GoPro, "Gopro MAX 360 action camera," 2023, online; accessed 04-Dec-2023. [Online]. Available: https://gopro.com/en/se/shop/cameras/max/CHDHZ-202-master.html

[135] P. Harvey, "Exiftool by phil harvey," 2023, online; accessed 04-Dec-2023. [Online]. Available: https://exiftool.org/

APPENDICES

A

Measurement Setup

FOUR of the papers included in this thesis use data recorded from a measurement system which was built for the MIMO-PAD project, financed in part by the Swedish Innovation Agency Vinnova. The measurement system receives and records downlink Fourth Generation (4G) signals, and high-resolution processing is subsequently performed offline. Simultaneously, observations are made of GNSS signals and inertial measurements from a high-grade ground truth system, which are also post-processed offline for highly-accurate estimations of vehicle position and pose. Finally, a 360° camera is used to examine any irregularities in the data. Each of the articles that use the measurements also contain a brief description of the setup, but because those articles were all subject to page limits that necessitated brevity, a more elaborate description is provided in this appendix.

Numerous test runs were made prior to the primary measurement campaign conducted on December 23, 2020, including a long drive test 2 days prior in which the experimenters discovered, at the end of the day, that a coax cable end had been broken early on and the data was useless.

As the adage goes regarding simulations and measurements, *No one believes in simulation results except the person who did the simulation. Everyone believes in measurement results except for the person who performed the measurements.* The data is not fudged or cherry-picked, but the system was designed for high-resolution operation, so trade-offs in the quality of aspects of the system for commercialization purposes, or designing another scaled-down system for verification and further development, would entail a trade-off in performance. The relevant aspects for the impressive performance achieved are mentioned in the articles where applicable and again in this appendix.

LTE SIGNAL RECEPTION

The most elaborate and novel part of the measurement system was designed by the author's close collaborator in the MIMO-PAD project, Junshi Chen. The goal was to perform channel sounding of commercial Long-Term Evolution (LTE) wireless channels with the maximum possible spatial resolution, for which a massive antenna array was a natural choice. While multi-antenna systems for receiving LTE signals have been demonstrated previously [59,129], these systems use parallel receivers, which places practical constraints on the number of antennas that can be used, and introduces non-trivial calibration challenges as well. Additionally, those systems employ dipole or monopole antennas with mostly overlapping gain patterns.

A different approach was taken for this system. A single receive chain was used and switching was done among antenna ports of a massive antenna array, which allows for an almost arbitrarily large number of receive antennas. A Stacked Uniform Circular Array (SUCA) with 128 ports was used, because this antenna architecture is well-suited for channel sounding, as explained in detail in [55, Chapter 3.3]. Rather than a snapshot entailing simultaneous sampling of the channel on all antenna ports, a single snapshot involves sequential sampling of antenna ports through an electrical switch. Switching among the antenna ports with the right timing requires an understanding of LTE synchronization signals and their timing.

In the time domain, LTE is divided into symbols (71 or 83 μs, depending on configuration), slots (0.5 ms), subframes (1 ms), half-frames (5 ms) and frames (10 ms). Synchronization signals are broadcast at regular intervals at predictable spots in the LTE resource grid (time and frequency allocation) [47]. The Primary Synchronization Signal (PSS) and Secondary Synchronization Signal (SSS) are transmitted once per half frame and used for acquiring network timing. Cell-specific Reference Signals (CRS) are used for coherent data modulation, and are transmitted the most frequently of any synchronization signals (twice per slot) to enable operation at high speed when channel coherence times are short. They span the entire channel bandwidth (20 MHz), but they are not broadcast on every subcarrier.

An overview of the timing for snapshots is shown in Figure A.1. The CRS switching interval was set to once per slot, 0.5 ms per antenna port. One snapshot involves observations with all 128 antenna ports, which requires 64 ms. This does not fit conveniently into the 10 ms frame structure, and an extra 11 ms are allocated to provide some buffering time for Automatic Gain Control (AGC) adjustment, bringing the total snapshot interval time to 75 ms. This amounts to seven full frames and one half frame per snapshot.
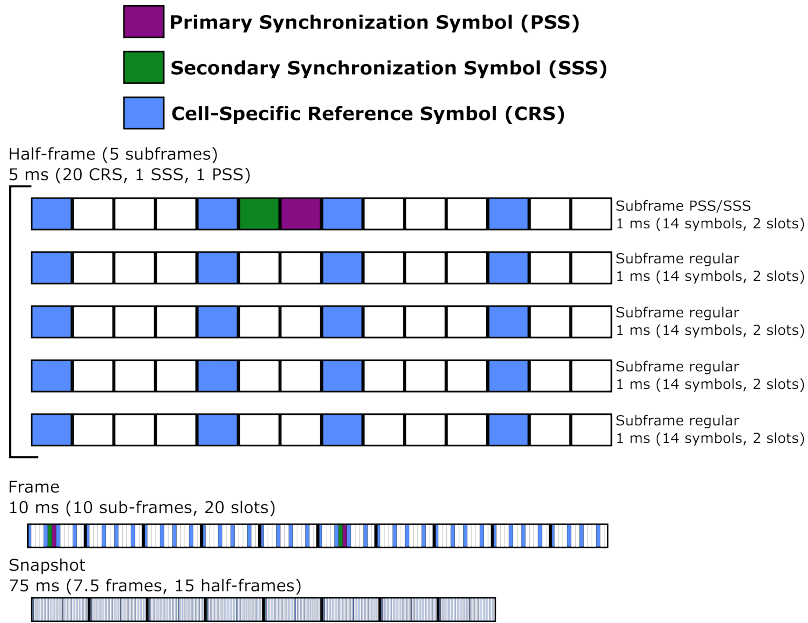
Figure A.1: Timing of LTE synchronization signals, which are built up from symbols in the time domain. Snapshot is not part of the LTE standard, but rather the interval used for high-resolution processing with the measurement system.

The attentive reader might be wondering whether every transmitter can provide unambiguous references in a global frame in the manner of GNSS as described in Chapter 4.1.1. The number of unique CRS sequences is the product of unique PSS (3) and SSS (168) sequences, a total of 504 [7, Table 38.1]. Global identifiers can be extracted in the additional information blocks that are broadcast in LTE, which include country codes, network codes, tracking area codes, and cell identities [130].

SOFTWARE-DEFINED RADIO AND ACCESSORIES

The LTE Framework software from National Instruments was employed to help with acquisition and timing described in the previous section [131], and this software is designed to run on one of National Instruments' Software-Defined Radios (SDRs). An SDR is essentially a Swiss Army knife for the reception and generation of radio signals. Commercial products like mobile phones are designed to operate in accordance with standardized communication protocols where the lower layers of the protocol stack are

well-defined and not variable, only configurable within standardized bounds. There is some room for optimization of receiver and transmitter hardware and firmware, but there is not typically much maneuvering room for the designers once the standard is complete. If someone thinks that the physical layer waveforms defined for a certain Wi-Fi standard are not up to snuff and need a re-design, they can either make their case in the standardization meetings for a future generation or develop a system that will be incompatible with other Wi-Fi radios. SDRs form the platform one is likely to use for such experimentation. Within broad boundaries, almost any aspect of radio communication, from the physical waveforms to the network protocols, can be adjusted.

A block diagram of the important components of the system is shown in Figure A.2. The SDR is the core of the system. It hosts the LabVIEW software with LTE Framework, which has a user interface displayed on an external laptop, sends the measured data to the laptop over a PCI Express interface, controls the antenna switch, and has the RF circuitry and FPGA for analog-to-digital conversion, and also has an integrated GPS receiver used not for positioning (the positioning performance is shown for illustration purposes in Paper III), but rather for time synchronization so received signals are timestamped with GPS time.
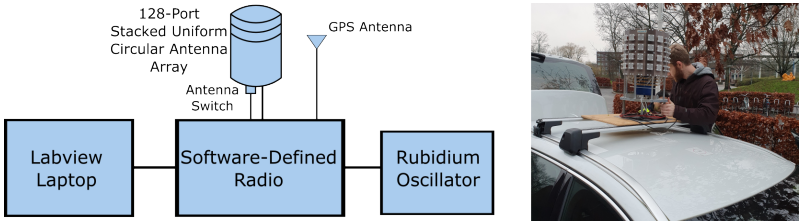
Figure A.2: Block diagram showing components used in high-resolution channel sounding system for LTE CRS. The author, cold and in a slightly irritable mood, is shown mounting the SUCA antenna on the vehicle.

A stable 10-MHz frequency reference is provided by a GPS-disciplined Rubidium oscillator [132]. Rubidium oscillators are frequently employed for channel modeling, because the transmitter and receiver clocks are derived from the oscillators, and if the two diverge there is no easy mechanism for achieving time-alignment again. Consumer devices almost universally employ crystal oscillators that have a much higher (worse) Allan deviation [12, Chapter 5.2]. As discussed in detail in Papers II, III, and IV, this level of clock stability minimizes the severity of one of the primary challenges for wireless positioning, which is timing synchronization between transmitter and

receiver, but in a way that is not easily applicable to large-scale deployment with today's clock technologies.

There are numerous other design decisions involved with the LTE channel sounding system which are not included here, such as the frequency of AGC updates or the interference cancellation scheme. The interested reader can attain some of these details from the paper *High-resolution channel sounding and parameter estimation in multi-site cellular networks* found in "Related Work".

GROUND TRUTH POSE AND MAP PROJECTION

An RT3003G ground truth reference system developed and sold by OXTS [133] is used to generate ground truth estimates of the vehicle position and orientation. The RT3003G is a dual-antenna, two-constellation system with a high-grade IMU and survey-grade GNSS receiver. RINEX observation data from three nearby reference stations in the SWEPOS network operated by the Swedish Mapping Authority Lantmäteriet are used to perform post-processing in OXTS' NAVSOLVE software. Forward and backward passes through the time series data are combined to create a "Post-processed" RTK trajectory, though it is apparent when examining these trajectories that there are hiccups in the Ground Truth trajectory as a consequence of very long, low-speed passes through the heavy multipath environment, and it is likely that the large antenna array on the roof causes problems with the carrier phase observable as well. This manifests itself most clearly as infeasible jumps in elevation, but those were deemed to not be consequential for the 2-D problems considered in the papers.

UTM Projections to SWEREF 99 13 30 (EPSG:3007) are used to translate the latitudes and longitudes to East-North coordinates for processing, but are translated to various other representations for visualizations in the papers. Openstreetmap data is used, either downloaded from geofabrik.de or fetched with the Mapnik Python toolkit, as well as Google Earth for 3-D renderings.

3-D CAMERA DATA

A GoPRO 360° camera [134] was mounted on top of the antenna array, to have a similar field of view as the antenna array. The camera has a built-in GPS receiver, and the locations and times are embedded into the recorded files as metadata. These times and positions were extracted using exiftool [135] to perform time-alignment with the ground truth system and cellular data. An example panorama image is shown in Figure A.3. The primary base station (BS A in Paper IV) is visible above the bus.

Figure A.3: Panorama image showing the view from the GoPRO camera, mounted on top of the antenna array. The SMA connections to the upper rows of patch antennas are visible in the lower part of the image, and the base station is visible above the bus.

Note that while the positioning performance of the GNSS receivers for both the SDR and the GoPRO camera is not particularly good in the challenging urban canyon environment, the timing accuracy is more than sufficient for the purposes of time synchronization with ground truth positioning. Timing accuracy is proportional with position accuracy, so even if the position estimates were off by 50 meters compared to the Ground Truth system, the equivalent distance traveled for the slowly-moving test vehicle would be less than a millimeter.

A NOTE ON THE DRIVING SPEED

Channel sounders are typically employed in the domain of channel modeling. Channel sounding entails transmitting a pre-determined sequence at a center frequency and bandwidth of interest*. Using opportunistic observations of signals broadcast by commercial networks as the basis for channel sounding means being at the mercy of the whims of the particular operator with license to use the spectrum, as well as the transmission protocol which is designed to maximize network data throughput rather than for the sake of science.

The decision to use a switched system resulted in a strong trade-off in channel coherence time. With the flexibility to design the transmitted waveform,

---

*Subject to legal constraints on spectral mask and duty cycles. The radio spectrum is an enormously valuable public resource and research ethics and national regulations dictate that one cannot blast energy at any frequency willy-nilly.

a rapid sequence would have been employed rather than the frequency of CRS transmission, which is sufficient for data communication but far from ideal for channel sounding at a non-zero velocity. The intention was to limit the drive speed so that less than half a wavelength (λ = 11.5 cm at 2.6 GHz) would be traversed during one snapshot, but for 75 ms snapshots (of which 64 ms is the duration of sampling) this is just under 1 m/s or 3.6 km/h. Speed governing functions (cruise control or adaptive cruise control) cannot be activated at this low speed, and the speedometer is not that granular either. The author attempted to maintain a constant speed and was mostly successful at hovering around 3-4 km/h, but occasionally exceeded these values when traffic conditions called for it.

PAPERS

Paper I

Paper I

Cellular Localization for Autonomous Driving
A function pull approach to safety-critical wireless localization

Russ Whiton

Abstract

Cellular localization has received marked attention in academia and in indus-try, as indicated by a rapidly expanding volume of literature specific to vehicular environments. Impressive results have been shown for a number of problems as measured by metrics such as accuracy and latency. This paper identifies five important requirements for cellular localization for safety-critical systems with a particular focus on autonomous driving, and puts them in the context of industrial and academic trends and standardization. We show why autonomous operation requires special consideration, and suggest research directions toward novel and practically implementable solutions, drawing lessons from decades of work on satellite-based localization for aviation landing systems. In addition, we highlight the benefit of cellular localization technology for safety-critical autonomous systems, showing the utility of a satellite-navigation independent absolute localization sensor with error overbounding.

I. INTRODUCTION

The challenge of Autonomous Driving (AD) has resulted in a surge of industrial activity and academic publications in the past 10 years. Novel proposals have been made for the associated hardware and software components, system architectures and even behavioral and societal impacts. Using the levels defined in the Society of Automotive Engineers' (SAE) widely-used J3016 taxonomy, companies, universities and research institutes are now developing, testing and validating level 3 and 4 automated driving features on public roads.

Functional architectures for AD are typically split into blocks from sensing through to actuation, enabling the vehicle to navigate the environment both on a large scale (lane selection and route planning) as well as on a small scale (lane position and orientation) [1]. This is most frequently accomplished with a broad suite of sensing technologies and a world map. *Localization* entails determination of position, orientation and velocity in an external reference frame, and provides context to AD beyond the horizon of the perception sensors. This context can be provided with a world map, which can be as simple as a road-level navigation map or as intricate as a High-Definition (HD) map rich with detail about road classification, lane markings, signs and other detectable objects.

Only Global Navigational Satellite Systems (GNSS) provide *absolute* estimates of position at coordinates surveyed in the same global reference frame in which map data is typically stored. GNSS has well-known limitations, primarily a strong dependence on physical view of satellites, weak signals at the Earth's surface, and is increasingly easy to jam and spoof by unsophisticated malicious actors.

Cellular localization has been developed as an enabling technology for use cases ranging from factory automation to AD, recognized in industry consortia such as the 5G Automotive Alliance (5GAA) and 3rd Generation Partnership Project (3GPP). The communications world sees the natural affinity for cellular systems with their widespread deployment, relatively high power, and large communication bandwidth and granular direction determination to address localization needs for increased robustness and for expansion of the Operational Design Domain (ODD) to locations where GNSS reliability is always low, such as urban canyons [2].

To take the next step towards deployment of cellular localization for safety-critical systems including AD, we believe it is necessary to take a *function pull* approach, in which the needs of the AD localization subsystem, and the role of cellular localization within that subsystem, are considered from an application and safety engineering standpoint. This is done in accordance with automotive industry-wide technical standards that allow safety principles to be shared across engineering teams with common vocabulary and practices. In doing so, we place new types of requirements on cellular localization that have not been addressed in prior literature, which has considered the *technology push* of cellular localization within the architecture of cellular networks in terms of signals, operating frequencies and bandwidths [3], or the performance achievable in isolation for automotive use cases without regard to sensor fusion or safety engineering principles, quantified by metrics like accuracy and latency [4].

We highlight performance metrics that we see would be most valued for AD, primarily the ability to establish *quantified confidence* in a localization solution in a reference frame that can be aligned with maps. We also show why multipath propagation poses difficult challenges for classic overbounding approaches adapted from aviation [5], and more generally the extent to which error overbounding can be ported from aviation landing systems to automotive use cases [6].

New constellations of researchers across disciplines are necessary to achieve this vision. This encompasses the fields of classical navigation, different sub-disciplines of wireless communications, geodesy as well as safety engineering. To this end we offer a list of research topics that need to be addressed to realize such a solution, drawing lessons from decades of work done on localization integrity in aviation.

The manuscript is organized as follows: Section II introduces AD localization architectures, safety-critical localization and the state of cellular localization in literature and standardization; Sections III-V identify novel requirements related to the gaps between the "pull" of AD functional needs and the "push" of cellular localization technology,

formulating requirements and exploring the reasoning behind them; finally, Section VI concludes with an overview of the requirements and the functional benefits of their eventual realization.

II. STATE OF THE ART - CELLULAR PUSH AND AD PULL

A. Localization for AD

1) Localization Function Goals: A localization function is responsible for providing the decision-making and actuation functions with the road geometry together with the position, orientation and movement of the vehicle inside that road geometry. This is closely related to the perception function that is responsible for identification and classification of static and dynamic objects immediately around the vehicle. The extent to which these two functionalities are separated in hardware and software is implementation dependent.

Simple driver support features such as lane departure warnings require estimation of *lateral* (cross-road) parameters like lane position. Higher-level AD requires *longitudinal* estimates (along road) and *global* estimates for lane selection and route-level navigation. Even co-operative maneuvering based on information sharing among vehicles is best understood in the context of both lane geometry and static infrastructure; traversing intersections or performing merging is done based on the rules and geometry of the road.

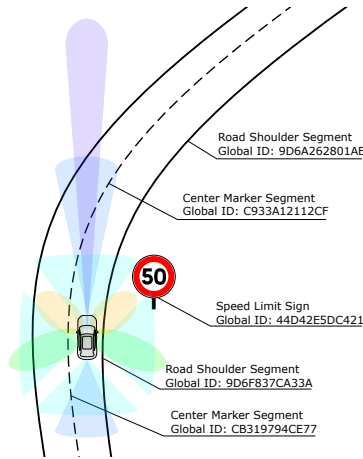Fig. 1. High-Definition map, which includes polynomial descriptions of dividing lines and road edges. Signage is also included, as well as semantic information describing road type (Rural Road) and Speed Limit. The perception sensor suite provides a 360-degree understanding of the immediate vicinity and GNSS provides absolute location to narrow the search space and to help identify map irregularities.

The understanding of the road comes from a geospatial database of map data. In the years since the Defense Advanced Research Projects Agency (DARPA) AD Grand Challenges, so-called "High-Definition" (HD) maps have grown to include more types of information, with competing offerings in development from a number of map suppliers and functional architectures for crowd-sourcing [7]. Figure 1 shows an example of an HD map segment.
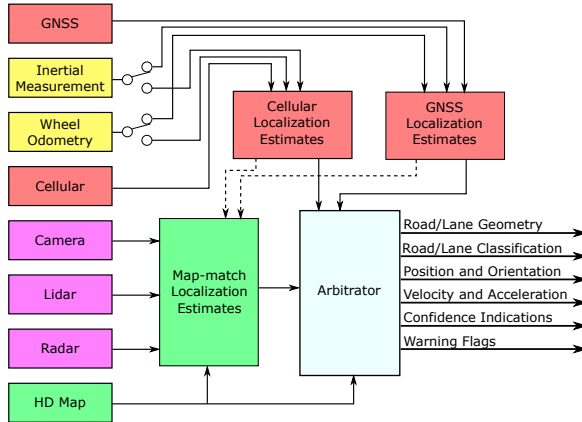
Fig. 2. Possible implementation of an AD localization architecture including cellular localization. Alternative sensor fusion paradigms can be implemented at every stage, including feedback loops for deeper sensor coupling. Maximum separation of inputs is shown to prevent dependent failures.

Sensors including lidar, radar and cameras match observations with map data in a two-step process of feature extraction and data association [8]. Absolute localization serves to narrow the search space for the initial search, bound probabilities of association and detect anomalies in the map database. An AD localization architecture, with a proposed integration of cellular localization, is shown in Figure 2. Absolute localization is supplemented through proprioception, and the fusion of these sensors produces global position and orientation estimates and seeds a map-matching algorithm. An arbitrator block looks for consistency between the sets of estimates and forwards the expected road geometry and confidence estimations for decision-making and actuation, serving in part as a safety mechanism.

There are at least two important lessons to draw from this architecture. First, absolute positioning is solely responsible for long-term unbiased estimates of position, even if observations are noisy or low-rate [9]. This is complementary to high-rate sensors sensors such as Inertial Measurement Units (IMUs), which can provide ≥ 100 Hz observations, or odometry. This means that the traditional metric of latency is not highly consequential for an absolute positioning sensor in a fused system.

Second, the centrality of GNSS shows why it can be a bottleneck for localization functionality. In anticipation of this need, investment in GNSS for mass-market appli-

cations has improved performance tremendously in recent years [10]. Among the chief improvements enabling mass-market use are new GNSS constellations coming online, updates to the broadcast satellite signals themselves, and production of inexpensive dual-frequency, multi-constellation receivers and State State Representation (SSR) correction services including regional atmospheric models. However, even with these improvements, fundamental limitations of satellite navigation justify investment in alternative technologies.

2) Safety-Critical Localization: For safety-critical systems, error distribution tails are of paramount concern because infrequent extreme errors, if multiplied by the number of hours of operation, can result in significant risk exposure in aggregate. Failures are inevitable and they need to be addressed systematically over the complete lifetime of the vehicle.

To provide an example outside the localization domain, traction battery overheating in an electric vehicle can lead to chemical fires. There are many plausible scenarios that could lead to overheating after the vehicle leaves the factory. The cooling system might incur a leak stemming from mechanical damage or a broken coolant pump. An incorrect control unit software flash or software bug might impact cooling system control, or cause an incorrect assessment of battery aging effects. None of these failures are effectively modeled as an extrapolation of nominal operation because, as with most practical engineering problems, tail errors are decidedly non-Gaussian even if such approximations may be of utility for normal operation. Detection, mitigation and recovery mechanisms are necessary to prevent rare failures leading to injury or death. A battery module temperature sensor (redundant sensors in practice) can help flag a module before it overheats. Disconnecting the overheating module from the rest of the battery pack allows for fail-safe operation. The goal in the end is to achieve *integrity*, real-time assessment of when a system is safe for use, and base control decisions on the most trustworthy of redundant systems.

Accomplishing integrity at an AD level requires structured ways of thinking about safety, as prescribed through multiple industry standards including ISO-26262 and ISO/PAS-21448 [11]. Before looking at the sensor level, Hazard Assessment and Risk Analysis (HARA) entails comprehensively listing potentially dangerous outcomes at a vehicle level, then assessing the risk of each in terms of severity, likelihood and controllability. Functional safety goals are developed from the HARA results, and subsequently safety requirements are generated which can be met with hardware and software elements.

A complete integrity solution in the localization domain entails generating real-time estimates of localization parameter error overbound and assigning *quantified* risk of violation of the overbounds that can help meet functional safety goals. In the parlance of the aviation world in which these concepts have been pioneered for localization estimate overbounding, the error overbound is referred to as a *Protection Level* and the quantified risk of violation is the *Integrity Risk*. Overbounding failures are called *Integrity Failures*, but errors are of course not observable in real-time.

While it does not necessarily need to be formulated this way, the Protection Level is typically compared to an application-specific error *Alert Limit*, a threshold that can lead to
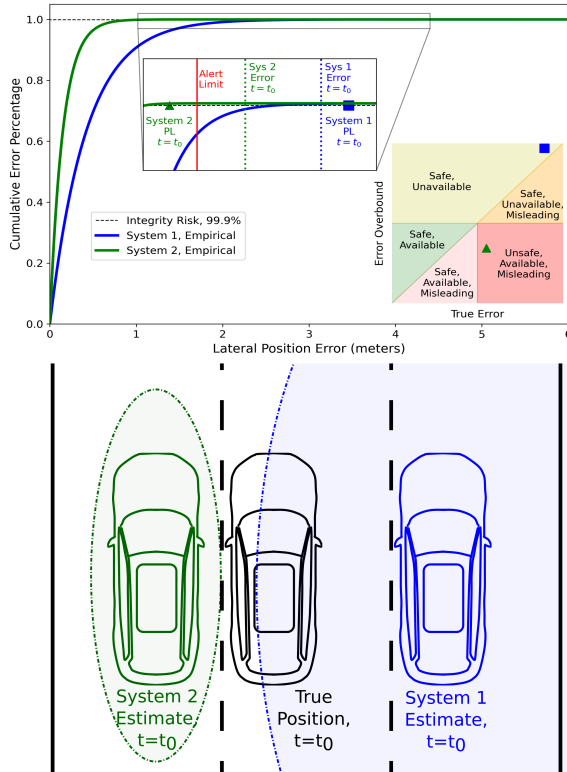
Fig. 3. A single localization epoch including instantaneous error and protection levels for two systems at time t_0. (Left) A backdrop of aggregate system performance shows that System 2 has better *average accuracy* than System 1. The inset graph shows a given navigation epoch t_0, where System 2 has smaller position error, but incorrectly underestimates the error overbound, leading to an integrity failure. Error distributions for localization can also include orientation or velocity estimation errors. Readers are referred to [6], [12] for longer discussions of the Stanford Diagram. (Right) Illustration of scenario. Note that the actual lane positions are incidental; the erroneous error bound determination below the Alert Limit would be considered an Integrity Failure regardless of the on-road position.

identifiable dangerous operation such as incorrect determination of road, lane or compass direction. This narrows the development and validation scope by excluding too-large or too-small failures. An overbound of 10 cm when the true error is 11 cm is not likely to be dangerous, nor is an overbound of 110 m when the true error is 111 m because the data will not be used downstream at this magnitude of uncertainty. An Alert Limit defines whether the system is *available* and suitable for use by the application, just as a temperature

threshold may lead to the exclusion of a battery module and force the combined system to rely on the remaining modules.

Figure 3 illustrates the idea of localization integrity for lateral position estimates by showing two localization systems operating simultaneously for a single time epoch, with an integrity failure at this epoch for one of the systems. System 1 (blue) is unavailable; the lateral position overbound is too large to perform lane determination. This is safe operation, but *unavailable* for lane determination. System 2 (green) is *available*; the overbound indicates it is suitable for lane determination, but from the right part of the figure we can see that judgment was an overestimation of confidence (*Misleading Information*); the true position is outside the Protection Level, in this case incorrect lane determination. GNSS error overbounds have proven to be frequently unavailable and even unsafe in urban areas [12], which has prompted significant interest in cellular localization.

B. Technology Push of Cellular Localization, in 3 Categories

Wireless localization, and cellular localization specifically, has a decades-long history. Readers are referred to [13] for an overview of fundamental wireless positioning techniques as well as a survey-of-surveys on wireless localization from 1977-2017. A number of new technologies spanning in maturity from recent commercial deployment to algorithms showing promise in simulations have been developed in recent years, which we generalize into three broad categories.

1) Machine Learning: Interest in statistical methods for wireless localization has increased since the year 2010 [14]. Supervised methods are most common. Location in space is used as the label and a representation of the wireless channel, a channel fingerprint, as the data.

Feature engineering holds promise in finding channel representations that are well-suited for scalability and transferability. Additionally, cellular signals are just one possible input; other types of signals such as Wi-Fi can be integrated into the same estimation framework for improved performance.

2) Triangulation and Multilateration: New measurements, including 3GPP Release 16's multi-cell round trip time (multi-RTT), downlink angle of departure (DL-AoD) and uplink angle of arrival (UL-AoA), were introduced to serve a multitude of envisioned future use cases such as factory automation and vehicle-to-everything communication [3]. Enhanced bandwidth (up to 400 MHz with 120 kHz carrier spacing) results in time resolution capabilities superior to those of previous generations for Positioning Reference Signals (PRS).

Opportunistic position estimation through observation of cellular pseudoranges (GNSS-like) has been demonstrated in academic literature for cellular transmitters, and error overbounding has even been applied (see, e.g., [5] and references therein). However, direct application of these methods has several limitations, which are discussed further

in Section V. Treating angles and delays of arrival as representative of actual transmitter-receiver geometry is sensitive to the "soft-onset" problem [14], when the direct path is much weaker than multipath components or not estimable. In the worst case, this can lead to hazardous operation when the receiver mistakenly considers multipath to be the direct path. Classic error overbounding approaches based on residuals testing such as [5] struggle in urban areas because of the strong correlation of errors [12]. Other mitigation strategies include statistical tests for non line-of-sight identification [14].

3) Simultaneous Location and Mapping Based on Multipath Component Reflections: Multipath components can be decomposed in both space and time, with larger antenna aperture and larger signal bandwidth, respectively. Work in propagation modeling led to the insight that such reflections can be used as physical references in a Simultaneous Location and Mapping (SLAM) problem formulation as "virtual transmitters". This method has attracted significant attention in the academic literature (see, e.g., [15]). It is therefore possible to use multipath information advantageously rather than as a problem to be mitigated. This holds great promise for solving positive ranging biasing, but introduces new challenges, as we discuss in our requirements.

III. Requirement Area 1: Reference Frames
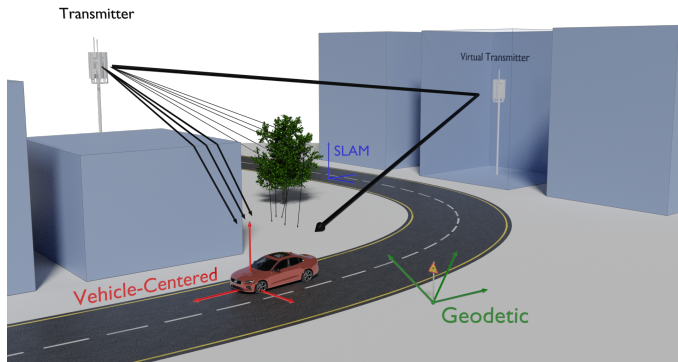
Fig. 4. A vehicle, transmitter, virtual transmitters and other objects in a map database with different wave propagation mechanisms including reflection, diffraction and scattering. Expressed equivalently in three Reference Frames: Geodetic, Vehicle-Centered, and SLAM. Note that items in the map database such as signs and road marker indications are surveyed in Geodetic coordinates. Map matching entails feature extraction from observations in a Vehicle Frame and data association of map data stored in the Geodetic Frame, including road geometry. Radio SLAM entails estimation of transmitters and virtual transmitters together with the vehicle itself in a SLAM Frame which has its origin as an arbitrary starting epoch of the Vehicle Frame.

Geospatial data (the data stored in a vehicle's map database) is expressed with reference systems, reference frames and geodetic datums. Common reference systems for map data include the International Terrestrial Reference System (ITRS) and the World Geodetic System (WGS). Representative and well-defined datums are critical for precision applications (see, e.g., Section II.F in [10]).

Different reference frames for the same vehicle-transmitter (and virtual transmitter) geometry are illustrated in Figure 4, which also includes map data in the form of road geometry and signage. Estimates of Figure 2 are expressed in geodetic coordinates, Earth-centered, Earth-fixed Cartesian coordinates in this case. Map-matching entails feature extraction in the vehicle-centered coordinate system (sometimes expressed as *body frame* [9]), and data association with the global identifier, such as in Figure 1. Wireless communication systems are powerful in their ability to easily multiplex globally unique identifiers making the data association problem simple; unique transmitter IDs can be embedded with observations, realized in GNSS as the pairing of the navigation message with pseudo-random noise sequences.

The localization function is responsible for providing road information together with the state estimates, and therefore the estimates should be in the same frame as the map data, and our first requirement enables us to perform absolute localization in the absence of GNSS. **Requirement 1: Localization estimates shall be generated in a well-defined geodetic reference frame.**

The three categories of cellular localization described in Section II have different relationships with the reference frames. Machine learning methods can have labels assigned in any coordinate system, but nominally it is logical to use a system directly transferable to the geodetic system realization. In this case, the performance bottleneck for anchoring in geodetic coordinates is the labeling noise for the surveyor collecting fingerprints. Multilateration and triangulation have the inverse limitation: if transmitter antenna array phase center is not accurately surveyed in a global reference frame (as well as orientation, for angular methods), subsequent vehicular estimates of position will be biased proportionally with the offset. Fortunately, the data association problem is trivial if transmitters have unique IDs.

Multipath SLAM has the most complicated relationship with geodetic coordinates. In the classic formulation of a SLAM problem, an agent is placed in an unknown environment and aims to localize itself in relation to landmarks corresponding to sensor observations, seeking to "close the loop". This is an inherently different problem than working from a map database known *a priori*. A vehicle coordinate system at a certain time point is initialized to generate a new coordinate system; a few car lengths of driven distance previously on the road, in the case of Figure 4.

From the perspective of the localization system of Figure 2, this is a similar function to inertial measurement and odometry, simultaneous with landmarks that are not consequential in the manner that other references like lane geometry are. To increase performance for

relative localization estimation, investment in the other sensors is feasible, but even a million-dollar strategic grade IMU cannot observe global position.

Anchoring in global coordinates for SLAM can be done at the receiver, in the propagation medium or the transmitter. Presuming knowledge of the global receiver position and orientation upon initialization is merely augmented proprioception. Assuming knowledge of relevant scattering objects [15] to anchor through the propagation medium would entail a dramatic expansion of the map database beyond the scope of road-level data. Anchoring through transmitters may hold more promise, even if virtual anchors lack a unique global identifier with a bijective mapping to their sender ID; they appear as time-delayed copies of the original transmitter. Additional parameterization of virtual transmitters, including angles of departure and relative time delay to the original transmitter, may be a viable strategy for global identification.

IV. Requirement Area 2: Tail risks

Hardware and software failures can lead to hazards at a vehicle level, as the example of battery overheating case shows. Certain failure modes (voltage supply, for example) are common across electronic systems, but identification of new fault modes unique to cellular localization will be necessary.

GNSS localization integrity in aviation provides a procedural template for how to perform systematic analysis of risks. Certain GNSS fault modes can be disregarded; rapid changes in ionospheric electron content are not a likely error source for a cellular system, for example. Other faults will be introduced that might be especially difficult to quantify using cellular base stations that do not provide the same integrity guarantees as navigational satellites, though future cellular systems may evolve in that direction. Receiver hardware will also be subjected to a new level of complexity. Something as trivial as oscillators or amplifiers failing to operate within their specification, for example, may lead to potentially dangerous operation.

Overdetermined systems permit for integrity checking, as decades of development in Receiver Autonomous Integrity Monitoring (RAIM) for GNSS receivers have shown [12]. Multiple-Input Multiple-Output (MIMO) systems offer new possibilities for monitoring, including diversified channel estimation, consistency checks across estimated parameters (angles and ranges), consistency across multiple frequencies, or consistency across systems (inertial and cellular, camera and cellular).

A multi-disciplinary approach is necessary to identify faults at a sensor level, as the weakest link in the chain will dominate the tail errors for the final localization estimates, expressed mathematically as a convolution of probability density functions. Both the faults themselves and areas for monitoring and mitigation flow naturally from the fault tree. This work is fundamental for development of a safety-critical system [11], and we should

therefore include this procedural matter as an explicit requirement: **Requirement 2: Fault Tree Analysis shall be used to identify and monitor faults and mitigate risks.**

Ultimately, the goal in localization integrity is to establish quantified error overbounds by determining the frequency at which faults are expected to occur. Fault monitors can be effective at reducing the frequency at which undetected faults are encountered and can reduce the risk of subsequent vehicle-level hazards by orders of magnitude. After decades of research in aviation, the vertical position error overbound was reduced to 10 meters with 10^{-7} failures/hr integrity risk [8], but a position overbound of 10 meters may not be a sufficiently powerful tool for an automotive use case. This leads to perhaps the most difficult requirement, but the most useful for the localization function. **Requirement 3: Localization estimates shall provide defined instantaneous upper error bounds.**

With this end goal, it is useful to start considering the placement of cellular localization in the architecture of Figure 2. Designing for accuracy and integrity are often in direct opposition, as choices that might lead to better accuracy, such as tighter filter tuning, may also lead to infrequent extreme errors. This is why the proposed architecture in Figure 2 does not use tighter feedback loops or permit downstream sharing of proprioception sensor data, to prevent dependent failures among systems (specifically common cause failures, in ISO 26262 taxonomy).

It is important to keep in mind that only some hazards in an automotive environment are a predictable function of absolute location and orientation, as collision risks are largely derived from dynamic objects. Drifting outside of a lane (see, e.g., [6]) can be hazardous, but because map data is by definition historical, AD vehicles are vulnerable to dynamic environmental changes to the semantic labels or physical geometry such as construction [7], or (less frequently) earthquakes. An important consequence of this is that to a much larger extent than aviation, absolute location certainty can only contribute to, but not satisfy, safety goals consequential to the localization system. Redundant systems are necessary and perception and localization are necessarily interwoven. If lanes are not visible, e.g. in snowy conditions or road construction, then driving within historically-defined lane boundaries is hazardous.

An illustrative example of a single AD hazard from a HARA analysis is shown in Figure 5. The vehicle-level hazard propagates down to functional safety requirements on a sensor level. The benefit of cellular localization for AD is the blue AND gate providing diversified redundancy. Satellite and cellular localization can work in a redundant fashion when both are available, but either can protect against hazards on an individual basis, and with cellular localization, absolute localization is possible in environments where GNSS is completely unavailable.
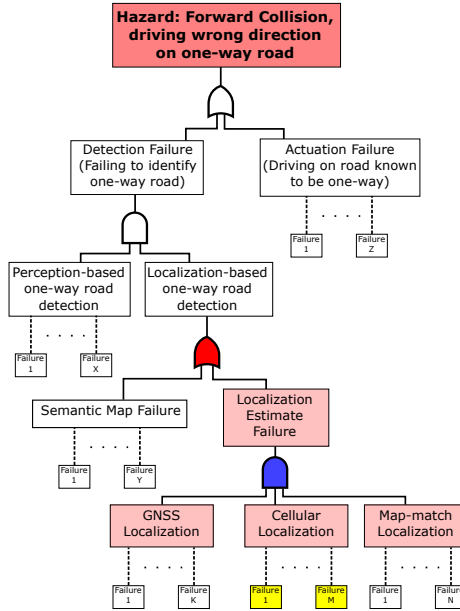
Fig. 5. Part of a fault tree for a functional safety concept. AND gates allow for a multiplication of risk probabilities (reduction in risk), in the absence of dependent faults. OR gates result in a summation of risk. Note that the OR gate between absolute localization and map data means that the map is a bottleneck for any safety goal met with the help of absolute localization. Cellular localization Faults (yellow) are unexplored in literature. GNSS or Cellular blocks can include fusion with proprioception.

V. REQUIREMENT AREA 3: WAVE PROPAGATION

Far-field propagation is typically modeled as a sum of plane waves and, for some more advanced propagation models, an additional "diffuse multipath component" term to capture components that are too strong collectively to ignore when estimating plane waves but not resembling a plane wave sufficiently (diffuse waves in an urban canyon, for example) to estimate individually [15]. Single-bounce reflections from the buildings shown in Figure 4 might result in estimable plane waves, and diffraction over rooftops or scattering might contribute to diffuse multipath, but the distinction is dependent on physical geometry, measurement aperture and signal processing capabilities.

A physical model well representative of the physical reality of wave propagation allows for more precise localization estimates. Multilateration methods, whether based on clock

synchronization or Time-of-Flight (RTTOF), typically presume that the first (and usually strongest) arriving wave is a direct path between the transmitter and receiver. They are therefore subject to ranging biasing because of multipath and blocked line-of-sight. Even if larger bandwidths offer improved time *resolution*, the very properties that have driven the MIMO revolution in wireless communication pose challenges for multilateration. In MIMO communication, the number of linearly independent paths from transmit array to receive array (which can increase the rank of the channel matrix) allows for linear scaling of data rate. Multipath is considered beneficial because it serves both to enable greater physical coverage and to achieve higher data transmission rates. This is a strong contrast to GNSS, in which signals and hardware are designed to push reality to fit the multilateration model better, with polarized antennas and signal design that explicitly aims to physically suppress multipath, leaving the first and strongest signal if it is present. Scientific measurements in geodesy even employ elaborate choke ring structures for multipath suppression.

The rich scattering environments in which GNSS is subject to range biasing are correlated with those in which cellular transmitters will also experience blocked line-of-sight signals and heavy multipath, such as urban canyons or parking garages. Mitigation strategies suggested for GNSS have included improved antenna polarization, map consistency checks or other cross sensor utilization (see [12] Table II). MIMO systems should be able to move from mitigation to utilization. With this in mind, we can formulate our next requirement to ensure performance works well when it matters most. **Requirement 4: The channel estimation shall resolve multipath components.**

One promising opportunity afforded by MIMO systems is the ability to both steer and estimate angles of departures and angles of arrival. This has potential benefits for integrity, as discussed in Section IV, but it also affords opportunities for velocity and orientation estimation.

Multi-antenna GNSS receivers (common in construction or agriculture, but not on passenger vehicles due to cost and packaging) can provide the ability to perform static orientation estimation, but cellular systems can estimate angles at both sender and receiver (and are not subject to International Traffic in Arms Regulation in the United States, as some multi-antenna GNSS receivers are). Three-dimensional receiver orientation estimation is possible if the physical geometry of the array permits angular resolution in both azimuth and elevation, so yaw, pitch and roll angles can be estimated without inertial measurement of gravity or magnetic measurement of compass direction. For a vehicle that is highly constrained in both pitch and roll, heading estimation is typically a primary constraining factor for localization system performance.

Similarly, the ability to perform Doppler estimation allows for an independent estimation of velocity. Dynamic objects in the environment such as other vehicles result in multipath Doppler contributions that are additive to ego-vehicle velocity vector, but reflections from a static transmitter off of static objects in the environment will have Doppler contributions derived only from ego-vehicle velocity and frequency mismatch. With the full dynamism

of the sensor in view, we can formulate our final requirement. **Requirement 5: Position, heading and velocity estimates shall be generated.**

VI. CONCLUSIONS

The five requirements introduced for safety-critical cellular localization for AD, together with a summary of the functional benefits and research directions for realization, are listed in Table I. We contend that a cellular localization sensor that can provide position, heading and velocity estimates with error overbounds in an external reference frame is a powerful tool for Autonomous Drive systems.

Safety-critical applications provide a unique set of challenges, as a long history of integrity systems for satellite navigation in aviation has shown. The natural affinity between advanced communication technologies and localization should make such solutions feasible to implement on a wide scale.

TABLE I
AD FUNCTION REQUIREMENTS, RESEARCH DIRECTIONS AND BENEFITS

Requirement	Function Benefits	Possible Research Directions
Localization estimates shall be generated in a well-defined geodetic reference frame	• Geographical expansion of AD Operational Design Domain to GNSS-denied areas • Relaxation of GNSS integrity requirements when cellular localization is available • Relaxation of bias drift specification for Inertial Measurement Units • Absolute localization reference sources that move seismically with other items in the map database	• Surveying and parameterization of transmitters and virtual transmitters in a global frame • Cross-sensor perception to correlate cellular localization references with observations from other sensors • Cellular fusion with proprioception
Fault Tree Analysis shall be used to identify and monitor faults and mitigate risks	• Procedural compliance with functional safety	• Identification of localization faults related to antennas, radio electronics and channels • Integrity monitoring techniques for different observation models
Localization estimates shall provide defined instantaneous upper error bounds	• Quantitative contribution to the Functional Safety Concept • Reduced search space and higher confidence for map-matching	• Novel statistical overbounding approaches • Scalable data collection hardware and software platforms for wireless systems
The channel estimation shall resolve multipath components	• Absolute localization in urban canyons, parking garages, indoors • Decorrelation of GNSS and cellular localization failures	• Propagation models providing more granular resolution of diffuse components • Computationally efficient and redundant channel estimation
Position, heading and velocity estimates shall be generated	• Stationary orientation estimates independent of inertial measurement • Odometry-independent source of velocity estimates • GNSS spoofing detection	• Ego-velocity estimation from Doppler observation • Dynamic receive phase calibration and antenna pattern characterization

ACKNOWLEDGMENT

REFERENCES

[1] E. Yurtsever, J. Lambert, A. Carballo, and K. Takeda, "A Survey of Autonomous Driving: Common Practices and Emerging Technologies," *IEEE Access*, vol. 8, pp. 58 443–58 469, 2020.

[2] Z. Kassas, J. Khalife, K. Shamaei, and J. Morales, "I Hear, Therefore I Know Where I Am: Compensating for GNSS Limitations with Cellular Signals," *IEEE Signal Processing Magazine*, vol. 34, no. 5, pp. 111–124, Sep. 2017.

[3] S. Dwivedi, R. Shreevastav, F. Munier, J. Nygren, I. Siomina, Y. Lyazidi, D. Shrestha, G. Lindmark, P. Ernström, E. Stare *et al.*, "Positioning in 5G Networks," *IEEE Communications Magazine*, vol. 59, no. 11, pp. 38–44, 2021.

[4] S. Bartoletti *et al.*, "Positioning and Sensing for Vehicular Safety Applications in 5G and Beyond," *IEEE Communications Magazine*, vol. 59, no. 11, pp. 15–21, 2021.

[5] M. Maaref and Z. M. Kassas, "Autonomous Integrity Monitoring for Vehicular Navigation With Cellular Signals of Opportunity and an IMU," *IEEE Transactions on Intelligent Transportation Systems*, 2021.

[6] T. G. Reid, S. E. Houts, R. Cammarata, G. Mills, S. Agarwal, A. Vora, and G. Pandey, "Localization Requirements for Autonomous Vehicles," *SAE International Journal of Connected and Automated Vehicles*, vol. 2, no. 12-02-03-0012, pp. 173–190, 2019.

[7] K. Jo, C. Kim, and M. Sunwoo, "Simultaneous Localization and Map Change Update for the High Definition Map-Based Autonomous Driving Car," *Sensors*, vol. 18, no. 9, p. 3145, 2018.

[8] M. Joerger and M. Spenko, "Towards Navigation Safety for Autonomous Cars," *Inside GNSS*, 2017.

[9] P. Groves, *Principles of GNSS, Inertial, and Multisensor Integrated Navigation Systems, Second Edition*. Artech House, March 2013.

[10] N. Joubert, T. G. Reid, and F. Noble, "Developments in Modern GNSS and its Impact On Autonomous Vehicle Architectures," in *2020 IEEE Intelligent Vehicles Symposium (IV)*. IEEE, 2020, pp. 2029–2036.

[11] O. Kirovskii and V. Gorelov, "Driver assistance systems: analysis, tests and the safety case. ISO 26262 and ISO PAS 21448," in *IOP Conference Series: Materials Science and Engineering*, vol. 534, no. 1. IOP Publishing, 2019, p. 012019.

[12] N. Zhu, J. Marais, D. Bétaille, and M. Berbineau, "GNSS Position Integrity in Urban Environments: A Review of Literature," *IEEE Transactions on Intelligent Transportation Systems*, vol. 19, no. 9, pp. 2762–2778, 2018.

[13] J. A. del Peral-Rosado, R. Raulefs, J. A. López-Salcedo, and G. Seco-Granados, "Survey of cellular mobile radio localization methods: From 1G to 5G," *IEEE Communications Surveys & Tutorials*, vol. 20, no. 2, pp. 1124–1148, 2017.

[14] D. Burghal, A. T. Ravi, V. Rao, A. A. Alghafis, and A. F. Molisch, "A Comprehensive Survey of Machine Learning Based Localization with Wireless Signals," 2020.

[15] K. Witrisal, P. Meissner, E. Leitinger, Y. Shen, C. Gustafson, F. Tufvesson, K. Haneda, D. Dardari, A. F. Molisch, A. Conti *et al.*, "High-Accuracy Localization for Assisted Living: 5G systems will turn multipath channels from foe to friend," *IEEE Signal Processing Magazine*, vol. 33, no. 2, pp. 59–70, 2016.

Paper II

Paper II

Urban Navigation with LTE using a Large Antenna Array and Machine Learning

Russ Whiton[*][†], Junshi Chen[*][‡], Tobias Johansson[†], and Fredrik Tufvesson[*]
[*]Department of Electrical and Information Technology, Lund University, Lund, Sweden
Email:{russell.whiton, junshi.chen, fredrik.tufvesson}@eit.lth.se
[‡]Terranet AB, Lund, Sweden
[†]Volvo Car Corporation, SE-405 31 Gothenburg, Sweden
Email:tobias.johansson@volvocars.com

Abstract

Channel fingerprinting entails associating a point in space with measured properties of a received wireless signal. If the propagation environment for that point in space remains reasonably static with time, then a receiver with no knowledge of its own position experiencing a similar channel in the future might reasonably infer proximity to the original surveyed point. In this article, measurements of downlink LTE Common Reference Symbols from one sector of an eNodeB are used to generate channel fingerprints for a passenger vehicle driving through a dense urban environment without line-of-sight to the transmitter. Channel estimates in the global azimuthal-delay domain are used to create a navigation solution with meter-level accuracy around a city block.

I. INTRODUCTION

Wireless signals are used for positioning on a massive scale, with end-users for such systems numbering in the billions. The expansion of Global Navigational Satellite System (GNSS) constellations and commodification of receivers means that any modern mass-market electronic consumer device including phones, watches or vehicles can tap into a network of high-accuracy positioning reference signals wherever the receiver antenna has an un-attenuated view of the sky [1]. The availability restriction of clean sky views, paired with other limitations like susceptibility to spoofing and jamming, create a desire for alternative wireless positioning solutions based on terrestrial transmitters. 4G Long-Term Evolution (LTE) commercial base stations provide a rich basis for opportunistic positioning [2].

Localization methods aside from trilateration (used in GNSS) are triangulation, proximity, and fingerprint matching, all of which have attracted attention in both industry and academia. The focus of this paper is on fingerprint matching using statistical tools, in which we seek to find a mapping from the received wireless signal to a position in space

through domain knowledge about electromagnetic wave propagation and signal processing [3]. This offers advantages in that no knowledge of transmitter locations is required, it allows for capturing of channel behavior in complicated propagation environments that are tough to model parametrically, and position estimates are provided in a reference frame of the user's choice.

The simplest feature available to the user by most commercial wireless receivers is received signal strength, but the low dimensionality of this parameter precludes anything close to a bijective mapping in a large outdoor environment, and the combination of large- and small-scale fading weakens the correlation even further in heavy multipath environments where alternatives to GNSS are most desirable. To benefit from the full richness of the wireless channel information, it is desirable to use an observation model that includes the geometrical information embedded in multipath propagation [4]. Channel State Information (CSI) is a raw form of measurement data, a complex-value for each subcarrier of the LTE signal per antenna. With a sufficiently large data set and network architecture, end-to-end learning from this information should be able to extract the relevant features. However, feature engineering allows for more computationally tractable and memory-efficient network design, portability to different hardware and software platforms, intuition about what the network is "learning" and the ability to augment the network with external information to attain better results with limited training data.

The problem of channel representation for outdoor fingerprinting with a single sector of a commercial base station is an interesting benchmark. In [5], 11 channel representations were investigated and 75-meter median error was achieved. In [6], 19-meter median accuracy was achieved with CSI vectors. [7] considers the problem of tracking with an angular-delay representation of the channel. Our research builds on these ideas, and contributions are as follows:

- We apply and extend [7], which suggests using an azimuthal-delay representation of the received signal as input to a Convolutional Neural Network (CNN). We demonstrate that the choice of a *global* azimuthal-delay domain allows for effective fingerprinting not only with CNNs, but through a non-parametric k-Nearest Neighbors (kNN) estimator.
- Downlink channel measurements are visualized in a world reference frame to motivate the choice of a global azimuth-delay domain representation.
- Results for the two estimators (CNN and kNN) are shown for both raw data and with a Kalman filter applied.

We demonstrate that without line-of-sight, a meter-level navigation solution can be generated with signals of limited bandwidth and no input regarding transmitter location. These results are predicated on having known User Equipment (UE) orientation and clock synchronization.

II. MEASUREMENT SETUP

Cell-Specific Reference Symbols (CRS) in LTE are signals that are known to the UE in advance as a function of physical cell identity, with 504 possible sequences distributed across resource blocks to facilitate down-link channel estimation [8]. What makes CRS appealing for channel estimation also makes them appealing for opportunistic localization, in that they are open, frequently transmitted, known to the UE *a priori* and of higher bandwidth than the Primary and Secondary Synchronization Sequences.
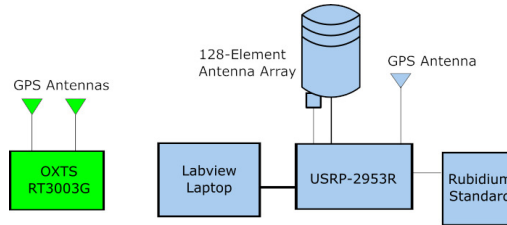
Fig. 1.   Block diagram of key measurement system components.

A system was built for receiving and logging CRS symbols from commercial LTE base stations operating at 2.6 GHz, based on a National Instruments USRP-2953R Software-Defined Radio. Sampling of CRS symbols was done at a rate of 30.72 MHz, or approximately 32.56 ns per sample and logged onto a laptop hard drive. The USRP-2953R also controlled a 128-element switched Stacked Uniform Circular Array consisting of 4 vertically-stacked rings of 16 dual-polarized antenna elements each, which was mounted on the roof of a passenger vehicle. A rubidium standard, disciplined by GPS, was used as a frequency reference and a GPS receiver provided an absolute time reference for correlation with localization ground truth data.

A high-end localization reference system [9] with a survey-grade GNSS receiver and high-grade Inertial Measurement Unit (IMU) was used to provide estimates of vehicle and antenna position and orientation, through Post-Processed Real-Time Kinematics. A block diagram of key system components is shown in Figure 1, and a photo of the test vehicle with all components mounted is shown in Figure 2.

Four laps of around 400 meters each were driven around one block in central Lund, Sweden for an aggregate distance of 1628 meters over 28 minutes and 17 seconds at an average speed of 0.96 m/s (driving speed was limited to 1.5 m/s to avoid exceeding the channel coherence time[1]). The driving area spanned 103 meters East-West and 108 meters North-South. Two laps were driven in each direction, as depicted in Figure 3.

---

[1]This is a limitation of the measurement system, which switches at the rate of CRS symbol transmission. Sampling antennas in parallel would negate limitations in speed.

Fig. 2. Photo of array antenna mounted on Volvo V90 Passenger Vehicle.

Fig. 3. Visualization of Ground Truth position for one of four laps driven in Lund, Sweden (55.71°N, 13.19°E). The approximate position of the Base Station (eNodeB) is displayed as well. Image created with Google Earth.

The surrounding buildings consist of four- to five-story residential or mixed-use buildings. The receive antenna array never had line-of-sight to the transmitting eNodeB, as the line-of-sight trajectory was always obstructed by multi-story buildings.

A sweep among all antenna elements (a channel snapshot) was completed every 75 LTE subframes (75 ms), and a total of 22,626 75-ms snapshots were generated over the drive trajectory.

III. Data Representation and Estimators

A. Channel and Position Representation

For every snapshot at time index i, a channel estimate in the UE frame, Y_i^{UE}, is associated with a localization vector x_i. Channel estimation is done using the Expectation-

Maximization-based RIMAX algorithm [10], and parameterized into a variable and discrete number L_i of multipath components, e.g., $Y_i^{UE} \triangleq [\tau_l, \alpha_l, \theta_l^{UE}, \phi_l^{UE}]$ where l spans from 1 to L_i. τ_l represents component delay[2], α_l represents component signal strength, and θ_l^{UE}, ϕ_l^{UE} represent component azimuth- and elevation-of-arrival in the UE frame, respectively. Doppler was not estimated, under the assumption that reflecting objects which contribute significant energy to the channel impulse response were static and that the ego-vehicle was moving slowly.

In [7], simulated channel data consisting of several multipath clusters based on a COST 2100 channel model realization are processed into the azimuth-delay domain, motivated as a sparse channel representation that maps to position $x_i \in \mathbb{R}^{2 \times 1}$ in a manner described as approaching bijective for most practical propagation scenarios. For this to hold true for a static transmitter and a mobile UE unconstrained in both position and orientation, a more complete parameterization of x_i is necessary. A complete 6 degree-of-freedom representation is $x_i \in \mathbb{R}^{6 \times 1} = [e_i, n_i, u_i, \gamma_i, \lambda_i, \eta_i]^T$, including three-dimensional position e_i, n_i, u_i (East-North-Up Cartesian Frame) and three-dimensional orientation[3] $\gamma_i, \lambda_i, \eta_i$ (yaw, pitch, and roll [11]). We extend [7] through our use of external orientation information $\gamma_i, \lambda_i, \eta_i$ to rotate the angles-of-arrival of multipath components from the UE coordinate system $y_{l,i}^{UE}$ to express them in an East-North-Up coordinate system $y_{l,i}^{ENU}$, expressed in Cartesian form in Equation 1.

$$y_{l,i}^{ENU} = y_{l,i}^{UE} \begin{bmatrix} 1 & 0 & 0 \\ 0 & cos(\eta_i) & sin(\eta_i) \\ 0 & -sin(\eta_i) & cos(\eta_i) \end{bmatrix} \begin{bmatrix} cos(\lambda_i) & 0 & -sin(\lambda_i) \\ 0 & 1 & 0 \\ sin(\lambda_i) & 0 & cos(\lambda_i) \end{bmatrix} \begin{bmatrix} cos(\gamma_i) & sin(\gamma_i) & 0 \\ -sin(\gamma_i) & cos(\gamma_i) & 0 \\ 0 & 0 & 1 \end{bmatrix}$$
(1)

The components $y_{l,i}^{ENU}$ constitute the global angular representation of the channel, $Y_i^{ENU} \triangleq [\tau_l, \alpha_l, \theta_l^{ENU}, \phi_l^{ENU}]$. The footprints were discretized into a matrix of azimuthal-delay bins with M delay bins and N azimuthal bins, $\mathbf{H}_i \in \mathbb{R}^{M \times N}$ with signal power α_l contributing to the power for a given azimuthal-delay bin. Elevation values are not considered in the formulation of $\mathbf{H}_i$, but extension to three dimensions, e.g., [12] is possible. The *M* azimuthal bins can be interpreted as a discretization of the full span of compass

---

[2]Delay measurements (equivalently expressed in meters) were biased, but not time-varying based on a visual inspection of delay domain data over the full test drive. Built into this representation is effectively absolute clock synchronization between transmitter and receiver, a parameter which is typically estimated on a per-epoch basis for time-of-arrival systems built on low-cost crystal oscillators on the UE side. CNNs are effective if the shape of information features is invariant to the location in the input space, but absolute time synchronization provides a large amount of information about proximity to the base station, even if the mapping is highly non-linear for an urban canyon scenario. We leave the investigation of sensitivity to time synchronization for future work.

[3]Non-isotropic UE antenna pattern and variable propagation environment (vegetation or dynamic objects such as traffic) will also preclude a bijective representation. Effective channel footprinting entails finding representations of Y_i that are both sparse and robust to these types of effects.

directions. We ignore the altitude u_i component of the position because the route does not have variable elevation for the same East and North coordinates[4], leaving us with the same two-dimensional localization estimate $x_i \in \mathbb{R}^{2 \times 1} = [e_i, n_i]^T$ that now accounts for freedom in orientation. A desirable extension which we leave for future work is to add orientation (primarily heading) as an estimable parameter.

B. Data Aggregation

Training on individual snapshots provides both higher-frequency position estimates at run-time and a larger training data set, but averaging over a longer time interval allows for more energy to be aggregated in each estimate. Using discretized multipath components as the basis for populating the matrix $\mathbf{H}_i$ results in very few non-zero angle-delay bins for an individual snapshot if the number of components L_i is low, resulting in most subsequent estimator operations being multiplication of zeros. Therefore, energy contributions from snapshots are summed, 20 at a time, into snapshot groups (indexed hereafter with k) to produce position estimates every 1.5 seconds, e.g., $\mathbf{G}_k = \sum_{i=1+20(k-1)}^{20+20(k-1)} \mathbf{H}_i$.

In a multi-sensor navigation system, unbiased and low-rate estimates of absolute position are complementary to high-rate sensors such as IMUs or wheel odometry with unbounded long-term bias [13], so for this application it is reasonable to produce position estimates at a lower rate.

C. Estimators

1) Convolutional Neural Network Estimator: The CNN estimator consists of three Convolution-Activation-Pooling (CAP) layers, a flattening layer, a fully-connected layer and an output layer estimating position e_k, n_k for each snapshot group k. Relevant parameters of the CNN estimator are summarized in Table I.

Moderate changes to parameters including number of layers, filters, kernel size and learning rate did not significantly impact performance and are not included in this text. Network optimizing is left to future work.

2) k-Nearest Neighbors Estimator: A kNN estimator was used, with the intention of establishing a performance benchmark for the CNN using the same underlying input data. Unlike the CNN estimator, there are no learned parameters. The two-dimensional azimuthal-delay representation from the CNN is flattened, and the same angular-frequency bins are used without any convolution operation that considers adjacent values within Y_i^{UE}. The estimator is described in Table II.

---

[4]Some driving scenarios could benefit from altitude estimates, such as parking garages, freeway over- and under-passes, stacked highways, etc.

TABLE I
CNN ESTIMATOR DESCRIPTION

Parameter	Value
Input Layer Dimensions	69 x 71
Delay Range (meters / ns)	0 to 700 / 0 to 2333
Azimuthal Range (degrees)	-180 to 180
Delay Resolution (meters / ns)	10.1 / 33.8
Azimuthal Resolution (degrees)	5.1
CAP Layer 1 Filters / Weights	16 / 272
CAP Layer 2 Filters / Weights	32 / 8224
CAP Layer 3 Filters / Weights	64 / 32832
Dense Layer 1 Weights	524416
Kernel Size (All conv. layers)	3
Pool Size (All pooling layers)	2x2
Output Layer Shape	2

TABLE II
KNN ESTIMATOR DESCRIPTION

Parameter	Value
Input Dimensions	4899 x 1
Delay Range (meters / ns)	0 to 700 / 0 to 2333
Azimuthal Range (degrees)	-180 to 180
Delay Resolution (meters / ns)	10.1 / 33.8
Azimuthal Resolution (degrees)	5.1
Neighbors n used	5
Neighbor weights	Uniform

D. Kalman Filtering

For each estimator, a Kalman Filter employing a constant velocity model is used to filter the series of independently predicted points from the kNN and CNN estimators. The state vector includes two-dimensional positions and velocities, e.g., $x_k = [e_k, n_k, e'_k, n'_k]^T$. The filter is initialized at $x_{k=1}$ with position estimates from the estimator predictions after the first snapshot group, velocities of zero (e.g., $\hat{e}'_{k=1} = \hat{n}'_{k=1} = 0$) and a covariance matrix $P_{k=1} = diag([9, 9, 1, 1])$.

IV. RESULTS

A. Channel Footprints

Azimuthal-delay domain spectra for four geographically proximate snapshot groups (spread within 2 meters), one on each lap, are shown in Figure 4. A visual inspection

of these channel footprints shows visibly similar clusters, even with position offsets on the order of tens of wavelengths and heading differences of 180 degrees, and dynamic environmental changes such as size and location of other vehicles. This supports the choice of global azimuthal-delay representation of $\mathbf{H}_i$.
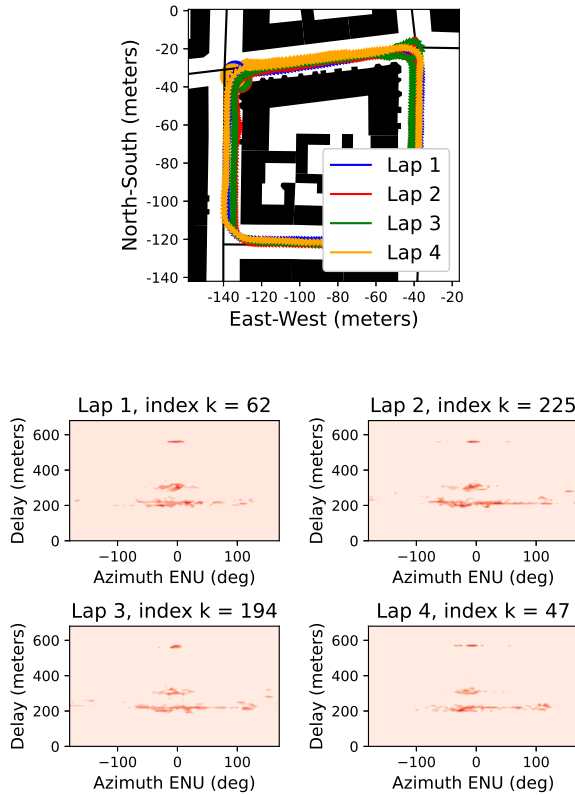
Fig. 4. Azimuthal (East-North) - Delay spectra for one snapshot group on each of four laps around Central Lund, Sweden. e_0, n_0 corresponds to 55.7107°N, 13.1898°E, and a Universal Transverse Mercator projection is applied to generate a two-dimensional representation of position. The points are taken from the Northwest corner of the route.

It is also clear that significant energy is contained in clusters that have path differences on the order of several hundred meters (several hundred nanoseconds), and that the channel estimation shows "smeared" angle-of-arrival estimates where clusters appear to occupy a broad range of azimuthal values.

B. Estimator Performance

Laps 1-3 were used as a training set in the case of the CNN and as the underlying search space in the case of the kNN estimator. Lap 4 was used for testing. The positioning performance for Lap 4 with each estimator is shown as a time series and error distribution function in Figure 5 and as a map in Figure 6. Performance metrics are listed in Table III. The kNN estimator is more prone to extreme errors, but still manages to produce a navigation solution that traces the trajectory of UE in a counter-clockwise manner around the block. Each estimator shows similar directional performance, with the exception of high East-West error for the kNN, possibly caused by a single point. This represents a performance improvement as compared with [5], [6], but different environmental conditions, survey areas and densities preclude such comparisons being considered comprehensive.
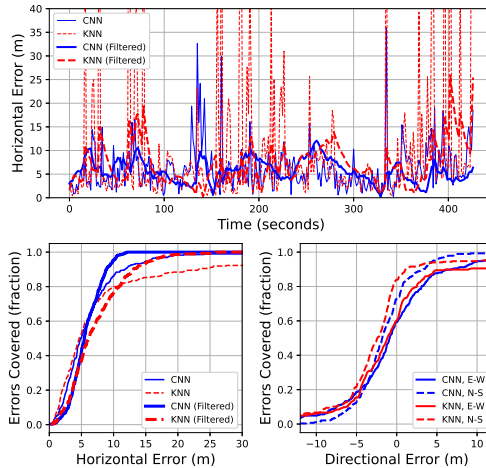
Fig. 5. Time series and cumulative distribution functions of absolute and directional position errors for Lap 4.

The CNN appears to be a superior estimator, likely owing to the ability to better integrate larger quantities of data in the individual estimates rather than discarding all but a few points, some of which may contain large errors.

V. CONCLUSIONS AND FURTHER WORK

The results show that with a single sector of a single eNodeB in non-line-of-sight conditions, meter-level estimations of absolute position can be generated based on limited
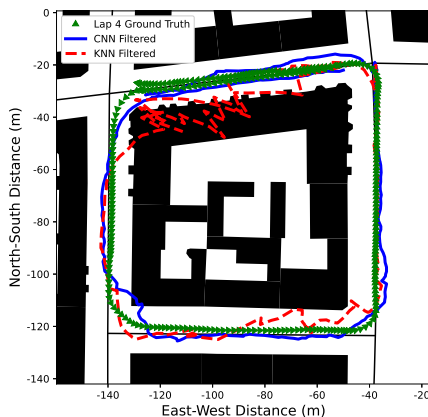
Fig. 6. Ground Truth vehicle trajectory, as well as Filtered Position Estimates from kNN and CNN.

TABLE III
HORIZONTAL ERROR VALUES FOR ESTIMATORS

Estimator	Avg. Error (m)	Error Std. (m)	Max Error (m)
CNN	6.2	4.9	35.9
kNN	10.4	17.3	108.8
CNN (Filtered)	5.7	2.4	12.1
kNN (Filtered)	7.2	4.5	25.9

drive data over the same road segment through an azimuthal-delay representation of the wireless channel. They show that the statistics of the wireless channel can be used to create a navigation solution even in non line-of-sight conditions. The estimates are augmented by external information regarding UE orientation and presume effective clock synchronization with the transmitter.

In future work, it would be interesting to alter the CNN architecture including input and output parameters, investigate sensitivity to timing errors, and to integrate multiple sectors and base stations.

ACKNOWLEDGMENT

REFERENCES

[1] N. Joubert, T. G. Reid, and F. Noble, "Developments in Modern GNSS and Its Impact on Autonomous Vehicle Architectures," in *2020 IEEE Intelligent Vehicles Symposium (IV)*. IEEE, 2020, pp. 2029–2036.

[2] Z. Kassas, J. Khalife, K. Shamaei, and J. Morales, "I Hear, Therefore I Know Where I Am: Compensating for GNSS Limitations with Cellular Signals," *IEEE Signal Processing Magazine*, vol. 34, no. 5, pp. 111–124, Sep. 2017.

[3] D. Burghal, A. T. Ravi, V. Rao, A. A. Alghafis, and A. F. Molisch, "A Comprehensive Survey of Machine Learning Based Localization with Wireless Signals," 2020. [Online]. Available: https://arxiv.org/pdf/2012.11171.pdf

[4] K. Witrisal, P. Meissner, E. Leitinger, Y. Shen, C. Gustafson, F. Tufvesson, K. Haneda, D. Dardari, A. F. Molisch, A. Conti *et al.*, "High-Accuracy Localization for Assisted Living: 5G systems will turn multipath channels from foe to friend," *IEEE Signal Processing Magazine*, vol. 33, no. 2, pp. 59–70, 2016.

[5] X. Ye, X. Yin, X. Cai, A. P. Yuste, and H. Xu, "Neural-Network-Assisted UE Localization Using Radio-Channel Fingerprints in LTE Networks," *Ieee Access*, vol. 5, pp. 12 071–12 087, 2017.

[6] H. Zhang, Z. Zhang, S. Zhang, S. Xu, and S. Cao, "Fingerprint-based Localization using Commercial LTE Signals: A Field-Trial Study," in *2019 IEEE 90th Vehicular Technology Conference (VTC2019-Fall)*. IEEE, 2019, pp. 1–5.

[7] J. Vieira, E. Leitinger, M. Sarajlic, X. Li, and F. Tufvesson, "Deep convolutional neural networks for massive mimo fingerprint-based positioning," in *2017 IEEE 28th Annual International Symposium on Personal, Indoor, and Mobile Radio Communications (PIMRC)*. IEEE, 2017, pp. 1–6.

[8] E. Dahlman, S. Parkvall, and J. Skold, *4G: LTE/LTE-advanced for mobile broadband*. Academic press, 2013.

[9] Oxford Technical Solutions Ltd, "Rt3000 v3," 2020, online; accessed 06-December-2021. [Online]. Available: https://www.oxts.com/products/rt3000/

[10] A. Richter, "Estimation of Radio Channel Parameters, Models and Algorithms," Ph.D. dissertation, Technische Universität Ilmenau, Germany, 2005.

[11] International Organization for Standardization, "Road vehicles — Vehicle dynamics and road-holding ability — Vocabulary," International Organization for Standardization, Geneva, CH, Standard, dec 2011.

[12] C. Wu, X. Yi, W. Wang, L. You, Q. Huang, X. Gao, and Q. Liu, "Learning to localize: A 3D CNN approach to user positioning in massive MIMO-OFDM systems," *IEEE Transactions on Wireless Communications*, 2021.

[13] P. Groves, *Principles of GNSS, Inertial, and Multisensor Integrated Navigation Systems, Second Edition*. Artech House, 03 2013.

Paper III

Paper III

Reproduced, with permission, from: ION

LTE NLOS Navigation and Channel Characterization

Russ Whiton[*‡], Junshi Chen[†‡], Fredrik Tufvesson[‡]
[*]Volvo Car Corporation, SE-405 31 Gothenburg, Sweden
[†]Terranet AB, Lund, Sweden
[‡]Dept. of Electrical and Information Technology, Lund University, Lund, Sweden
Email: {russell.whiton, junshi.chen, fredrik.tufvesson}@eit.lth.se

ABSTRACT

Navigation with terrestrial wireless infrastructure is appealing to overcome geometrical limitations of satellite navigation for users in environments with limited sky views. However, terrestrial signals are also prone to multipath that can result in angular and range estimates that are not representative of actual transmitter-receiver geometry. In this paper, some of these propagation effects are quantified for a particular urban non line-of-sight (NLOS) scenario, based on measurements of downlink reference symbols transmitted by a commercial Long Term Evolution (LTE) base station (eNodeB) and received by a massive antenna array mounted on a passenger vehicle. Empirical results indicate that large-scale statistics for a user making multiple passes through the same urban environment look similar when represented in terms of angles and delays despite changes in orientation and drive direction. Additionally, it is demonstrated that multipath effects can be utilized advantageously; it is possible to estimate not only user position but also orientation through wireless fingerprinting.

I. INTRODUCTION

The most well-known and widely-used wireless navigation systems are Global Navigational Satellite Systems (GNSS), including the United States Department of Defense's Global Positioning System (GPS), that provide positioning references in semi-synchronous Medium Earth Orbit (MEO). Users on the ground with an inexpensive GNSS receiver and antenna can localize themselves in real-time in a global reference frame with meter-level accuracy without external augmentation or sensor fusion. However, indoor areas, areas with heavy foliage, urban canyons, and other places with obstructed views of the sky face tougher challenges for achieving accurate and robust navigation.

Numerous applications would benefit from GNSS-like localization capabilities in these environments. The most promising technology for replicating the ubiquity of GNSS is cellular communication, which is rolled out across the world and offers generous bandwidth and transmit power [1]. For these reasons, use of cellular communication has been explored

and deployed as a GNSS complement or alternative for decades [2], with a focus on base station localizing of User Equipment (UE). While not widely commercially deployed, Fourth Generation (4G) Long-Term Evolution (LTE) systems introduced several Positioning Reference Symbols (PRS) already in 3rd Generation Partnership Project (3GPP) Release 9. Fifth-Generation (5G) systems built on 3GPP Release 16 have new dedicated signals for both uplink and downlink positioning using angles and delays [3].

However, the use of cellular signals for localization in GNSS-challenged environments is not trivial. The physical mechanisms of wave propagation mean that the dominant energy contribution of the received channel response may not correlate strongly with the physical transmitter-receiver geometry, resulting in systematic biases of delay estimates [4]. Researchers have expressed significant interest in determining how LTE, and specifically LTE based on Time-of-Arrival (TOA), performs in multipath environments through both simulation and measurement. Much work has been done to understand the large-scale statistics of multipath propagation [5], and to characterize various techniques for TOA estimation [6]. Innovative techniques have been introduced to mitigate multipath at a signal processing level, including multipath-estimating delay locked loops [7], machine learning [8], or even at an application level through environmental maps [9]. Another school of thought is to try to exploit the environmental information embedded in multipath propagation for improved fingerprinting [10], Simultaneous Location and Mapping (SLAM) [11], or for establishing a shared reference frame among users [12].

In this work, physical channel behavior is characterized in terms of TOA and Angle-of-Arrival (AOA) statistics for a particular urban canyon scenario. For a passenger vehicle following a similar trajectory through multiple passes of an urban canyon environment, propagation statistics show consistency when expressed in these domains. Furthermore, equipped with an advanced understanding of the channel, multipath propagation is used opportunistically for improved navigation. A channel fingerprint is introduced that enables a passenger vehicle to predict not only position, but orientation from a single sector of one eNodeB operating at 2.6 GHz in NLOS conditions. While previous work has used external sensory data to augment fingerprints, see, e.g., Table IV in [13] regarding "Side Information", one insight absent from fingerprinting literature is that information about UE orientation is embedded in channel fingerprints, even if angular resolution on the UE side may be limited for many practical scenarios. Our research contributions are as follows:

- A channel fingerprint utilizing multipath propagation is introduced to enable estimation of both position and heading, and the concept is verified with measurement data recorded in an urban canyon of signals received from a commercial eNodeB.
- Delay biases and, owing to the advanced spatial resolution of the measurement system employed, angular spreads are quantified for this NLOS scenario.

The manuscript is organized as follows: basics of LTE signal demodulation and channel representation are introduced in Section II; details of the measurement campaign, including the measurement system and drive route are provided in Section III. The estimators are

briefly described in Section IV; channel statistics and estimator performance from the test drive are presented in Section V; and finally, conclusions are drawn in Section VI.

II. CHANNEL CHARACTERIZATION

A. LTE Downlink Channel State Information

Numerous synchronization signals are frequently broadcast in LTE, including Primary Synchronization Symbols (PSS) and Secondary Synchronization Symbols (SSS) which allow the UE to synchronize with network time and deduce Cell Identification Numbers (CID). Cell-Specific Reference Signals (CRS) are used by the UE for channel estimation for coherent demodulation and to obtain Channel State Information (CSI) [14]. CRS are particularly appealing for navigation because they span the channel bandwidth, are transmitted frequently, and unlike PRS they are transmitted regardless of network operator configuration. The sequences are known *a priori* to the UE, which can multiply the Discrete Fourier Transform (DFT) of the received signal with the conjugate of the known transmitted signal to obtain the CSI estimate. For the multiple-receive antenna system introduced in Section III, this is done on a per-antenna basis, and estimated CSI is expressed as a complex value at each time index t per subcarrier, per antenna, $\hat{\mathbf{F}}_t$:

$$\hat{\mathbf{F}}_t \in \mathbb{C}^{M \times S} \tag{1}$$

Where M is the number of receive antennas and S is the number of subcarriers.

B. Channel Representation

CSI is a raw form of channel information, and propagation channels are often modeled as the superposition of a discrete number of plane waves, including a direct Line-of-Sight (LOS) path and Specular Multipath Components (SMCs). If the LOS path is attenuated to the point of being unresolvable but other components are resolvable, it is called a NLOS scenario. Such a model is useful for many tasks in communication and localization, but there are several limitations. For one, the plane wave model alone necessarily discards some of the energy contained in the Channel Impulse Response (CIR) from propagation mechanisms other than specular reflection, or even specular reflection that is unresolvable for a given channel bandwidth and measurement aperture. So-called Diffuse Multipath Components (DMCs), which can be understood as the superposition of many components of lesser power that are too small to effectively estimate individually, also contain information. Another problem is that decomposition into plane waves requires the additional step of channel estimation which requires processing power, particularly for methods based on expectation maximization or subspace searches. Yet another problem in plane wave modeling is that model order number can vary dramatically, which is consequential for both communication and localization.

A somewhat less cumbersome approach to decompose the channel into a domain with intuitive and sparse properties, an approach without matrix inversions or subspace searches, is to use a matched filter [15]. The effects of the antenna pattern can be compensated for through matrix multiplication with the Hermitian transpose of the per-antenna measured complex radiation pattern $\mathbf{A}$, which is measured for M antennas at the center frequency in discrete steps of $\Delta\theta$ for elevation angles θ and steps of $\Delta\phi$ for azimuthal angles ϕ, e.g., [16]:

$$\mathbf{A} \in \mathbb{C}^{M \times ((\frac{\pi}{\Delta\theta}+1)*(\frac{2\pi}{\Delta\phi}))} \tag{2}$$

Similarly, decomposition into the time domain is done through multiplication with the conjugate of the matrix of per-subcarrier phase shifts $\mathbf{D}$ at frequency indexes of the subcarriers f_1 to f_S for the desired length of the channel into T discrete time steps from τ_0 to τ_{T-1}:

$$\mathbf{D} = \begin{bmatrix} 1 & e^{2\pi f_1 \tau_1} & \cdots & e^{2\pi f_1 \tau_{(T-1)}} \\ \vdots & \vdots & \ddots & \vdots \\ 1 & e^{2\pi f_S \tau_1} & \cdots & e^{2\pi f_S \tau_{(T-1)}} \end{bmatrix} \in \mathbb{C}^{S \times T} \tag{3}$$

By performing a matrix multiplication of the CSI $\hat{\mathbf{F}}$ with the Hermitian transpose of the combined antenna pattern across antennas, $\mathbf{A}^{\mathbf{H}}$, and the conjugate per-subcarrier phase shifts $\mathbf{D}^*$, the CSI is transformed into an angular-delay bin channel estimate $\hat{\mathbf{Y}}$, with granularity according to the sampling interval of the antenna pattern and delay according to the per-subcarrier phase shift matrix $\mathbf{D}$:

$$\hat{\mathbf{Y}}_t = \mathbf{A}^{\mathbf{H}}\hat{\mathbf{F}}_t\mathbf{D}^* \in \mathbb{C}^{((\frac{\pi}{\Delta\theta}+1)*(\frac{2\pi}{\Delta\phi})) \times T} \tag{4}$$

Rearranging into a three-dimensional tensor $\hat{\mathbf{Z}}_t$ in the order of elevation, azimuth and delay:

$$\hat{\mathbf{Y}}_t \in \mathbb{C}^{((\frac{\pi}{\Delta\theta}+1)*(\frac{2\pi}{\Delta\phi})) \times T} \rightarrow \hat{\mathbf{Z}}_t \in \mathbb{C}^{(\frac{\pi}{\Delta\theta}+1) \times (\frac{2\pi}{\Delta\phi}) \times T} \tag{5}$$

This matrix multiplication, while still computationally intensive for a massive antenna array with narrow sampling of the complex antenna pattern, yields an intuitive result for viewing of the channel in the angular and delay domains and is well-suited for rich multipath channels at lower frequencies that are not well-characterized by plane-wave modeling.

III. MEASUREMENTS FROM LTE ENODEB

A. LTE Signal Measurement and Hardware

Signals transmitted by a commercial LTE eNodeB were recorded using a USRP-2593R Software Defined Radio (SDR) and LABView from National Instruments. PSS and SSS were used to establish frame timing, and PSS/SSS/CRS symbols in the time domain were subsequently logged on a test laptop for offline data processing. The USRP also included a GPS receiver which was used for synchronization with GPS time and as a point of comparison for Results in Section V. The frequency reference for the USRP was generated by an FS725 Rubidium Frequency Standard from Stanford Research Systems (disciplined by a GPS receiver-generated 1 pulse-per-second output prior to testing) to provide a more stable oscillator reference than the USRP's internal oscillator. The SDR served as both a receiver and an antenna switch controller, connected to a 128-element (4 vertical rings of 16 patch antennas with 2 cross-polarized elements per patch) Stacked Uniform Circular Array (SUCA) , which switched at the rate of 2 CRS symbols per antenna[1], or equivalently 0.5 ms. The complete measurement set-up is depicted in Figure 1.
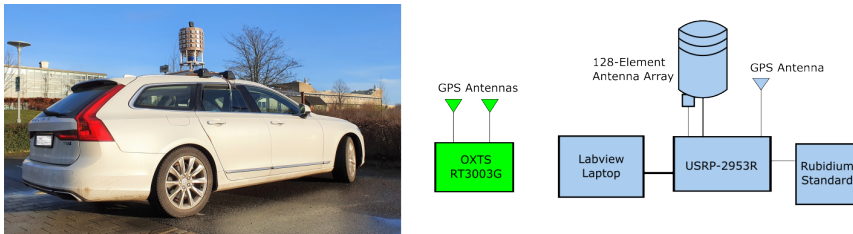
Fig. 1: (Left) Photo of test vehicle. (Right) Block diagram of measurement set-up.

Ground truth vehicle pose, including orientation, was generated by a dual-constellation, dual-antenna, dual-frequency Oxford Systems RT3003G system with Post-Processed Real-Time Kinematics (RTK). A GoPRO MAX $360°$ camera was mounted on the top of the antenna array to check for data irregularities.

B. Drive Route

A deep urban environment and LTE eNodeB were selected for testing with a presumption that various propagation mechanisms would contribute appreciable amounts of energy to the CIR, including diffraction over rooftops, wave guiding down streets, scattering from

---

[1]Note that switching at the rate of CRS symbol transmission imposes strict limitations on driving speed to avoid exceeding channel coherence time. Sampling antennas in parallel would negate limitations in speed, but significantly increase data logging or real-time data processing requirements.

surrounding objects including other vehicles and specular reflections from smooth surfaces. At all points along the test route the direct path to the transmitter was heavily attenuated by multi-story buildings. Reception of GNSS signals was possible in this environment, but measurements derived from GPS-only measurements exhibited errors on the order of tens of meters, as shown in Section V. The ground truth system benefitted from post-processing (smoothing), inertial fusion and the Eastern section of the route which had an open sky view on three sides.

The geometry of the drive laps relative to the transmitting eNodeB is shown on the left side of Figure 2. Two laps were driven clockwise (laps two and three, defined as the positive direction for odometry in Section V) and two were driven counter-clockwise (one and four). There are lateral position offsets on the order of a few meters for the Eastern and Western sections of the route which are multi-lane. The route spanned slightly more than 100 meters North-South and East-West, and each lap was about 400 meters of driven distance. Average speed was about 1 meter/second to avoid exceeding channel coherence time for the slowly switched system.
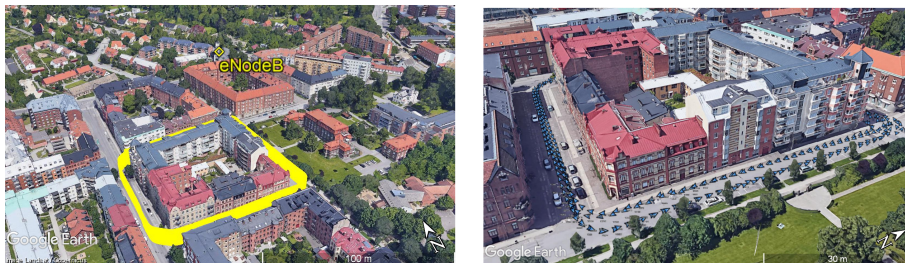
Fig. 2: (Left) Visualization of drive lap area and transmitting eNodeB in Lund, Sweden (approx. location 55.71°N, 13.19°E). (Right) Position and heading for selected snapshots on each of the four laps to illustrate lateral offsets and drive direction differences. Images created with Google Earth.

There is uncertainty in the absolute position of the phase center of the transmitting eNodeB, as well as with the time-varying absolute clock offset beween the measurement system and eNodeB. A manual calibration was done in post-processing to try to refine estimates of the antenna phase center's three-dimensional location and a static absolute clock offset, based on LOS data collected before and after the four drive laps from approximately the same starting point. Visual results in the delay and azimuthal domains, presented in Section V, show minimal variation over time, but these ambiguities mean that the absolute numbers can be considered accurate on a meter-level at best. The measurement system's absolute time synchronization with the disciplined Rubidium oscillator appears to be adequate for at least a visual analysis. The oscillator of the eNodeB was unknown

because it was a commercially operating mobile network, and the test system oscillator was subject to vibration and changes in temperature over a period of about an hour.

This should not be confused with ambiguity in the position domain for the vehicle position estimator presented in Section IV, because ground truth estimates are accurate on a centimeter-level and not derived from eNodeB position. Rather, the opposite is the case that eNodeB position is derived from vehicle pose that is well-anchored in a geodetic frame.

IV. ESTIMATORS FOR CHANNEL REPRESENTATION AND LOCALIZATION

A. Estimator for TOA Channel Characterization

The LTE positioning problem is often formulated as a trilateration problem where ranges (pseudoranges including transmitter-receiver clock mismatch, in practice) are taken to known reference points. TOA estimators of varied complexity and performance have been considered for LTE estimation, and previous work has considered performance as a function of signal-to-noise ratio and environmental conditions using Geometry-Based Stochastic Channel Models (GBSCMs) [6].

Using the measurement set-up described in Section III, a simple peak-detector p_{ranges} is implemented to estimate L delay peaks from d_1 to d_L for a CIR as shown in the left subfigure of Figure 3:

$$p_{ranges} : CIR \rightarrow \{d_1, d_2, ...d_L\} \tag{6}$$
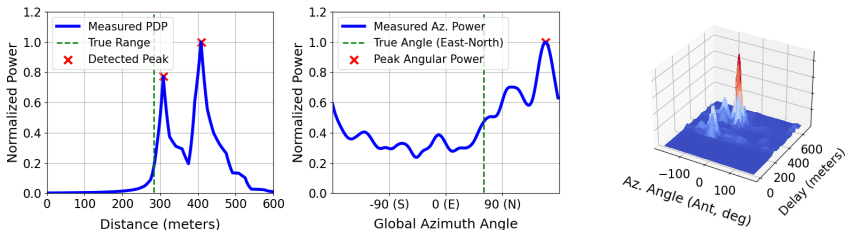
Fig. 3: Channel data for one snapshot. (Left) CIR with peak detection. (Middle) Azimuthal spectra. (Right) Azimuthal-delay spectra in antenna reference frame.

Next, the CIR is generated as a compression across the tensor elements $\hat{z}_{(i,j,k),t}$ of $\hat{\mathbf{Z}}_t$ which compresses the channel into the time domain, and the delay bias κ_t per snapshot is calculated as the difference between the true distance at time t to the eNodeB η_t^{BS} and the first peak d_1:

$$\kappa_t = p_{ranges}(\sum_{i=1}^{I}\sum_{j=1}^{J}\hat{z}_{(i,j,k),t})_1 - \eta_t^{BS} \qquad (7)$$

B. Estimator for AOA Channel Characterization

A similar analysis is done for AOA, a compression across the tensor elements $\hat{z}_{(i,j,k),t}$ of $\hat{\mathbf{Z}}_t$ in the dimensions of elevation and delay. The absolute difference in degrees ξ_t between the absolute peak angular power of the azimuthal spectra and the geometric angle to the eNodeB γ_t^{BS}, as is shown in the middle subfigure of Figure 3.

$$\xi_t = min(\gamma_t^{BS} - max(\sum_{i=1}^{I}\sum_{k=1}^{K}\hat{z}_{(i,j,k),t}), 2\pi - (\gamma_t^{BS} - max(\sum_{i=1}^{I}\sum_{k=1}^{K}\hat{z}_{(i,j,k),t}))) \qquad (8)$$

C. CNN Estimator and Kalman Filter for Position and Heading Estimation

A Convolutional Neural Network (CNN) is used to generate estimations of two-dimensional position together with heading. The goal with the estimator f_{CNN} is to take a channel fingerprint $\mathbf{Y}_t$ and generate a three-dimensional measurement $\hat{\mathbf{y}}_t$ of UE pose including East-West position $\hat{y}_e$, North-South position $\hat{y}_n$ and heading angle $\hat{y}_\gamma$:

$$f_{CNN}(\mathbf{Y}_t) \rightarrow \hat{\mathbf{y}}_t = [\hat{y}_e, \hat{y}_n, \hat{y}_\gamma]^T \in \mathbb{R}^3 \qquad (9)$$

The SUCA antenna has significantly better resolution in the azimuthal domain than in elevation, so the input fingerprints are compressed in the elevation direction to reduce the computational complexity for both training and run-time. The parameters of the CNN are given in Table I. Rather than performing three-dimensional convolutions on the tensor $\hat{\mathbf{Z}}_t$, the footprints used in this case, $\hat{\mathbf{Z}}_{az\_del,t}$, are two-dimensional in the azimuthal-delay domain, as shown in the right side sub-figure of Figure 3:

$$\hat{\mathbf{Z}}_{az\_del,t} = \sum_{i=1}^{I}\hat{z}_{(i,j,k),t} \qquad (10)$$

Complete state estimates generated at each snapshot at discrete time t are filtered with an Extended Kalman Filter (EKF) employing a coordinated turn process model, where three of the parameters are observed directly by the output of the CNN, and velocity $\hat{x}_v$ and turn rate estimates $\hat{x}_\omega$ are treated as stochastic parameters, for a complete state vector $\hat{\mathbf{x}}_t = [\hat{x}_e, \hat{x}_n, \hat{x}_v, \hat{x}_\gamma, \hat{x}_\omega]^T$. The state estimates at each time step t of duration $\Delta t = 75$ ms are from a prediction step:

TABLE I: CNN Estimator Description

Parameter	Value
Input Layer Dimensions	90 x 82
Delay Range (meters / ns)	0 to 675 / 0 to 2083
Azimuthal Range (degrees)	-180 to 180
Delay Resolution (meters / ns)	8.2 / 25.4
Azimuthal Resolution (degrees)	4
CAP Layer 1 Filters / Weights	16 / 160
CAP Layer 2 Filters / Weights	32 / 4640
CAP Layer 3 Filters / Weights	64 / 18,496
Dense Layer 1 Weights	901,248
Dense Layer 2 Weights	8256
Kernel Size (All conv. layers)	3
Pool Size (All pooling layers)	2x2
Output Layer Shape	3
Trainable parameters	932,995

$$\hat{\mathbf{x}}_{t|t-1} = \begin{bmatrix} \hat{x}_{e,t-1} + \Delta t \cdot \hat{x}_{v,t-1} \cdot cos(\hat{x}_{\gamma,t-1}) \\ \hat{x}_{n,t-1} + \Delta t \cdot \hat{x}_{v,t-1} \cdot sin(\hat{x}_{\gamma,t-1}) \\ \hat{x}_{v,t-1} \\ \hat{x}_{\gamma,t-1} + \Delta t \cdot \hat{x}_{\omega,t-1} \\ \hat{x}_{\omega,t-1} \end{bmatrix} + \mathbf{w}_t \quad (11)$$

Where $\mathbf{w}_t$ is a zero-mean sequence with covariance $\mathbf{Q} = diag([q_e, q_n, q_v, q_\gamma, q_\omega])$. Observations are linear in the state space:

$$\hat{\mathbf{y}}_t = \begin{bmatrix} 1 & 0 & 0 & 0 & 0 \\ 0 & 1 & 0 & 0 & 0 \\ 0 & 0 & 0 & 1 & 0 \end{bmatrix} \hat{\mathbf{x}}_t + \mathbf{r}_t \quad (12)$$

Where $\mathbf{r}_t$ is zero-mean with covariance $\mathbf{R} = diag([r_e, r_n, r_\gamma])$.

V. RESULTS

A. Channel Measurements

A critical factor for localization using fingerprinting is whether the fingerprint representation is consistent across space and time. A fingerprint that is sensitive to minor perturbations in the environment will be of limited utility; the differences between data collection and run-time will make inferences less meaningful. Figure 4 shows the delay spectra for the four laps as a function of odometry (the x-axis is inverted for counter-clockwise drive laps). The Euclidian distance from the vehicle to the eNodeB antenna itself is shown in

blue. There are visibly similar patterns in each of the laps both in terms of the absolute value of delay spectra and the relative spacing of the major energy contributions. Several lessons can be drawn from these results, both about the channel behavior and about the measurement system.
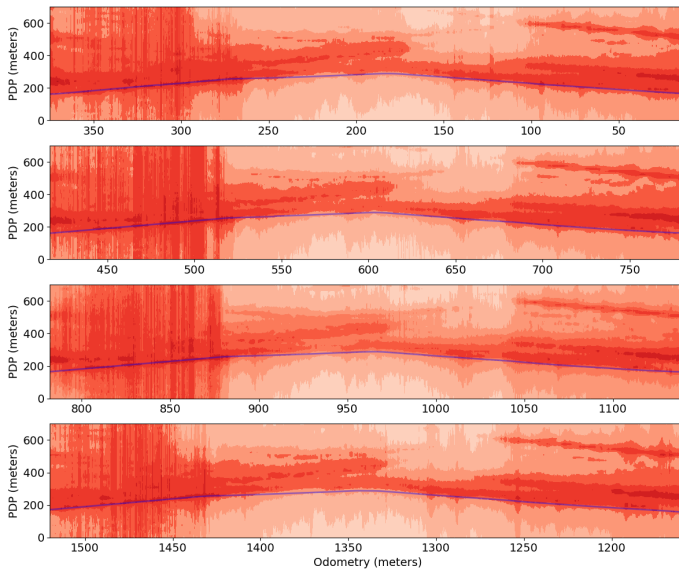

Fig. 4: Power Delay Profile as a function of odometry from one sector of one eNodeB for four drive laps, as well as the Euclidian distance from the vehicle to the eNodeB (blue).

At the beginning of the route (the Eastern section) there is an apparent smearing of energy; it is an artifact of interference from another eNodeB that has strong signal power and a cell ID that entails transmission on the same resource blocks. Interference cancellation allows for data communication, but complicates propagation modeling for this section.

With regard to the channel behavior itself, the peaks of the delay spectra lag the Euclidian distance from the vehicle to the eNodeB, as expected for this NLOS scenario. Given the 20 MHz channel bandwidth with 200 subcarriers used in the estimation, it is unsurprising that an effective discrete representation of the channel under these conditions appears difficult, as propagation mechanisms other than specular reflection are contributing energy to the CIR and the resolution is limited. For an urban scenario with similar bandwidth and number of antennas, DMCs were previously found to comprise 10-30% of the impulse response energy [17]. The last segment (Northernmost) part of the route shows strong multipath components with delay-distance components in excess of 300 meters from the early peaks.

This is not surprising for LTE, which supports Cyclic Prefix (CP) lengths corresponding to over a kilometer of propagation distance even in normal CP mode. The consistency of the spacing between components shows that it is reasonable to infer information about position based on delay spreads, and provides further evidence that there is information which can be retrieved for localization [18].

Figure 5 shows global (East-North) azimuthal spectra for the same drive laps. The spectra are again visibly consistent in spite of lateral offsets in the drive route and differences in driving direction. Strong discontinuities are visible that are consistent across drive laps, and at intersections the energy appears to shift compass directions, following the North-South and East-West layout of the surrounding buildings. This is highly consequential if AOA is to be used for state estimation, see, e.g., [19].
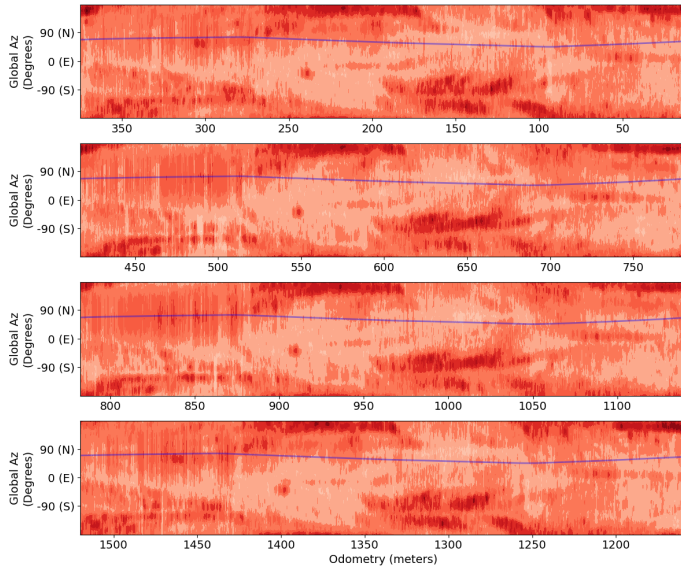
Fig. 5: Azimuthal spectra for four laps as well as the calculated angle to the eNodeB (blue).

B. Bias Characterization

The biases of the TOA estimator and AOA estimators described in Section IV are shown in Figure 6. For the TOA estimator, a normal distribution with a mean of 30 meters and standard deviation of 12 meters is plotted for comparison. Previous work has utilized a skew-t distribution [5] with the intention of combining both LOS and NLOS scenarios, but

of course the distribution parameters in that case will depend heavily on the mix of the two in the underlying data set. All measurements in this data set are NLOS.

Note that data from the Eastern section of the route, for which significant interference from a separate eNodeB was observed (visible on the left side of the laps in Figure 4), was excluded from the statistics because this interference results in distortion of the CIR and false local maxima when applying the peak detector p_{range}. Future work will employ better interference cancellation techniques to address this problem. The choice of peak detector applied to the time domain measurements is consequential, but was not found to significantly impact the shape of the results for these drives or to reduce lap-to-lap consistency.
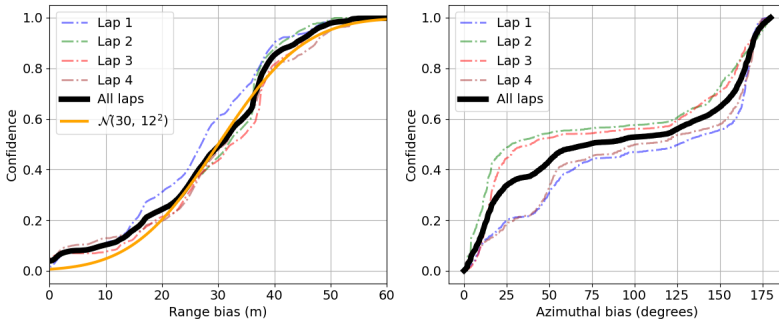
Fig. 6: (Left) Cumulative distribution function of range biases κ_t. (Right) Cumulative distribution function of azimuthal biases ξ_t.

C. Localization with CNN

The results of the position and heading estimator described in Section IV-C are shown in a map view and time series in Figure 7, both for the unfiltered and filtered estimates. Comparison with the GPS L1 receiver integrated into the SDR is also given as a reference.

From the map view, it is apparent that the estimator is capable of differentiating the different segments of the lap, but it suffers in differentiating the Northwest and Southeast corners. Part of the trouble in the Southeast corner may be attributable to interference from the other eNodeB. The settings of the filter in the SDR GPS receiver are opaque, but total position error is similar in this environment. One important advantage of the CNN estimator is that it provides independent heading estimates, as opposed to the SDR GPS receiver which must assume that the traversed path of the antenna corresponds with direction of travel without consideration for the vehicle body frame.

Velocity estimates at the output of the estimator appear to be particularly poor, which is in part owing to the lack of observability of the parameter with this choice of motion

Fig. 7: Results of position and heading estimation for filtered and unfiltered CNN estimates. (Left) Map view of fourth lap ground truth and estimates. (Right) Time series view of estimates.
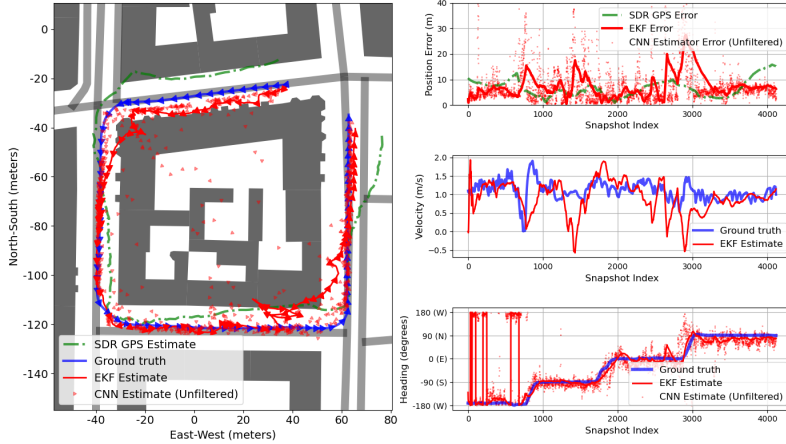
model with measurements of position and heading. Augmentation with wheel odometry or inertial measurement would likely be effective at addressing this deficiency.

A cumulative distribution function of the errors in position and heading are shown in Figure 8. The position estimation of the CNN performs similarly to the SDR GPS receiver, but this is strongly influenced by the poor CNN performance in the section of the drive route that suffers from interference. CNN heading estimation appears to be effective for the unfiltered estimates, correctly estimating the direction of travel (less than $90°$ heading error) well over 95% of the time, which demonstrates that there is potential for fingerprinting to provide observations of more of the state vector than position alone. CNN estimates are based on 75 ms snapshots, but aggregation of energy into multiple snapshots would likely result in more stable estimates at the expense of longer update times.

VI. CONCLUSIONS

Four drive laps through the urban canyon showed visual and statistical similarity in the angular and delay spectra. In NLOS scenarios there is a tendency toward absolute delay biases on the order of tens of meters, but delay biases that are not sensitive to meter-level offsets in lateral and longitudinal position. Angular spectra are dominated by the surrounding building geometry, and the peaks of the received power spectra have little correlation with the actual receiver-transmitter geometry for such scenarios when direct transmission is heavily attenuated.
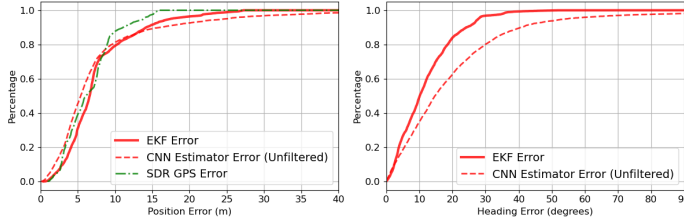
Fig. 8: Cumulative distribution functions of CNN estimator errors. (Left) Filtered and unfiltered position errors. (Right) Filtered and unfiltered heading errors.

The moderate success of the Convolutional Neural Network in generating fingerprint-based estimations of both position and heading at 75 millisecond intervals also shows that there is promise in this channel representation. Fingerprints can represent more than just position, angular information can be taken into consideration as well when antenna arrays are utilized. Even with a single transmitting antenna, multipath reflection is shown to be effective at providing a basis for orientation estimation, which is desirable for many problems in navigation. Performance shown by the test system, for a challenging scenario, was similar to that of an unaugmented GPS L1 receiver, but with the benefits of a faster update rate and independent heading updates in the UE frame.

Matched filter representation of the channel allows for the preservation of information that might otherwise be lost if representing the channel as the summation of a discrete number of plane waves, and can reduce the complexity of performing a computationally intensive super resolution algorithm.

In the future, it would be interesting to integrate multiple sectors and multiple eNodeBs into the estimation, to investigate the sensitivity of such a representation to absolute timing error, and to add memory to the neural network rather than filtering neural network outputs with a Kalman filter.

ACKNOWLEDGEMENTS

REFERENCES

[1] Z. Kassas, J. Khalife, K. Shamaei, and J. Morales, "I Hear, Therefore I Know Where I Am: Compensating for GNSS Limitations with Cellular Signals," *IEEE Signal Processing Magazine*, vol. 34, no. 5, pp. 111–124, Sep. 2017.

[2] J. A. del Peral-Rosado, R. Raulefs, J. A. López-Salcedo, and G. Seco-Granados, "Survey of cellular mobile radio localization methods: From 1G to 5G," *IEEE Communications Surveys & Tutorials*, vol. 20, no. 2, pp. 1124–1148, 2017.

[3] S. Dwivedi, R. Shreevastav, F. Munier, J. Nygren, I. Siomina, Y. Lyazidi, D. Shrestha, G. Lindmark, P. Ernström, E. Stare *et al.*, "Positioning in 5G networks," *IEEE Communications Magazine*, vol. 59, no. 11, pp. 38–44, 2021.

[4] S. Aditya, A. F. Molisch, and H. M. Behairy, "A Survey on the Impact of Multipath on Wideband Time-of-Arrival-Based Localization," *Proceedings of the IEEE*, vol. 106, no. 7, pp. 1183–1203, 2018.

[5] P. Müller, J. A. del Peral-Rosado, R. Piche, and G. Seco-Granados, "Statistical Trilateration With Skew-t Distributed Errors in LTE Networks," *IEEE Transactions on Wireless Communications*, vol. 15, no. 10, pp. 7114–7127, 2016.

[6] P. Wang and Y. J. Morton, "Performance comparison of time-of-arrival estimation techniques for LTE signals in realistic multipath propagation channels," *NAVIGATION: Journal of the Institute of Navigation*, vol. 67, no. 4, pp. 691–712, 2020.

[7] P. Wang and Y. J. Morton, "Multipath Estimating Delay Lock Loop for LTE Signal TOA Estimation in Indoor and Urban Environments," *IEEE Transactions on Wireless Communications*, vol. 19, no. 8, pp. 5518–5530, 2020.

[8] M. Orabi, A. A. Abdallah, J. Khalife, and Z. M. Kassas, "A Machine Learning Multipath Mitigation Approach for Opportunistic Navigation with 5G Signals," in *Proceedings of the 34th International Technical Meeting of the Satellite Division of The Institute of Navigation (ION GNSS+ 2021)*, 2021, pp. 2895–2909.

[9] K. Strandjord, Y. Morton, and P. Wang, "Evaluating the Urban Signal Environment for GNSS and LTE Signals," in *Proceedings of the 34th International Technical Meeting of the Satellite Division of The Institute of Navigation (ION GNSS+ 2021)*, 2021, pp. 2166–2182.

[10] J. Vieira, E. Leitinger, M. Sarajlic, X. Li, and F. Tufvesson, "Deep Convolutional Neural Networks for Massive MIMO Fingerprint-Based Positioning," in *2017 IEEE 28th Annual International Symposium on Personal, Indoor, and Mobile Radio Communications (PIMRC)*. IEEE, 2017, pp. 1–6.

[11] C. Gentner, T. Jost, W. Wang, S. Zhang, A. Dammann, and U.-C. Fiebig, "Multipath Assisted Positioning with Simultaneous Localization and Mapping," *IEEE Transactions on Wireless Communications*, vol. 15, no. 9, pp. 6104–6117, 2016.

[12] M. Ulmschneider, C. Gentner, and A. Dammann, "Cooperative Estimation of Maps of Physical and Virtual Radio Transmitters," in *Proceedings of the 34th International Technical Meeting of the Satellite Division of The Institute of Navigation (ION GNSS+ 2021)*, 2021, pp. 2307–2317.

[13] D. Burghal, A. T. Ravi, V. Rao, A. A. Alghafis, and A. F. Molisch, "A Comprehensive Survey of Machine Learning Based Localization with Wireless Signals," 2020. [Online]. Available: https://arxiv.org/pdf/2012.11171.pdf

[14] E. Dahlman, S. Parkvall, and J. Skold, *LTE/LTE-Advanced for Mobile Broadband*. Academic Press, 2013.

[15] Y. Luo, L.-T. Hsu, and Y. Pan, "A Super-Resolution Algorithm with FRFT Towards GNSS TOA Estimation for Multipath Channel," in *Proceedings of the 34th International Technical Meeting of the Satellite Division of The Institute of Navigation (ION GNSS+ 2021)*, 2021, pp. 3350–3359.

[16] M. Landmann and G. Del Galdo, "Efficient Antenna Description for MIMO Channel Modelling and Estimation," in *7th European Conference on Wireless Technology, 2004*. IEEE, 2004, pp. 217–220.

[17] S. Sangodoyin, V. Kristem, C. U. Bas, M. Käske, J. Lee, C. Schneider, G. Sommerkorn, C. J. Zhang, R. Thomä, and A. F. Molisch, "Cluster Characterization of 3D MIMO Propagation Channel in an Urban Macrocellular Environment," *IEEE Transactions on Wireless Communications*, vol. 17, no. 8, pp. 5076–5091, 2018.

[18] A. Niitsoo, T. Edelhäußer, E. Eberlein, N. Hadaschik, and C. Mutschler, "A Deep Learning Approach to Position Estimation from Channel Impulse Responses," *Sensors*, vol. 19, no. 5, p. 1064, 2019.

[19] K. Shamaei, J. Khalife, and Z. M. Kassas, "A Joint TOA and DOA Approach for Positioning with LTE Signals," in *2018 IEEE/ION Position, Location and Navigation Symposium (PLANS)*, 2018, pp. 81–91.

Paper IV

Paper IV

Reproduced, with permission, from: IEEE

Wiometrics: Comparative Performance of Artificial Neural Networks for Wireless Navigation

Russ Whiton, Junshi Chen, Fredrik Tufvesson

Abstract

Radio signals are used broadly as navigation aids, and current and future terrestrial wireless communication systems have properties that make their dual-use for this purpose attractive. Sub-6 GHz carrier frequencies enable widespread coverage for data communication and navigation, but typically offer smaller bandwidths and limited resolution for precise estimation of geometries, particularly in environments where propagation channels are diffuse in time and/or space. Non-parametric methods have been employed with some success for such scenarios both commercially and in literature, but often with an emphasis on low-cost hardware and simple models of propagation, or with simulations that do not fully capture hardware impairments and complex propagation mechanisms. In this article, we make opportunistic observations of downlink signals transmitted by commercial cellular networks by using a software-defined radio and massive antenna array mounted on a ground vehicle in an urban non line-of-sight scenario, together with a ground truth reference for vehicle pose. With these observations as inputs, we employ artificial neural networks to generate estimates of vehicle location and heading for various artificial neural network architectures and different representations of the input observation data, which we call wiometrics, and compare the performance for navigation. Position accuracy on the order of a few meters, and heading accuracy of a few degrees, are achieved for the best-performing combinations of networks and wiometrics. Based on the results of the experiments we draw conclusions regarding possible future directions for wireless navigation using statistical methods.

I. INTRODUCTION

Wireless systems are used ubiquitously for navigation. Global Navigational Satellite Systems (GNSS) including the US Department of Defense's Global Positioning System (GPS) deploy satellites in Medium Earth Orbit (MEO) which allow users anywhere on Earth with an unobstructed view of the sky to generate estimates of global position and time with meter-level and microsecond-level accuracies using inexpensive mass-market

hardware [1]. Real-Time Kinematic (RTK) methods have been developed to enhance GNSS accuracy to just a few centimeters [2], and millimeter-level accuracy is even achievable for scientific applications including measurement of tectonic plate velocities with sophisticated hardware and post-processing algorithms [3].

With this impressive performance in mind, one could consider MEO navigational satellites to have solved the problem of positioning on Earth. However, numerous applications of interest face practical limitations that preclude using GNSS as the sole source for navigation. GNSS signal reception is limited to non-existent indoors [4], for example, and in urban environments observations are frequently not of sufficient quality to meet application requirements for accuracy, availability, continuity, or integrity [5]. More conspicuously, GNSS receivers are vulnerable to intentional and unintentional jamming, as well as deliberate spoofing [6]. Augmentation with complementary proprioceptive sensing such as odometry, inertial measurement, or altimeters can help mitigate some of these limitations (dead-reckoning), but even sensor-fused systems still have utility for absolute navigation estimates in a global frame (position fixing) [7].

Terrestrial wireless systems are particularly well-suited to provide global position estimates [8], and cellular communications systems boast a decades-long history of dual-use for navigation driven primarily by legislation intended to assist first responders in emergencies [9]. Such systems have a natural affinity for use in navigation owing to their ubiquity of deployment and the large bandwidths and link budgets that enable high data-rate communication [10]. Fifth Generation (5G) systems from the Third Generation Partnership Project (3GPP) have dedicated measurements for performing triangulation and multi-lateration [11], measurements which are expected to offer unprecedented accuracy compared with what previous cellular systems could achieve.

However, the same physical obstructions which prevent utilization of satellite signals in some environments can cause similar challenges for navigation systems utilizing terrestrial transmitters. Position fixing methods based on ranging or bearing (angular) measurements will face difficulties in the face of multipath, manifesting as positive range biasing [12] and angular biases [13]. A broad set of methods have been proposed for line-of-sight (LoS) identification and multipath mitigation, including multipath-estimating tracking loops [14], statistical methods [15], and residuals testing [16]. An even more promising solution for multipath is to exploit the additional information that it provides to improve performance rather than trying to mitigate it [17], [18]. Tracking of individual Multipath Components (MPCs) allows for the construction of multiple ranging and bearing observations from a single transmitter, but this too is not without challenges. Such methods are best suited for large channel bandwidths, antenna arrays, dense transmitter infrastructure, and limited mobility, or dense multipath may preclude reliable ranging and bearing measurements [19].

Feature-matching [7] (or *non-parametric*) navigation techniques rely on comparisons of observations with databases rather than using explicit calculation of ranges and bearing to known landmarks. With wireless navigation, these methods are referred to as *proximity*

or *fingerprinting*, and are often used for lower carrier frequencies [20], [21]. Billions of devices are in use today that can provide users with a coarse location based on a non-parametric "network-provided" location, using massive databases of Wi-Fi and cellular transmitters aggregated from many users over a long time [22]. The breakthrough success of machine learning in areas like computer vision and natural language processing has inspired significant recent interest in applying statistical learning techniques, primarily Artificial Neural Networks (ANNs) to wireless positioning [23], in order to make the leap from the coarse position provided by commercial systems to highly precise estimates. Such techniques are frequently predicated on the use of massive-Multiple-Input Multiple-Output (MIMO) [24], in which multiple transmitting and/or multiple receiving antennas provide separate observations for a single link.

In this work, a massive-MIMO receiver is used to provide navigation state estimates for a ground vehicle in a complicated urban propagation environment, building on previous work from the authors in [25]. ANNs are used to estimate navigation states based on opportunistic measurements from commercial Long Term Evolution (LTE) Base Stations (BSs). Wireless fingerprinting[1] is analyzed broadly, and we offer the humble suggestion that this method might more appropriately be renamed *wiometric navigation*, analogous to *biometrics*, for which human fingerprinting is merely one tool (see Section II for more exposition). This manuscript includes a number of extensions beyond our previous work in [25], including the following:

- Multiple channel representations and ANN architectures are proposed and evaluated, as well as two train/test splits representing high and low levels of epistemic uncertainty.
- The navigation state and learning models are updated to include estimates of heading, as opposed to [25], which used heading as a network input rather than a predicted state at the output.
- Performance of the network is analyzed when signals are received concurrently from a neighboring BS, and an architecture is proposed for additional sectors and BSs.

The manuscript is organized as follows: Section II discusses channel fingerprinting and specifies the four channel representations (wiometrics) used in the main body of the paper; Section III discusses the types of algorithms used for association between the surveyed data and inferences at run-time; Section IV discusses the LTE signal structure, the vehicular test bed, and the data set with the two training and test splits; Section V provides the results for the channel measurements, train/test splits and the neural networks; Section VI offers exposition on the results; and finally the conclusions are drawn in Section VII together with suggestions for future work.

Notes on mathematical representation:

---

[1]Somewhat confusingly, "fingerprinting" is also used in literature for performing transmitter identification by capturing characteristic device-level hardware variations [26]. In this work, fingerprinting refers to non-parametric feature matching for navigation.

- $(\cdot)^T$, $(\cdot)^H$, and $(\cdot)^*$ represent the transpose, Hermitian transpose and conjugate of a complex-valued vector/matrix, respectively.
- $\mathcal{F}_{m,n}$ indicates a two-dimensional m- and n-point Fourier Transform (FT).
- $\mathbf{col_j(F)}$ and $\mathbf{row_k(F)}$ indicate taking the i-th column and the k-th row of a matrix, respectively.

II. Channel Wiometrics

A. Channel and User State Representation

As formulated in [27], the intention with non-parametric wireless channel-based navigation methods is to learn an inverse function that maps a set of channel measurements $\mathbf{Y}_i$ to their associated navigation state vectors $\mathbf{x}_i$ in a maximally-bijective fashion:

$$f^{-1} : \{\mathbf{Y}_i\} \to \{\mathbf{x}_i\}. \tag{1}$$

Literature addressing this basic problem formulation can be found as early as 1993 [28], when a "calibration matrix" was proposed to construct an effective radio map that compensated for the limitations that complex propagation phenomena imposed on angle-of-arrival methods in a prison environment for Very High Frequency (VHF) signals. Literature on the subject expanded to encompass other technologies such as WaveLAN [29] and Wi-Fi, the well-known successor to WaveLAN [30]. Application using cellular-based technology has been investigated from Second Generation (2G) systems [31] through 5G systems [32].

Much of this body of work on the subject has come from the Internet-of-Things domain, employing commercial hardware that is easy to use but which provides limited insight into the internal hardware states. Received Signal Strength (RSS) values were a logical starting point [29], reducing the dimensionality of the channel to a single scalar value corresponding to received power (a function of channel gain). A simple extension of this, which was enabled by network cards such as the Intel IWL-5300, was to consider the frequency-dependent channel gain or equivalently Channel State Information (CSI) [33]. CSI-based solutions to the problem formulation of Equation (1) are so thoroughly investigated that they have spawned dedicated survey papers [34] and derivative methods including feature engineering of the CSI vectors [35], multi-antenna CSI [36], [37], or stacking of subsequent CSI samples in the time domain [38]. We formulate the expression of CSI at each time index i for M receive antenna ports ($M = P*M_I*M_{II}$ for a two-dimensional antenna array with P polarizations, M_I first and M_{II} second dimensions of the array) and S frequency samples, typically orthogonal frequency-division multiplexing (OFDM) subcarriers[2], as the complex-valued matrix $\mathbf{F}_i$:

---

[2]The measurement system described in Section IV utilizes LTE signals. We formulate our definitions accordingly as generic for OFDM systems and note that use of OFDM is likely to continue for many use cases even with the advent of 6G systems [39].

$$\mathbf{F}_i \in \mathbb{C}^{S \times M}. \tag{2}$$

Numerous other representations have been tested that employ additional signal processing to produce representations that are intuitive or hypothesized to provide compelling performance gains in the face of aleatoric or epistemic uncertainty. The domains tested include angles of arrival [40]; channel impulse responses [41], [32]; delay spreads or number of MPCs [42]; hybrids of various measurements defined in 3GPP standards [43]; angular-delay domain [27], [44], [45], [46]; and RSS augmented by Reconfigurable Intelligent Surfaces (RIS) [47].

The user navigation state representation $\mathbf{x}_i$ is similarly flexible. Most works on the subject consider a two-dimensional Cartesian position and formulate a two-dimensional regression problem, but it is feasible to parameterize user position discretely in a grid, by building and floor [48], [49], or as any other kind of classification problem. Information about uncertainties (practical for many navigation problems) is also directly estimable via a network, as has been demonstrated through direct estimation [50] and through probability maps [51]. The user states estimated in this paper are position and orientation in a two-dimensional plane: an East-West coordinate x_e, a North-South coordinate x_n, and a heading (or equivalently, yaw) value x_γ in degrees ranging from $[-180°, 180°]$:

$$\mathbf{x}_i = [x_e, x_n, x_\gamma]^T \in \mathbb{R}^3. \tag{3}$$

Remark 1
Some "fingerprinting" literature for multi-antenna systems formulates a tracking problem, where inferences are made about a mobile agent's state based on multi-antenna measurements on the network side. The measurement system in this work (described in Section IV) employs a massive antenna array for a mobile receiver, which provides high-resolution observation of signals transmitted by a single antenna port from a BS. In our previous work, we noted that user orientation is either interesting to use as an input to improve performance [25] or to add as an estimable parameter if the channel representation is rich enough to allow for it [13].

B. Fingerprinting to Wiometrics

In fingerprinting in the literal sense with human fingers, the goal is to effectively capture friction ridges on the fingers as a proxy for identity for the purpose of *verification*, confirming a one-to-one comparison with a database entry, or for *classification*, conducting a one-to-many match [52]. The recorded pattern from the individual's fingers is analogous to $\mathbf{Y}_i$ in Equation (1), and identity to $\mathbf{x}_i$. Channel fingerprinting can be formulated similarly as a *proximity* problem with a binary one-to-one hypothesis, as a one-to-many database *region classification* problem, or as a continuously-defined output space in multiple dimensions [23].

The analogy between channel fingerprinting and human fingerprinting is reasonably apt if judged by the performance criteria in each case. The proxy values $\mathbf{Y}_i$ should be as invariant as possible to environmental or measurement aperture changes; variability for wireless fingerprints is introduced by changes in scatterer geometry or differences in receiver hardware. For human fingerprint recording, variability can stem from non-uniform contact, variable skin condition, and dirty sensor plates [53]. The proxy values in either case should be *collectable*, in that the measurement apparatus should be reasonable in terms of hardware and software cost and complexity. Critically, the inherent challenge in developing reliable parametric models for human fingerprints or wireless channels in complex propagation environments means that statistical methods are attractive.

The analogy fails in that human fingerprints are a specific and unchanging trait for an individual, whereas wireless channel "fingerprints" can be almost arbitrarily imaginative, as the numerous representations cited in the previous subsection demonstrate. The analogy to human fingerprinting may have made sense when hardware limitations meant that a scalar value for signal strength was the only easily realizable form for $\mathbf{Y}_i$ to take, but a more appropriate analogy is to *biometric authentication*, of which human fingerprinting is just one subcategory [54]. Facial and voice recognition are also well-known biometric authentication methods, but even less well-known methods such as gait recognition or hand geometry recognition are also proxies for identity, useful when discretion or non-intrusiveness are desirable for inference. With this in mind, we suggest that all such non-parametric wireless navigation approaches (which do not explicitly calculate bearings and ranges to landmarks) should be renamed *wiometric navigation*, and the underlying channel representations to *wiometrics*, for wireless observation metric or simply wireless metrics in homage to biometrics. Four wiometrics are presented for analysis in the following subsection and examined for the duration of the manuscript.

C. A Selection of Wiometrics for Analysis

Four channel representations are chosen for analysis, using the same measurement aperture with varying degrees of feature engineering, listed in ascending order of computational complexity and illustrated briefly in Fig. 1. As the figure shows, the CSI representation (complex-valued transfer function per antenna) is the basis for further signal processing to create real-valued representations[3] used for training ANNs.

For the remainder of the manuscript the subscript indicating time index i is dropped for brevity, and elements of the matrix $\mathbf{F}$ are indicated with subscripts for the j-th row and k-th column as $f_{j,k}$.

---

[3]Complex-Valued Neural Networks (CVNNs) have shown promise for signal processing problems in speech, sonar, and wireless communications. Real-valued representations separating the amplitude and phase components can create a "dangerous" degree of freedom [55] and may be prone to over-fitting. Employment of CVNNs is included in the Conclusions (Section VII) as suggested future work.
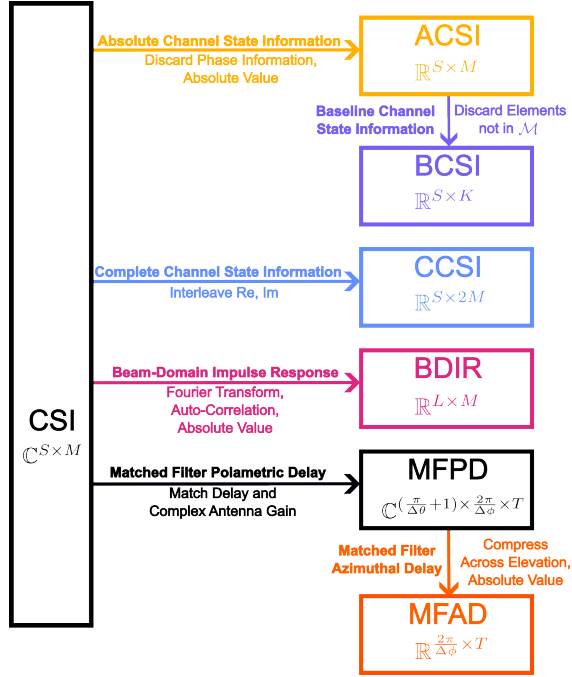
Fig. 1. Block diagram of channel representations (wiometrics). Note that Channel State Information, the complex-valued transfer function for each antenna, is the basis for all subsequent representations.

1) ACSI/BCSI/CCSI - Absolute/Baseline/Complete Channel State Information: As discussed in Section II-A, the frequency-dependent transfer function has long been used for non-parametric positioning methods, including the frequency response of multiple antennas for multi-receive antenna systems. The relationship of the phases among subcarriers is influenced by the complex antenna gain pattern as well as the total path length (delay) of individual MPCs. Physical movement in the direction of an arriving MPC entails a phase rotation as the path length decreases, and correspondingly higher power contribution. If the individual MPCs can be resolved, this geometric relationship can even be used for precise (differential) tracking of movement [56]. Taking the absolute value of the frequency response is equivalent to discarding that phase information, but this is frequently done for convenience (owing to the difficulty of implementing CVNNs). The Absolute Channel State Information (ACSI) is denoted as $\mathbf{Y}_{ACSI}$:

$$\mathbf{Y}_{ACSI} = |\mathbf{F}| \in \mathbb{R}^{S \times M}. \tag{4}$$

The measurement system described in Section IV employs a large number of antennas, and to offer a baseline performance comparison representative of much of the previous work summarized in Section II-A, a reduced version is also offered with only a subset of the antenna ports $\mathcal{M} \subset m_1, m_2, \ldots m_K$. This reduced version of ACSI is called Baseline Channel State Information (BCSI) and denoted as $\mathbf{Y}_{BCSI}$:

$$\mathbf{Y}_{BCSI} = \begin{bmatrix} \mathbf{col_{m_1}}(\mathbf{Y}_{ACSI}) \ldots \mathbf{col_{m_K}}(\mathbf{Y}_{ACSI}) \end{bmatrix} \in \mathbb{R}^{S \times K}. \tag{5}$$

Intuitively, $\mathbf{Y}_{ACSI}/\mathbf{Y}_{BCSI}$ should not perform as well as systems that retain phase information because the absolute and relative phases of signals are the fundamental tool for calculation of ranges and bearings; GNSS uses code and carrier phase to set up the multi-lateration problem, for example. However, information about position and orientation can still be inferred through signal magnitude and the relationships among magnitudes in frequency and among antennas.

An alternative representation to retain the phase information is to split out the real and imaginary components of $\mathbf{F}$ by interleaving on a column-by-column basis to form a new matrix, with twice the number of columns. Phase and amplitude are both maintained and no information is discarded, so the representation is referred to as Complete Channel State Information (CCSI) and $\mathbf{Y}_{CCSI}$ is defined as follows:

$$\mathbf{Y}_{CCSI} = \begin{bmatrix} Re(f_{1,1}) & Im(f_{1,1}) & \ldots & Im(f_{1,M}) \\ Re(f_{2,1}) & Im(f_{2,1}) & \ldots & Im(f_{2,M}) \\ \vdots & \vdots & \ddots & \vdots \\ Re(f_{S,1}) & Im(f_{S,1}) & \ldots & Im(f_{S,M}) \end{bmatrix} \in \mathbb{R}^{S \times 2M}. \tag{6}$$

The components are interleaved rather than stacking all real components and all imaginary components into sub-matrices to capture the relationships in phase for adjacent subcarriers with convolutional methods, discussed in Section III-B2. Although all the information is preserved, the relationships between the real and complex components are decoupled.

2) BDIR - Beam-Domain Impulse Response: Several methods have been proposed which exploit auto-correlation of received signals, under the hypothesis that auto-correlation across time, frequency, and/or space should serve as an effective proxy for position. If used as the input for an ANN, this can be regarded as a form of feature engineering. In [57], the authors propose using a vectorized form of the matrix $\mathbf{F}$, by stacking the columns of the CSI matrix $\mathbf{F}$ into a "radio geometry" vector $\mathbf{f}_{RG}$:

$$\mathbf{f}_{RG} = \begin{bmatrix} \mathbf{col_1(F)} \\ \mathbf{col_2(F)} \\ \vdots \\ \mathbf{col_S(F)} \end{bmatrix} \in \mathbb{C}^{(M*S) \times 1}. \tag{7}$$

Taking the outer product $\mathbf{f}_{RG} * \mathbf{f}_{RG}^H$ "lifts" the vectorized form to a higher dimensional feature geometry space which has dimensionality corresponding to the number of subcarriers and antennas multiplied $\mathbb{C}^{(M*S)\times(M*S)}$. This may subsequently be scaled or other transforms applied before dimensionality reduction (the Channel Charting function) is used to create a low-dimensional representation that is useful for network functions as an effective proxy for user position. This has been extended to be mixed with labeled data for enhanced positioning [58], [59]. The enormous dimensionality of the "space lifted" channel provides a large input space for pattern finding, but also entails computationally intensive matrix operations that grow as the square of the number of subcarriers and number of antennas.

In [49], the authors also seek to do feature design for multi-antenna CSI in order to construct a channel representation that is robust against hardware impairments, computationally efficient, and which retains the essential information relevant for positioning. First, a two-dimensional FT is taken across the two physical dimensions of a planar antenna array M_I and M_{II} for transformation into the beam domain. As with Channel Charting, auto-correlation is used, but a decimated frequency-domain version rather than across a space-lifted version, creating a shortened impulse response. The subsequent representation is referred to here as the Beam-Domain Impulse Response (BDIR).

More precisely, the beam-domain transformation entails first rearranging $\mathbf{F}$ into a four-dimensional array. The four-dimensional beam-domain version $\mathbf{Y}_{BD,4D}$ is then formed by taking the FT across the M_I and M_{II} dimensions of the two-dimensional antenna array[4], and then rearranging back into the original shape along the same dimensions:

$$
\begin{aligned}
\mathbf{F} \in \mathbb{C}^{S\times M} &\rightarrow \mathbf{F}_{4D} \in \mathbb{C}^{S\times M_I \times M_{II} \times P} \\
\mathbf{Y}_{BD,4D} &= \mathcal{F}_{M_I, M_{II}}\{\mathbf{F}_{4D}\} \\
\mathbf{Y}_{BD,4D} &\rightarrow \mathbf{Y}_{BD} \in \mathbb{C}^{S\times M}.
\end{aligned}
\tag{8}
$$

Auto-correlation is subsequently applied along the frequency domain of $\mathbf{Y}_{BD}$ to remove the impact of timing advance and certain other hardware impairments. Both a decimation (downsampling) rate δ_{dec} (not every possible subcarrier spacing is considered) and a maximum number of adjacent frequency bins δ_{max} are used. In the original paper [49], a maximum subcarrier spacing of $\delta_{max} = 64$ is used with a decimation rate of $\delta_{dec} = 4$, resulting in $L = \lfloor \frac{\delta_{max}}{\delta_{rate}} \rfloor = 16$ subcarrier spacings $\delta_l \in [4, 8, ..., 64]$. The auto-correlation function R_{δ_l} for an offset of δ_l is expressed $R_{\delta_l}(\mathbf{y}) = \sum_{n=1}^{\delta_{max}} y(n)y^*(n+\delta_l)$ and applied for each antenna and time offset of $\mathbf{Y}_{BD}$:

$$
Y_{BDIR} = \begin{bmatrix} |R_{\delta_1}(\mathbf{col_1}(\mathbf{Y}_{BD}))| & \dots & |R_{\delta_1}(\mathbf{col_M}(\mathbf{Y}_{BD}))| \\ \vdots & \ddots & \vdots \\ |R_{\delta_L}(\mathbf{col_1}(\mathbf{Y}_{BD}))| & \dots & |R_{\delta_L}(\mathbf{col_M}(\mathbf{Y}_{BD}))| \end{bmatrix} \in \mathbb{C}^{L\times M}.
\tag{9}
$$

[4]For the measurement platform described in Section IV, the two dimensions of the antenna array are considered as rings (four) and patches per ring (sixteen).

BDIR can be understood intuitively as a set of bins of frequency selectivity (concatenated to length L) across the beams of the receive antenna array. Rotation or movement will impact both dimensions simultaneously. Note that the FT across elements to formulate the beamspace representation in Equation (8) does not use the measured antenna pattern. This is advantageous in terms of computational efficiency, and the invariance to certain hardware calibration errors and timing mismatch is useful for practical systems. However, for the sake of maximizing performance, one more wiometric is suggested in the following subsection.

3) MFPD/MFAD - Matched Filter Polametric/Azimuthal-Delay: Decomposition of the channel into the temporal and spatial domains, as a discretized number of temporal-angular "bins", is appealing because it lends itself well to human intuition about what is happening as the geometry of the scenario changes. MPC path lengths and angles-of-arrival/departure change intuitively with the geometry of the scattering environment. As the user rotates in place, power is shifted along the angular bins. As the user moves closer or farther from the source of each arriving MPC, power is shifted in the delay bins. First proposed by [27] for a two-dimensional simulated scenario, variations of this Angle-Delay Channel Amplitude/Power Matrix (ADCAM or ADCPM) [44], [60], [46], [61] or Angle-Delay Profile (ADP) [45], [62], have been popular in literature.

We use the abbreviation Matched Filter Polametric-Delay (MFPD) to emphasize that the complete three-dimensional radiation pattern per antenna port is used for formulating the angular response as in [13]. The antenna response matrix for all antennas in discrete steps of $\Delta\theta$ for the elevation domain and azimuthal angle steps of $\Delta\phi$ is given as $\mathbf{A}$:

$$\mathbf{A} \in \mathbb{C}^{M \times ((\frac{\pi}{\Delta\theta}+1)*(\frac{2\pi}{\Delta\phi}))}. \tag{10}$$

A tacit assumption in the MFPD/Matched Filter Azimuthal-Delay (MFAD) representation of the channel is that transmitter-receiver time synchronization is guaranteed and does not drift. In [49], the authors make the point that such a representation presumes absolute time synchronization between sender and receiver, with little allowance for timing advance, hardware impairments, or oscillator drift. Timing mismatch is discussed further in Section IV; for now we formulate the matched filter time-domain response per antenna and discrete time step τ for a maximum number of time steps T as the matrix $\mathbf{D}$:

$$\mathbf{D} = \begin{bmatrix} 1 & e^{2\pi f_1 \tau} & \dots & e^{2\pi f_1 \tau (T-1)} \\ \vdots & \vdots & \ddots & \vdots \\ 1 & e^{2\pi f_S \tau} & \dots & e^{2\pi f_S \tau (T-1)} \end{bmatrix} \in \mathbb{C}^{S \times T}. \tag{11}$$

Combining both the antenna and phase-delay elements of the matched filter response with the per-antenna and per-subcarrier matrix $\mathbf{F}$ yields the two-dimensional MFPD matrix $\mathbf{Y}_{MFPD,2D}$:

$$\mathbf{Y}_{MFPD,2D} = \mathbf{A}^H \mathbf{F} \mathbf{D}^* \in \mathbb{C}^{((\frac{\pi}{\Delta\theta}+1)*(\frac{2\pi}{\Delta\phi}))\times T}, \tag{12}$$

which can be rearranged into a three-dimensional array in the order of elevation, azimuth, and delay:

$$\mathbf{Y}_{MFPD,2D} \in \mathbb{C}^{((\frac{\pi}{\Delta\theta}+1)*(\frac{2\pi}{\Delta\phi}))\times T} \rightarrow \mathbf{Y}_{MFPD} \in \mathbb{C}^{(\frac{\pi}{\Delta\theta}+1)\times(\frac{2\pi}{\Delta\phi})\times T}. \tag{13}$$

Summation (incoherent) across the elevation dimension (the n rows in the first dimension a of the three dimensions abc of the absolute value of the $\mathbf{Y}_{MFPD}$ matrix) yields the MFAD representation, which is the wiometric used in the remainder of the manuscript. For a system with limited resolution in elevation (as many terrestrial systems have), the simplification of working in two dimensions with a smaller input is a desirable trade-off.

$$\mathbf{Y}_{MFAD} = \sum_{a=1}^{\frac{\pi}{\Delta\theta}+1} |\mathbf{Y}_{MFPD,abc}| \in \mathbb{R}^{(\frac{2\pi}{\Delta\phi})\times T}. \tag{14}$$

III. Learning Frameworks

A. Standard Methods and Deep Learning

Feature-matching for navigation encompasses a broad family of technologies and methods, from Terrain-Referenced Navigation in aviation to gravity gradiometry on submarines [7]. A recent comprehensive survey on machine learning with a particular focus on wireless navigation follows a common grouping convention that includes supervised, semi-supervised, and unsupervised methods [23]. Within the supervised category two subcategories are identified. The first subcategory is "Standard Methods" including k-Nearest Neighbor (kNN), Kernel Based Methods, Gaussian Process-based methods, and Trees/Ensemble methods. The second category is "Deep Learning" methods, with particular emphasis on Deep Learning, which has been the primary solution for most learning problems in recent years[5]. We compared one "standard" method (kNN) and deep learning in our previous work [25].

Popular classifiers for computer vision competitions such as AlexNet [63] or ResNet [64] and object classifiers such as YOLO [65] have inspired use of ANNs in virtually every domain (see, e.g., "Applications of Machine Learning" in [66]). An even more recent trend dominating machine learning literature, not mentioned in [23], is the trend of using Transformers [67]. This has dominated Natural Language Processing (NLP) research, and has already attracted interest in computer vision [68]. No Transformers are implemented

---

[5]Deep Learning is technically a subcategory of ANNs, but few ANNs are employed that do not meet the criterion of being "deep" (having hidden layers).

in this work, but suggestions about their future potential for navigation are considered in the Discussion (Section VI).

B. Artificial Neural Networks

ANNs come in many shapes, sizes, and architectures. Networks in computer vision have evolved toward larger and deeper networks for achieving breakthrough performance gains [65]. For wireless navigation using ANNs, hierarchical structures have been proposed to reduce total processing time, even for a single transmitter scenario [61]. This section is not intended to be a comprehensive survey of recent ANN use for wireless navigation, but aims to provide a sampling of recent results; and, for a set of ANNs described in the following subsections, together with the wiometrics of Section II and dataset generated from Section IV, we attempt to draw lessons of general interest for wireless navigation with ANNs in Section VI.

1) Fully-Connected Networks: The simplest ANN structures are Fully-Connected Neural Networks (FCNNs), in which all layers are flattened into one-dimensional structures and adjacent layers have direct connections among all nodes. For the wiometrics of Section II, this vectorization entails equal treatment of all input bins, and any apparent differences in the order of vectorization (drawing) are merely different drawings of the same graph with all nodes in adjacent layers having connecting edges. The manner in which the CSI rows and columns were interleaved to create the CCSI matrix becomes irrelevant, for example. The same is true for the azimuthal-frequency bins of the MFAD representation, every angular-delay bin will be represented.

Previous work on the subject has shown markedly worse performance for FCNNs compared to similarly-sized networks employing parameter sharing [69]. In this work, this is tested again employing FCNNs that are given a moderate advantage to parameter-sharing architectures in terms of the total number of weights employed. Approximately 8 million parameters are used for each of the FCNNs. Precise network dimensions are listed in the appendix under the heading **Fully-Connected Networks**.

2) Convolutional Neural Network: Convolutional Neural Networks (CNNs) are learning structures that apply parallel kernels to adjacent input values through convolution operations for each convolutional layer, typically before a vectorization (flattening) operation is used for the final few fully-connected layers including the output layer. CNNs in the MFAD domain were first suggested by Vieira et al. in [27], under the hypothesis that they should prove superior for the same reasons that CNNs have become ubiquitous in computer vision. CNNs that have input sizes comparable to well-known image recognition networks are used in this paper as a baseline for performance analysis. It is common practice to sub-sample ImageNet images [70] down to 256x256 or similar, for example, and the parameters in Fig. 1 are tuned accordingly. Specific network sizes are listed in the appendix, but the models employed in this work are comparatively modest in terms of trainable parameters. Approximately 4 million parameters are used as a baseline for establishing

CNN performance, with an additional round of experiments testing around 40 million parameters. They are listed under the headings **Convolutional Networks (Small)** and **Convolutional Networks (Large)** respectively in the appendix. This is far fewer parameters than the hundreds of millions employed by popular ImageNet winners for classification to tens of thousands of categories.

IV. GROUND VEHICLE MEASUREMENTS

A. LTE Signals

The signals in LTE are split into frames and subframes. A number of synchronization symbols are defined that are necessary for a User Equipment (UE) to acquire basic network information and to perform coherent data demodulation [71]. The idea of using these symbols for multilateration (a pseudorange model similar to GNSS) has been explored by multiple research groups [12], [72], [73]. For a detailed description of how such symbols can be acquired and used, readers are referred to [74]. The signals of interest, which can be decoded opportunistically (without network collaboration or knowledge) are the Primary Synchronization Signal (PSS), Secondary Synchronization Signal (SSS), and Cell-specific Reference Signals (CRS). Fig. 2 shows how these symbols are structured in LTE Frequency Division Duplexing (FDD) subframes and frames.
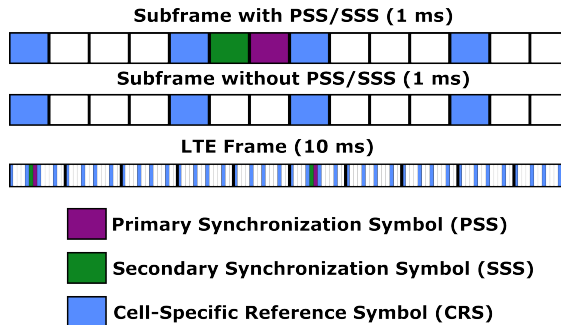
Fig. 2. LTE Symbol timing for downlink reference symbols. CRS are broadcast most frequently and, though the frequency dimension of the LTE resource grid is not illustrated, span the whole channel bandwidth, offering better time resolution and more frequent observation than PSS/SSS.

CRS are transmitted with the highest frequency and span a larger bandwidth than PSS/SSS, so they offer better time resolution and more frequent observations for channel estimation. Explicit signals for positioning were introduced in LTE release 9, but are not widely deployed by network operators.

Fig. 3. Picture and block diagram of LTE measurement system. A GoPro MAX panoramic camera was used to capture video of the environment as seen by the antenna array, and an OXTS 3003G system was used for ground truth pose estimates. All systems held time synchronization with GPS Time as a time base.

B. Measurement System

The primary components for our measurement system are shown together with a photograph in Fig. 3. The backbone of the measurement system is a Software-Defined Radio (SDR) from National Instruments, USRP-2953R, together with the LabVIEW Communications Application Framework. A Stacked Uniform Circular Array (SUCA) antenna with 128 ports (64 dual-polarized patch antennas in four layers of 16 elements each) was mounted on top of the vehicle. Such arrays are used in channel sounding [75] and provide significant array gain and angular resolution, particularly in the azimuthal domain. After network acquisition of Base Station A, samples in the time domain of PSS, SSS, and CRS were continuously logged on a laptop for post-processing and subsequent channel estimation. A rubidium frequency standard, disciplined by GPS prior to the measurements, was used to provide a highly stable time reference. It should be noted that the measurement system switches at the speed of two CRS transmissions per antenna (see Fig. 2); with four symbols per subframe, that means at least 64 subframes are required to cycle among all antennas. Sampling on all antennas (one snapshot) is completed every 75 ms, allowing time for adjusting the Automatic Gain Control (AGC) in the receiver. This sequential sampling of antennas implements sharp practical limitations on driving speed, because even with a speed of 1.0 m/s, the array moves half a wavelength over one snapshot. This limitation is applicable to our single RF-receiver measurement set-up, but could be negated with a more complicated measurement system employing parallel RF receive chains.

Ground truth estimates of vehicle position and orientation are generated using a dual-antenna, dual-constellation high-precision GNSS-Inertial system from OXTS, the RT3003G, which advertises 1 cm position accuracy and 0.05° heading accuracy, though these data sheet values might not be fully realized with long and slow trajectories through obstructed-sky environments. Post-Processed RTK was performed using observation data from the SWEPOS network to give the best possible pose estimates. The single-band GPS receiver of the SDR was used primarily for time synchronization among systems, but

the positioning performance of a commercial GPS receiver in the test environment is an interesting comparison, and is included in Section V, denoted SDR GPS-L1. Panoramic video from a GoPro MAX camera mounted on the antenna array was used for manual inspection in the event of unexpected results from the other systems. The steps for the measurement are shown in Figure 4.
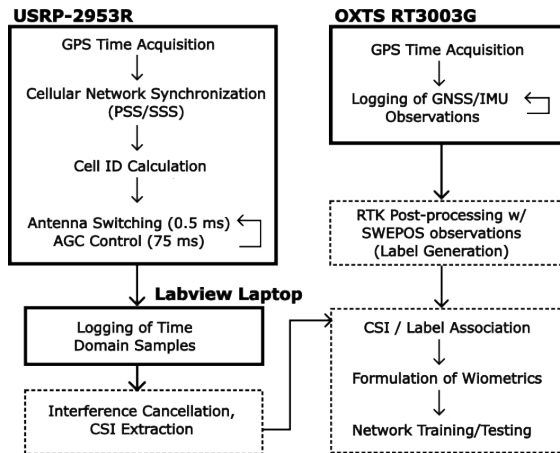

Fig. 4. Flow chart for vehicle measurements. The dashed lines indicate steps performed offline, but in operation the inferences with the trained network would be made online. The interference cancellation scheme is described in detail in [76].

C. Test Route

A test route was driven in an urban canyon environment in downtown Lund, Sweden. Four laps were driven (starting point 55.71055°N, 13.18919°E). Two laps were driven in the counterclockwise (CCW) direction and two were driven clockwise (CW). The commercial base stations and their locations relative to the test vehicle driving route are shown in Fig. 5, together with the inset plot showing the three-dimensional building geometry. The total distance traversed for each lap was about 400 m, spanning just over 100 m East-West and North-South. The average driving speed[6] was 1.0 m/s with a total of about 22,000 snapshots, each with a duration of 75 ms.

The commercial LTE BSs are from a single operator broadcasting at a center frequency of 2.66 GHz ($\lambda = 11 \ cm$). A single sector (cell ID 376) of the the primary transmitter BS

---

[6]As stated in the previous subsection, the switching of the array is done at the rate of two CRS per antenna, which governs the channel coherence time and subsequent limitation on speed. A parallel receive apparatus would not have such a limitation but represents a significant increase in measurement complexity.
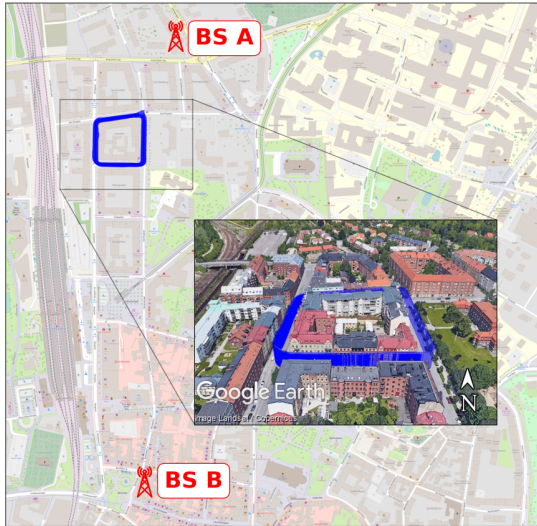
Fig. 5. The two commercial base stations in Lund, Sweden (55.71°N, 13.19°E) and the drive route for the four laps. The inset plot shows the urban canyon three-dimensional geometry of the route, courtesy of Google Earth. Note that base station locations are not used for navigation.

A is used as the only data input for all of the single base station (-S-) networks listed in the appendix. One sector (179) of a second base station is used as the additional input for the double base station (-D-) networks[7]. BS A is not physically visible for any section of the route, it is entirely non-LoS. BS B is physically visible in the Eastern section of the route at a distance of about 650-750 m. It provides at least one strong LoS path for most of the Eastern section and limited non-LoS energy for some other sections of the route. A novel scheme for handling interference among base stations was employed, described in previous work [76].

The Eastern and Western sections of the drive route are multi-lane roads with offsets in the lateral direction (lane-center to lane-center) of at least 3 m for opposing driving directions. The Northern and Southern sections are only a single car width with parked vehicles on each side.

The data are split into training sets in two different ways as shown in Fig. 6 together with the approximate perimeter of the route. First, in the Low Epistemic Uncertainty (LEU)

[7]In a parametric navigation problem, this would entail improved Geometric Dilution of Precision (GDOP), but the concept is not directly translatable here. Intuitively, one would expect more information to result in better performance.

test case, the complete data from all four laps are pooled together and a random subset of 25% of the whole measurement series is reserved for testing. Next, in the High Epistemic Uncertainty (HEU) test case, one of the four laps is reserved as a test set while the other three laps are used as training data. Having a dedicated test lap (the HEU case) entails having combinations of position and heading in testing that deviate from all training data by several meters and tens of degrees. Additionally, starts and stops occur at different locations and the scatterering environment varies with traffic in a way not fully captured in any training data; other cars and buses appear at different sections of the drive route with each loop. Additionally, only one of the three HEU training laps represents the vehicle traveling in the same direction as the test data, or in the same lane for the two-lane sections. The LEU training set includes drive data in both directions, and it is unlikely that relevant objects in the dynamic traffic environment (a passing bus, for example) will not be captured in any training samples.
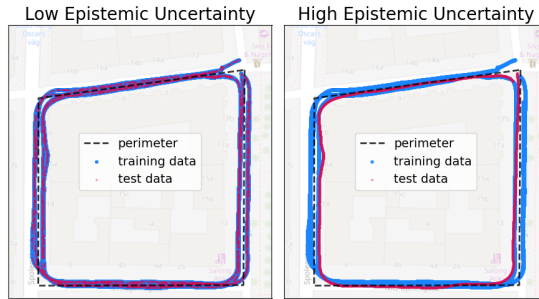

Fig. 6. Two test/train splits representing very different levels of epistemic uncertainty with approximately the same number of training and test points in each. In the "Low Epistemic Uncertainty" (left) plot, a randomly-chosen 25% of data points from the four laps are reserved for testing. In the "High Epistemic Uncertainty" (right) plot, one of the four laps is reserved for testing. The approximate perimeter of the route is also shown.

The main parameters of the measurement system and the specific test campaign are summarized in Table I.

Remark 2

Scaling systems of the sort described here for broad deployment would require solving a number of practical interrelated challenges. Large quantities of labeled data are needed [77], the underlying data is impacted by seasonal and environmental changes and is therefore non-stationary, and centralizing training requires massive data storage and transfer. While vehicular applications employing crowd-sourced HD Maps [78], [79] and numerous ANNs [80] are in some ways well-suited for such problems, solutions specific to wiometrics are desirable. For example, labels could be generated with an annotation pipeline using either

TABLE I
TABLE OF PARAMETERS FOR EXPERIMENT

Parameter Name				Value	
Center Frequency f_0				2660 MHz	
Channel Bandwidth				20 MHz	
Num. Subcarriers				200	
Antenna Ports				128	
Snapshot Duration				75 ms	
Lap number	1	2	3	4	Total
Num. Snapshots	4831	5378	5052	4618	19879
Distance (m)	363	365	359	362	1449
Avg. Speed (m/s)	1.00	0.91	0.95	1.05	0.97
Direction	CCW	CW	CW	CCW	-

HD Maps [81] or with Post-Processed RTK (see Figure 4), or a combination of the two. Requirements for labeled data could also be relaxed and distribution shift mitigated by employing weakly or semi-supervised methods [59], and data storage and transfer needs reduced with federated learning [82].

V. RESULTS

A. Channel Results

A single channel measurement (derived from CSI values, see Fig. 1) is shown as each of the four wiometrics, illustrated in Fig. 7. The ACSI representation is reasonably intuitive; certain antenna ports receive significantly more energy than others, because the SUCA antenna consists of elements with high directionality. There is some frequency dependence, but over the limited bandwidth of the channel it does not lend itself to intuition. The CCSI representation shows a similar pattern but with more information than is contained by ACSI; taking absolute values of the complex CSI entails information loss. As the only representation that takes on both positive and negative values, the color scheme for CCSI represents larger negative values as darker blue and larger positive values as darker red. The beam-domain transformation of BDIR results in clear patterns across the beam dimension, but not at the same indexes as those corresponding directly with antenna ports, as ACSI and CCSI have. The correlation across frequencies uses only a subset of frequency offsets, representing a significant compression in input dimension compared with using all S subcarriers (see the appendix for dimensions of each representation). Finally, the MFAD wiometric provides a highly intuitive spatial interpretation. Energy is received primarily from the rear and left (90 to 180 degrees in azimuth) for the first arriving path around time index 50, and then subsequent incoming energy arrives from the left side up until around time index 130.
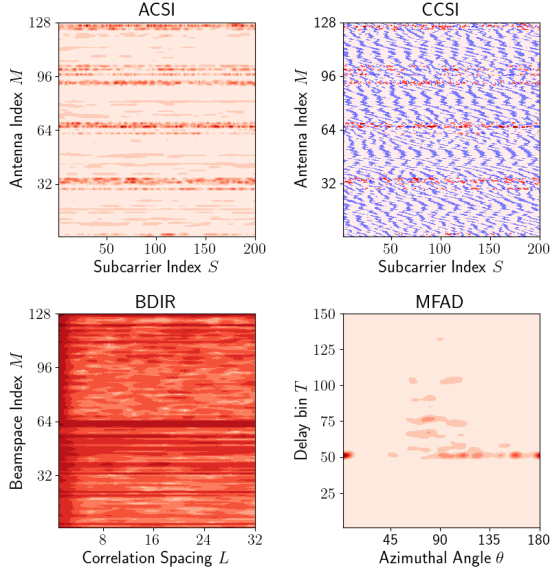
Fig. 7. Visualization of the same channel measurement in the four wiometrics for snapshot index 11,000, in the Southeast corner of the route. Note that CCSI uses a color scheme that permits for negative values, (shown as increasingly blue for higher negative values).

B. Baseline Performance

The baseline performance is illustrated for the BCSI wiometric as well as for the SDR GPS-L1 receiver in Figure 8. Performance is visualized through cumulative distribution functions showing horizontal position error in meters, as well as heading error spanning from $[0°, 180°]$. Selected values for all combinations are also included in Tables II and III. Note that the GPS receiver is treated as a point source and does not estimate heading, though differential position estimates are frequently employed as a proxy for course. The GPS receiver also filters position estimates, but in a manner that is opaque to the end user. Even in the urban canyon environment, the GPS receiver performs better than the baseline wiometric representation BCSI, especially at the upper end of the error distribution where BCSI has a long error tail.

The performances for BCSI and SDR GPS-L1 are also illustrated in map form in Figure 9. BCSI incurs extreme errors with some regularity, usually resulting in an incorrect projection to other parts of the route. Occasionally, estimates of position and heading are generated that, while inside the bounds of training data for individual input components, are far from any combination encountered in the training set. SDR GPS-L1 errors are
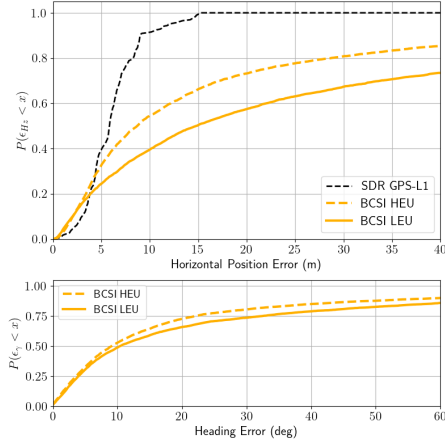
Fig. 8. Baseline position errors and heading errors for the SDR GPS-L1 receiver and baseline representation BCSI. BCSI experiences large tail errors. The GPS receiver is a point source and does not estimate heading.

primarily lateral to the direction of travel, corresponding with the expected excess MPC length from satellites observations in the directions where the sky is blocked in the urban canyons.

C. Network Size and Architecture

Comparison of the wiometrics using CNNs (see the appendix under the heading **Convolutional Networks (Small)**) is shown in Fig. 10. Position errors and heading errors are both higher for the HEU case where the test set includes combinations of position and heading that are less representative of the training set. The MFAD representation performs best for both position and heading for the LEU and HEU cases, but performs only marginally better than the other wiometrics for the HEU case. ACSI performs worse than CCSI, indicating that the information loss incurred when discarding phase information negatively impacts performance. The CNNs seem to be capable of exploiting phase information and making inferences about position and heading.

To provide additional intuition beyond the error distributions, the HEU result from Fig. 10 for the MFAD representation (CNN-MFAD-S-3.8M in the appendix) is overlaid on a map in Fig. 11 with the training data, test data (ground truth), and estimated states. Predictions are effectively mapped to the input space of the training set, but the network does not extrapolate beyond the exterior of the training data bounds. Three sections where this is particularly visible are emphasized with red ellipses. In the Southeast corner and Western
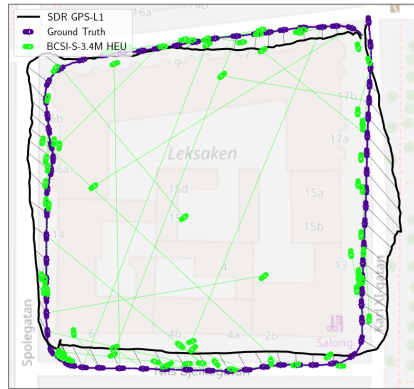
Fig. 9. Map view illustrating the position errors for the baseline BCSI network and the SDR GPS-L1 receiver. The GPS-L1 receiver suffers from multipath and experiences error primarily perpendicular to the direction of travel.
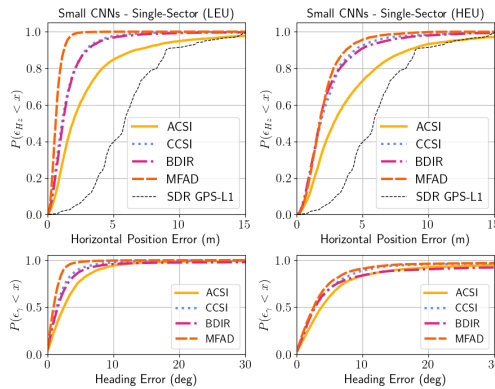
Fig. 10. Position errors and heading errors for similarly-sized networks for the various channel representations with low epistemic uncertainty (left) and high epistemic uncertainty (right). See Fig. 6 for an illustration of the test/train split.

section the vehicle cuts farther to the inside than was experienced in the training set, and predictions are mapped closer to points from training. In the Northeast corner, the first few points of the test set are not covered by the training set, but are projected to the wrong side of the training data (inside rather than outside).

Fig. 11. Predictions and ground truth for the MFAD representation CNN-MFAD-S-3.8M HEU overlaid on a map for the high epistemic uncertainty case. Note that the network does not tend to project to places outside the training set (emphasized with dashed red ellipses).

Repeating the experiment using different training laps yielded similar results in terms of error distributions as well as the underlying pattern of effectively projecting test data to data in the training set. While this might be an indication of over-fitting, using a smaller number of training epochs or smaller learning rate did not decrease the error or improve the ability of the network to extrapolate effectively toward the correct position and heading.

The experiment was repeated using approximately an order of magnitude higher number of weights in each of the networks (see the appendix under the heading **Convolutional Networks (Large)**) and the results are shown in Fig. 12. Performance is marginally better than with the smaller networks, for the MFAD and BDIR representations, but worse especially in the error tails of the ACSI and CCSI representations.

The results of the same input data with FCNNs (see the appendix under the heading **Fully-Connected Networks**) are shown in Fig. 13. Performance is markedly degraded compared with the baseline CNNs of the previous section, despite the networks having twice the number of trainable parameters, with the exception of the MFAD representation, which has similar performance. This indicates that the convolution operations are extracting useful information for all the wiometrics, but that the feature engineering going into creation of MFAD may be performing a function similar to what is being learned by the network. Heading estimates in particular are significantly degraded, and for the BDIR representation even more than for the other representations which use either antenna indexes or the complex radiation pattern. The BDIR heading performs similarly to blind
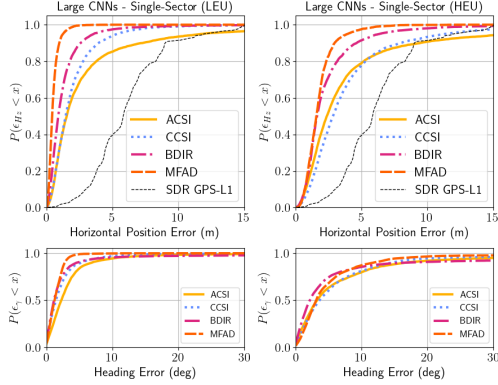
Fig. 12. Position errors and heading errors for the four representations with larger convolutional neural networks. Each network has tens of millions of parameters, approximately an order of magnitude more than is shown in Fig. 10.

sampling of a uniform distribution from $[-180°, 180°]$. Another curiosity is that for the LEU case, ACSI performs better than CCSI, indicating that the information loss from discarding phase information is actually beneficial, possibly because values learned for phase over the spacing of a few wavelengths tend to only contribute to overfitting, whereas the convolutional operations in the CNNs learn more meaningful features about adjacent frequencies and antennas.

D. Multiple Base Stations

Finally, results for CNNs utilizing both BSs (both BS A and BS B from Fig. 5) are shown in Fig. 14 and Fig. 15. For the MFAD and BDIR representations the use of the second BS results in superior performance (except for large heading tail errors for BDIR-HEU). Addition of the second BS leads to significantly worse performance for ACSI and CCSI in the HEU case, even if it improves performance nominally in the LEU case. Performing three-dimensional convolutions significantly increases training time and inference at run-time, and for these representations it results in worse performance.

E. Summary of Results

Position and heading error values for the 68th, 95th, and 99th percentiles are included in Table II and Table III, under the network names from the appendix. Individual wiometrics are sorted into adjacent rows to facilitate comparison. It is apparent that LEU almost always performs better than HEU; it is unsurprising that generalization to new data is difficult.
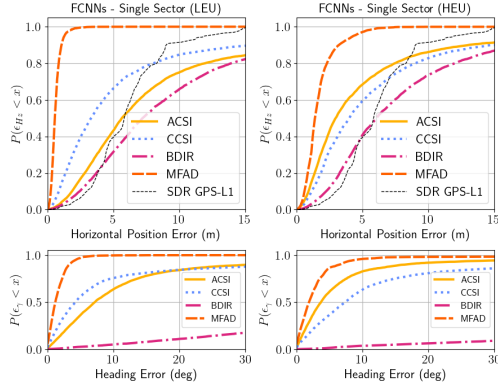
Fig. 13. Position errors and heading errors for the four representations with fully-connected neural networks. Each value of the input space is treated as a particular bin which is weighted in the first layer irrespective of adjacent bins in the original form.

Fig. 14. Position errors and heading errors for the four channel representations trained with data from two sectors and the two levels of epistemic uncertainty, one from each of BS A and BS B (see Fig. 5). The input data from each sector is stacked, and the convolutions are two-dimensional.

Some wiometrics are clearly superior to others; specifically, MFAD outperforms the other representations in all cases, while ACSI tends to perform the worst in most cases.
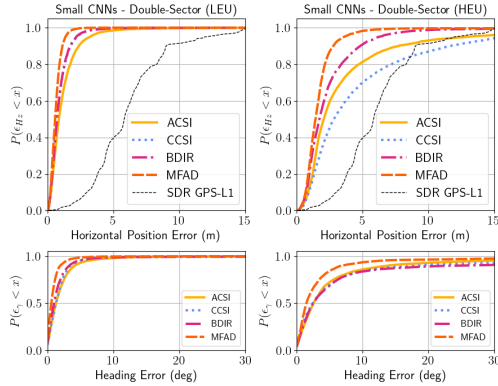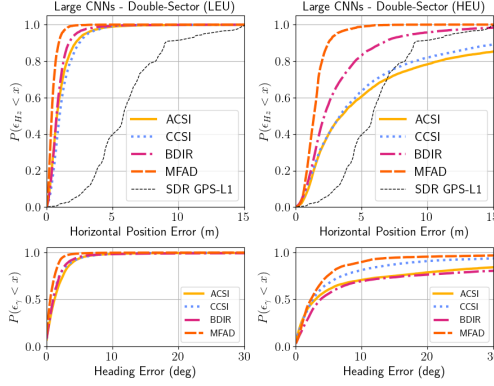
Fig. 15. Position errors and heading errors for the four channel representations trained with data from two sectors and the two levels of epistemic uncertainty, one from each of BS A and BS B (see Fig. 5). The data from each sector is stacked, and the convolutions are two-dimensional.

TABLE II
TABLE OF HORIZONTAL POSITION ERROR VALUES

Network Name	LEU Error (m)			HEU Error (m)		
Error Percentile (%)	68	95	99	68	95	99
SDR GPS-L1	6.8	9.0	12	6.8	9.0	12
CNN-BCSI-S-3.4M	31	98	112	16	89	108
FCNN-ACSI-S-7.5M	8.2	58	92	4.9	25	94
CNN-ACSI-S-3.9M	2.9	10	20	4.3	12	21
CNN-ACSI-S-30.6M	2.4	12	25	3.4	16	33
CNN-ACSI-D-4.5M	1.2	3.2	5.7	3.2	13	36
CNN-ACSI-D-33.0M	1.1	2.9	5.1	6.2	34	68
FCNN-CCSI-S-7.3M	5.2	37	86	6.3	28	86
CNN-CCSI-S-3.8M	1.6	3.9	6.7	2.6	5.9	12
CNN-CCSI-S-27.0M	2.0	5.3	9.7	3.9	11	21
CNN-CCSI-D-4.0M	1.0	2.2	3.4	4.7	16	25
CNN-CCSI-D-31.0M	1.4	3.1	4.8	5.6	21	36
FCNN-BDIR-S-7.5M	10	30	74	8.8	23	64
CNN-BDIR-S-3.3M	1.6	4.0	8.6	2.4	6.7	13
CNN-BDIR-S-39.9M	1.3	3.6	8.2	2.3	6.4	13
CNN-BDIR-D-3.8M	1.0	2.2	3.7	2.4	6.2	11
CNN-BDIR-D-35.7M	1.0	2.2	4.3	3.9	9.8	17
FCNN-MFAD-S-7.7M	0.7	1.3	2.0	1.8	4.3	6.0
CNN-MFAD-S-3.8M	0.8	1.5	2.1	2.3	4.8	8.0
CNN-MFAD-S-30.8M	0.6	1.2	2.0	1.9	4.0	6.2
CNN-MFAD-D-3.8M	0.7	1.4	2.0	1.8	3.5	5.9
CNN-MFAD-D-30.9M	0.5	1.1	1.7	1.7	3.1	5.1

TABLE III
TABLE OF HEADING ERROR VALUES

Network Name	LEU Error (deg)			HEU Error (deg)		
Error Percentile (%)	68	95	99	68	95	99
SDR GPS-L1	-	-	-	-	-	-
CNN-BCSI-S-3.4M	22	101	164	17	91	158
FCNN-ACSI-S-7.5M	11	60	134	5.9	35	129
CNN-ACSI-S-3.9M	3.8	11	30	5.7	32	122
CNN-ACSI-S-30.6M	3.2	11	31	5.9	31	124
CNN-ACSI-D-4.5M	2.1	6.0	14	4.1	29	114
CNN-ACSI-D-33.0M	2.0	5.4	14	7.9	92	146
FCNN-CCSI-S-7.3M	7.2	92	170	11	110	174
CNN-CCSI-S-3.8M	2.1	6.9	15	4.6	18	111
CNN-CCSI-S-27.0M	2.3	8.0	17	6.1	23	121
CNN-CCSI-D-4.0M	1.9	4.8	10	4.5	52	142
CNN-CCSI-D-31.0M	1.5	5.5	12	5.0	42	146
FCNN-BDIR-S-7.5M	97	157	174	134	170	178
CNN-BDIR-S-3.3M	2.3	8.8	102	4.7	71	170
CNN-BDIR-S-39.9M	1.8	8.8	116	3.8	60	163
CNN-BDIR-D-3.8M	1.4	4.5	14	4.9	120	178
CNN-BDIR-D-35.7M	1.6	4.9	23	23	148	176
FCNN-MFAD-S-7.7M	1.8	4.2	6.7	2.9	9.0	71
CNN-MFAD-S-3.8M	1.3	3.2	6.9	3.9	15	107
CNN-MFAD-S-30.8M	1.8	3.3	5.5	4.9	17	98
CNN-MFAD-D-3.8M	0.9	2.9	6.3	2.5	13	102
CNN-MFAD-D-30.9M	1.0	2.5	5.3	3.8	17.6	94.4

VI. DISCUSSION

The results demonstrate that a single commercial LTE BS in non-LoS conditions can be used to attain meter-level horizontal positioning accuracy as well as heading accuracy ranging from a few degrees to tens of degrees by employing deep learning architectures that are well-established in computer vision. This is achieved by using the richness of the multipath channel in a complicated urban propagation environment populated with irregular surfaces and variation in the geometry of scatterers. Even with limited training data and varied channel representations (wiometrics) ranging from bulky ones with minimal processing (ACSI and CCSI) to more intricate feature engineering (BDIR and MFAD), both position and heading estimates perform well on a snapshot-by-snapshot basis without prior knowledge of navigation states.

As originally hypothesized by Vieira et al. in [27], the feature engineering involved in generating the MFAD representation offers compelling performance. This representation takes full advantage of consistent clock synchronization between sender and receiver and integrates the complete radiation pattern of the receive antenna array. The representation is so effective that performance was essentially the same even when employing a simpler FCNN network architecture, when adding the information provided by a second BS, or using a convolutional network with an order of magnitude more training weights. None of the other wiometrics achieve the same performance under any circumstances, and, consistent with [69], FCNNs are inferior to CNNs for all cases. Particularly for BDIR, the convolution operations appear to be critical to attaining reasonable performance. The network architecture is more consequential for the simpler representations, and it is worthwhile to explore more intricate network architectures (particularly Transformers) for these, or to explore the use of Transformers for the integration of multiple BSs.

The difference in performance between the HEU and LEU training and testing splits is pronounced for all channel representations and network architectures. The input space in this paper draws from only four passes over the same route, two in each direction, and it is reasonable to suspect that a more thorough surveying of the test area with more combinations of position and heading would result in improved performance, particularly for the error tails, which in the HEU case correspond strongly with test points that are not representative of the training set.

The performance floor of position estimates for the best-performing representations is well under the length of a vehicle (4 or 5 meters) but still does not quite approach the sampling distance which is on the order of one decimeter. Higher resolution in terms of bandwidth could push the error down further, and Remark 2 may offer some clues on how to improve the performance and scalability of wiometric solutions. On the high end, tail errors are significant for most representations especially in terms of heading estimation for HEU data. Out-of-distribution detection and similar methods could be explored to mitigate these limitations.

There is significant room for wiometric navigation literature to explore robustness to environmental changes in a manner similar to what has been done in computer vision for positioning [83]. While a larger training set as compared to the HEU case visualized in Fig. 6 would presumably improve performance, multiple parameters are still not challenged. All testing was done in the winter and vegetation will change, creating a different scattering environment seasonally. Some non-parametric wireless positioning literature considers measurements taken spaced over the course of months [49]. In our data collection, there were few changes in the arrangement of cars parked along the side of the road and traffic density did not change significantly even if certain scatterers (buses and other vehicles) were variable from lap to lap. More critically for the CCSI and MFAD representations, absolute time synchronization is effectively maintained between transmitter and receiver, which requires first an accurate initialization and then an oscillator on both sides with an Allan deviation not representative of technologies used in today's commercial devices (see [1] Fig. 5.4).

VII. Conclusion

In this manuscript, a massive-MIMO antenna and receiver system was mounted on a passenger vehicle to opportunistically receive downlink CRS from commercial LTE BSs and to use them to generate two-dimensional estimates of position and heading from wiometrics using various deep learning architectures. In non-LoS conditions without knowledge of the transmitter location, meter-level estimates of position and heading errors of a few degrees are realized.

Given the superiority of the MFAD representation, future work should explore some of the practical challenges involved in realizing this at scale, including maintaining stable clock synchronization, designing antenna arrays with high spatial resolution that can be integrated into the form factor of a vehicle, and addressing calibration for the receive chains.

Another line of future work is to improve performance by exploring alternative network architectures (Transformers in particular), implementing complex-valued ANNs, and testing the environmental conditions under which performance can be shown to be variable in order to attain more robust navigation estimates. Annotation pipelines and learning methods such as weakly or semi-supervised methods could be investigated to address scalability. Alternative wiometrics beyond those explored in this manuscript may also be useful, and performance in different environments and with different channel bandwidths, carrier frequencies, and measurement apertures are also interesting. Considering that the results shown in Section V are achieved with LTE signals that have limited bandwidth, it seems likely that statistical methods will out-perform state-of-the-art parametric methods for many problems in wireless navigation as they have in computer vision.

APPENDIX A

Network names follow the following convention XXX-YYYY-B-NNM. Where:

- XXX is either CNN (convolutional) or FCNN (fully-connected)
- YYY is one of the four-letter wiometrics (see Fig. 1)
- B is either S for single base station or D for double base station
- NN is the approximate number of weights of the network, rounded to the nearest 100,000 and expressed in millions (M)

Each network shape is randomly initialized and trained twice, once each for the LEU or HEU training and test sets.

TABLE IV
TABLE OF NETWORK VALUES

Network Name	Input Shape	Layers	Convolutional Filters	Fully-Connected Layer Nodes
Fully-Connected Networks				
FCNN-ACSI-S-7.6M	200×128	7		256, 1024, 512, 256, 256, 128, 64
FCNN-CCSI-S-7.6M	200×256	7		128, 256, 1024, 512, 256, 256, 128
FCNN-BDIR-S-7.6M	32×128	7		1024, 2048, 512, 256, 256, 128, 64
FCNN-MFAD-S-7.4M	150×90	7		512, 512, 256, 256, 128, 128, 64
Convolutional Networks (Small)				
CNN-BCSI-S-3.4M	200×8	7	16, 32, 32	64, 256, 128, 32
CNN-ACSI-S-3.9M	200×128	8	16, 32, 64, 128	256, 1024, 256, 128
CNN-CCSI-S-3.8M	200×256	8	16, 32, 64, 128	128, 1024, 256, 128
CNN-BDIR-S-3.3M	32×128	7	16, 32, 64	512, 1024, 512, 128
CNN-MFAD-S-3.8M	150×90	7	16, 32, 64	256, 1024, 256, 128
Convolutional Networks (Large)				
CNN-ACSI-S-30.6M	200×128	8	32, 64, 128, 256	1024, 2056, 1024, 512
CNN-CCSI-S-27.0M	200×256	8	32, 64, 128, 256	512, 1024, 512, 256
CNN-BDIR-S-39.9M	32×128	7	32, 64, 128	2048, 5096, 2048, 1024
CNN-MFAD-S-30.8M	150×90	7	32, 64, 128	1024, 2048, 1024, 512
Double Base Station Networks (Small)				
CNN-ACSI-D-4.5M	$200 \times 128 \times 2$	8	16, 32, 64, 128	1024, 1024, 256, 128
CNN-CCSI-D-4.0M	$200 \times 256 \times 2$	8	16, 32, 64, 128	512, 1024, 256, 128
CNN-BDIR-D-3.8M	$32 \times 128 \times 2$	7	16, 32, 64	1024, 1024, 512, 128
CNN-MFAD-D-3.8M	$150 \times 90 \times 2$	7	16, 32, 64	512, 1024, 256, 128
Double Base Station Networks (Large)				
CNN-ACSI-D-33.0M	$200 \times 128 \times 2$	7	32, 64, 128	2048, 2048, 1024, 512
CNN-CCSI-D-31.0M	$200 \times 256 \times 2$	7	32, 64, 128	1024, 2048, 1024, 512
CNN-BDIR-D-35.7M	$32 \times 128 \times 2$	7	32, 64, 128	4096, 4096, 2048, 1024
CNN-MFAD-D-31.9M	$150 \times 90 \times 2$	7	32, 64, 128	2048, 4096, 2048, 1024

A kernel size of 4 is used for convolutions. Max pooling is applied[8] after convolution and activation with a pool size of 2×2 for single base station two-dimensional convolutions

---

[8]With the exception of BCSI-S-3.4M, to keep the total number of weights similar considering the smaller input size.

and $1 \times 2 \times 2$ for double base station three-dimensional convolutions. An Adam optimizer is used for all training, and a learning rate of 0.001. Dimensioning networks for variable input shapes is not an exact science, and there are small variations in the same category to target a similar number of weights for comparison.

REFERENCES

[1] P. Teunissen and O. Montenbruck, *Springer Handbook of Global Navigation Satellite Systems*, ser. Springer Handbooks. Springer International Publishing, 2017.

[2] V. Janssen, "A comparison of the VRS and the MAC principles for network RTK," in *International Global Navigation Satellite Systems Society (IGNSS) Symposium*, 2009, pp. 1–13.

[3] K. M. Larson, J. T. Freymueller, and S. Philipsen, "Global plate velocities from the Global Positioning System," *Journal of Geophysical Research: Solid Earth*, vol. 102, no. B5, pp. 9961–9981, 1997.

[4] M. B. Kjærgaard, H. Blunck, T. Godsk, T. Toftkjær, D. L. Christensen, and K. Grønbæk, "Indoor Positioning Using GPS Revisited," in *International conference on pervasive computing*. Springer, 2010, pp. 38–56.

[5] N. Zhu, J. Marais, D. Bétaille, and M. Berbineau, "GNSS Position Integrity in Urban Environments: A Review of Literature," *IEEE Transactions on Intelligent Transportation Systems*, vol. 19, no. 9, pp. 2762–2778, 2018.

[6] M. L. Psiaki and T. E. Humphreys, "GNSS Spoofing and Detection," *Proceedings of the IEEE*, vol. 104, no. 6, pp. 1258–1270, 2016.

[7] P. Groves, *Principles of GNSS, Inertial, and Multisensor Integrated Navigation Systems, Second Edition*. Artech House, 03 2013.

[8] R. Whiton, "Cellular localization for autonomous driving: A function pull approach to safety-critical wireless localization," *IEEE Vehicular Technology Magazine*, 2022.

[9] J. A. del Peral-Rosado, R. Raulefs, J. A. López-Salcedo, and G. Seco-Granados, "Survey of cellular mobile radio localization methods: From 1G to 5G," *IEEE Communications Surveys & Tutorials*, vol. 20, no. 2, pp. 1124–1148, 2017.

[10] Z. Kassas, J. Khalife, K. Shamaei, and J. Morales, "I Hear, Therefore I Know Where I Am: Compensating for GNSS Limitations with Cellular Signals," *IEEE Signal Processing Magazine*, vol. 34, no. 5, pp. 111–124, Sep. 2017.

[11] S. Dwivedi, R. Shreevastav, F. Munier *et al.*, "Positioning in 5G Networks," *IEEE Communications Magazine*, vol. 59, no. 11, pp. 38–44, 2021.

[12] P. Müller, J. A. del Peral-Rosado, R. Piche, and G. Seco-Granados, "Statistical Trilateration With Skew-t Distributed Errors in LTE Networks," *IEEE Transactions on Wireless Communications*, vol. 15, no. 10, pp. 7114–7127, 2016.

[13] R. Whiton, J. Chen, and F. Tufvesson, "LTE NLOS navigation and channel characterization," in *Proceedings of the 35th International Technical Meeting of the Satellite Division of The Institute of Navigation (ION GNSS+ 2022)*, 2022, pp. 2398–2408.

[14] Z. Liu, L. Chen, X. Zhou, N. Shen, and R. Chen, "Multipath tracking with LTE signals for accurate TOA estimation in the application of indoor positioning," *Geo-spatial Information Science*, pp. 1–13, 2022.

[15] M. Orabi, A. A. Abdallah, J. Khalife, and Z. M. Kassas, "A Machine Learning Multipath Mitigation Approach for Opportunistic Navigation with 5G Signals," in *Proceedings of the 34th International Technical Meeting of the Satellite Division of The Institute of Navigation (ION GNSS+ 2021)*, 2021, pp. 2895–2909.

[16] M. Maaref and Z. M. Kassas, "Autonomous integrity monitoring for vehicular navigation with cellular signals of opportunity and an IMU," *IEEE Transactions on Intelligent Transportation Systems*, vol. 23, no. 6, pp. 5586–5601, 2021.

[17] C. Gentner, T. Jost, W. Wang, S. Zhang, A. Dammann, and U.-C. Fiebig, "Multipath Assisted Positioning with Simultaneous Localization and Mapping," *IEEE Transactions on Wireless Communications*, vol. 15, no. 9, pp. 6104–6117, 2016.

[18] K. Witrisal, P. Meissner, E. Leitinger *et al.*, "High-Accuracy Localization for Assisted Living: 5G systems will turn multipath channels from foe to friend," *IEEE Signal Processing Magazine*, vol. 33, no. 2, pp. 59–70, 2016.

[19] S. Jiang, W. Wang, Y. Miao, W. Fan, and A. F. Molisch, "A survey of dense multipath and its impact on wireless systems," *IEEE Open Journal of Antennas and Propagation*, 2022.

[20] I. Sharp and K. Yu, *Wireless Positioning: Principles and Practice*. Springer, 2019.

[21] E. Björnson and E. Larsson, "Wireless localization and sensing (with Henk Wymeersch)," Podbean, Dec. 2021. [Online]. Available: https://wirelessfuture.podbean.com/e/23-wireless-localization-and-sensing-with-henk-wymeersch/

[22] F. Nedelkov, D.-K. Lee, D. Miralles, and D. Akos, "Accuracy and performance of the network location provider in android devices," in *Proceedings of the 33rd International Technical Meeting of the Satellite Division of The Institute of Navigation (ION GNSS+ 2020)*, 2020, pp. 2152–2165.

[23] D. Burghal, A. T. Ravi, V. Rao, A. A. Alghafis, and A. F. Molisch, "A Comprehensive Survey of Machine Learning Based Localization with Wireless Signals," 2020. [Online]. Available: https://arxiv.org/pdf/2012.11171.pdf

[24] T. L. Marzetta, E. G. Larsson, and H. Yang, *Fundamentals of massive MIMO*. Cambridge University Press, 2016.

[25] R. Whiton, J. Chen, T. Johansson, and F. Tufvesson, "Urban navigation with LTE using a large antenna array and machine learning," in *2022 IEEE 95th Vehicular Technology Conference:(VTC2022-Spring)*. IEEE, 2022, pp. 1–5.

[26] K. Merchant, S. Revay, G. Stantchev, and B. Nousain, "Deep learning for RF device fingerprinting in cognitive communication networks," *IEEE journal of selected topics in signal processing*, vol. 12, no. 1, pp. 160–167, 2018.

[27] J. Vieira, E. Leitinger, M. Sarajlic, X. Li, and F. Tufvesson, "Deep Convolutional Neural Networks for Massive MIMO Fingerprint-Based Positioning," in *2017 IEEE 28th Annual International Symposium on Personal, Indoor, and Mobile Radio Communications (PIMRC)*. IEEE, 2017, pp. 1–6.

[28] Christ, Godwin, and Lavigne, "A prison guard duress alarm location system," in *1993 Proceedings of IEEE International Carnahan Conference on Security Technology*, 1993, pp. 106–116.

[29] P. Bahl and V. N. Padmanabhan, "Radar: An in-building RF-based user location and tracking system," in *Proceedings IEEE INFOCOM 2000. Conference on computer communications. Nineteenth annual joint conference of the IEEE computer and communications societies (Cat. No. 00CH37064)*, vol. 2. Ieee, 2000, pp. 775–784.

[30] A. Khalajmehrabadi, N. Gatsis, and D. Akopian, "Modern WLAN fingerprinting indoor positioning methods and deployment challenges," *IEEE Communications Surveys & Tutorials*, vol. 19, no. 3, pp. 1974–2002, 2017.

[31] C. Takenga and K. Kyamakya, "A low-cost fingerprint positioning system in cellular networks," in *2007 Second International Conference on Communications and Networking in China*, 2007, pp. 915–920.

[32] M. Stahlke, T. Feigl, M. H. C. García, R. A. Stirling-Gallacher, J. Seitz, and C. Mutschler, "Transfer learning to adapt 5G AI-based fingerprint localization across environments," in *2022 IEEE 95th Vehicular Technology Conference: (VTC2022-Spring)*, 2022, pp. 1–5.

[33] X. Wang, L. Gao, S. Mao, and S. Pandey, "CSI-based Fingerprinting for Indoor Localization: A Deep Learning Approach," *IEEE Transactions on Vehicular Technology*, vol. 66, no. 1, pp. 763–776, 2016.

[34] W. Liu, Q. Cheng, Z. Deng *et al.*, "Survey on CSI-based Indoor Positioning Systems and Recent Advances," in *2019 International Conference on Indoor Positioning and Indoor Navigation (IPIN)*. IEEE, 2019, pp. 1–8.

[35] G. Pecoraro, S. Di Domenico, E. Cianca, and M. De Sanctis, "CSI-based fingerprinting for indoor

localization using LTE signals," *EURASIP Journal on Advances in Signal Processing*, vol. 2018, no. 1, pp. 1–18, 2018.

[36] Y. Chapre, A. Ignjatovic, A. Seneviratne, and S. Jha, "CSI-MIMO: An efficient Wi-Fi fingerprinting using Channel State Information with MIMO," *Pervasive and Mobile Computing*, vol. 23, pp. 89–103, 2015.

[37] M. Arnold, J. Hoydis, and S. ten Brink, "Novel Massive MIMO Channel Sounding Data Applied to Deep Learning-based Indoor Positioning," in *SCC 2019; 12th International ITG Conference on Systems, Communications and Coding*. VDE, 2019, pp. 1–6.

[38] H. Chen, Y. Zhang, W. Li, X. Tao, and P. Zhang, "ConFi: Convolutional Neural Networks Based Indoor Wi-Fi Localization Using Channel State Information," *IEEE Access*, vol. 5, pp. 18 066–18 074, 2017.

[39] H. Tataria, M. Shafi, A. F. Molisch, M. Dohler, H. Sjöland, and F. Tufvesson, "6G Wireless Systems: Vision, Requirements, Challenges, Insights, and Opportunities," *Proceedings of the IEEE*, vol. 109, no. 7, pp. 1166–1199, 2021.

[40] X. Wang, X. Wang, and S. Mao, "Deep Convolutional Neural Networks for Indoor Localization with CSI Images," *IEEE Transactions on Network Science and Engineering*, vol. 7, pp. 316–327, 2018.

[41] A. Niitsoo, T. Edelhäußer, E. Eberlein, N. Hadaschik, and C. Mutschler, "A Deep Learning Approach to Position Estimation from Channel Impulse Responses," *Sensors*, vol. 19, no. 5, p. 1064, 2019.

[42] X. Ye, X. Yin, X. Cai, A. P. Yuste, and H. Xu, "Neural-Network-Assisted UE Localization Using Radio-Channel Fingerprints in LTE Networks," *IEEE Access*, vol. 5, pp. 12 071–12 087, 2017.

[43] D. Li and Y. Lei, "Deep Learning for Fingerprint-Based Outdoor Positioning via LTE Networks," *Sensors*, vol. 19, no. 23, p. 5180, 2019.

[44] X. Sun, X. Gao, G. Y. Li, and W. Han, "Single-site localization based on a new type of fingerprint for massive MIMO-OFDM systems," *IEEE Transactions on Vehicular Technology*, vol. 67, no. 7, pp. 6134–6145, 2018.

[45] F. Hejazi, K. Vuckovic, and N. Rahnavard, "Dyloc: Dynamic localization for massive MIMO using predictive recurrent neural networks," in *IEEE INFOCOM 2021-IEEE Conference on Computer Communications*. IEEE, 2021, pp. 1–9.

[46] C. Wu, X. Yi, W. Wang *et al.*, "Learning to localize: A 3D CNN approach to user positioning in massive MIMO-OFDM systems," *IEEE Transactions on Wireless Communications*, 2021.

[47] Y. Wang, I. W.-H. Ho, S. Zhang, and Y. Wang, "Intelligent reflecting surface enabled fingerprinting-based localization with deep reinforcement learning," *IEEE Transactions on Vehicular Technology*, 2023.

[48] J.-W. Jang and S.-N. Hong, "Indoor localization with WiFi fingerprinting using convolutional neural network," in *2018 Tenth International Conference on Ubiquitous and Future Networks (ICUFN)*, 2018, pp. 753–758.

[49] P. Ferrand, A. Decurninge, and M. Guillaud, "DNN-based localization from channel estimates: Feature design and experimental results," in *GLOBECOM 2020-2020 IEEE Global Communications Conference*. IEEE, 2020, pp. 1–6.

[50] Y. Li, Z. Gao, Z. He *et al.*, "Wireless Fingerprinting Uncertainty Prediction Based on Machine Learning," *Sensors*, vol. 19, no. 2, p. 324, 2019.

[51] E. Gönültaş, E. Lei, J. Langerman, H. Huang, and C. Studer, "CSI-based multi-antenna and multi-point indoor positioning using probability fusion," *IEEE Transactions on Wireless Communications*, vol. 21, no. 4, pp. 2162–2176, 2021.

[52] D. Maltoni, D. Maio, A. K. Jain, and S. Prabhakar, *Handbook of Fingerprint Recognition*. Springer Science & Business Media, 2009.

[53] E. Tabassi, C. Wilson, and C. Schlenoff, "Fingerprint image quality," Apr 2004.

[54] A. K. Jain, A. A. Ross, and R. Nandakumar, *Introduction to Biometrics*. Springer, 2011.

[55] J. Bassey, L. Qian, and X. Li, "A survey of complex-valued neural networks," *arXiv preprint arXiv:2101.12249*, 2021.

[56] X. Li, E. Leitinger, M. Oskarsson, K. Åström, and F. Tufvesson, "Massive MIMO-based localization and mapping exploiting phase information of multipath components," *IEEE transactions on wireless communications*, vol. 18, no. 9, pp. 4254–4267, 2019.

[57] C. Studer, S. Medjkouh, E. Gonultaş, T. Goldstein, and O. Tirkkonen, "Channel Charting: Locating Users Within the Radio Environment Using Channel State Information," *IEEE Access*, vol. 6, pp. 47 682–47 698, 2018.

[58] Q. Zhang and W. Saad, "Semi-supervised learning for channel charting-aided iot localization in millimeter wave networks," in *2021 IEEE Global Communications Conference (GLOBECOM)*, 2021, pp. 1–6.

[59] M. Stahlke, G. Yammine, T. Feigl, B. M. Eskofier, and C. Mutschler, "Indoor localization with robust global channel charting: A time-distance-based approach," *IEEE Transactions on Machine Learning in Communications and Networking*, vol. 1, pp. 3–17, 2023.

[60] X. Sun, C. Wu, X. Gao, and G. Y. Li, "Fingerprint-based localization for massive MIMO-OFDM system with deep convolutional neural networks," *IEEE Transactions on Vehicular Technology*, vol. 68, no. 11, pp. 10 846–10 857, 2019.

[61] X. Wang, L. Liu, Y. Lin, and X. Chen, "A fast single-site fingerprint localization method in massive MIMO system," in *2019 11th International Conference on Wireless Communications and Signal Processing (WCSP)*, 2019, pp. 1–6.

[62] L. Chu, A. Alghafis, and A. F. Molisch, "SA-Loc: Scenario adaptive localization in highly dynamic environment using adversarial regressive domain adaptation," in *2022 IEEE International Conference on RFID (RFID)*. IEEE, 2022, pp. 132–137.

[63] A. Krizhevsky, I. Sutskever, and G. E. Hinton, "Imagenet classification with deep convolutional neural networks," *Communications of the ACM*, vol. 60, no. 6, pp. 84–90, 2017.

[64] K. He, X. Zhang, S. Ren, and J. Sun, "Deep residual learning for image recognition," in *Proceedings of the IEEE conference on computer vision and pattern recognition*, 2016, pp. 770–778.

[65] J. Redmon and A. Farhadi, "YOLO9000: Better, faster, stronger," in *Proceedings of the IEEE Conference on Computer Vision and Pattern Recognition (CVPR)*, July 2017.

[66] I. H. Sarker, "Machine learning: Algorithms, real-world applications and research directions," *SN computer science*, vol. 2, no. 3, p. 160, 2021.

[67] A. Vaswani, N. Shazeer, N. Parmar *et al.*, "Attention is all you need," *Advances in neural information processing systems*, vol. 30, 2017.

[68] S. Khan, M. Naseer, M. Hayat, S. W. Zamir, F. S. Khan, and M. Shah, "Transformers in vision: A survey," *ACM computing surveys (CSUR)*, vol. 54, no. 10s, pp. 1–41, 2022.

[69] W.-L. Chin, C.-C. Hsieh, D. Shiung, and T. Jiang, "Intelligent indoor positioning based on artificial neural networks," *IEEE Network*, vol. 34, no. 6, pp. 164–170, 2020.

[70] O. Russakovsky, J. Deng, H. Su *et al.*, "Imagenet large scale visual recognition challenge," *International journal of computer vision*, vol. 115, pp. 211–252, 2015.

[71] E. Dahlman, S. Parkvall, and J. Skold, *4G: LTE/LTE-advanced for mobile broadband*. Academic press, 2013.

[72] M. Driusso, C. Marshall, M. Sabathy, F. Knutti, H. Mathis, and F. Babich, "Vehicular position tracking using LTE signals," *IEEE Transactions on Vehicular Technology*, vol. 66, no. 4, pp. 3376–3391, 2017.

[73] P. Wang and Y. J. Morton, "Performance comparison of time-of-arrival estimation techniques for LTE signals in realistic multipath propagation channels," *NAVIGATION: Journal of the Institute of Navigation*, vol. 67, no. 4, pp. 691–712, 2020.

[74] K. Shamaei, J. Khalife, and Z. M. Kassas, "Exploiting LTE Signals for Navigation: Theory to Implementation," *IEEE Transactions on Wireless Communications*, vol. 17, no. 4, pp. 2173–2189, April 2018.

[75] A. Richter, "Estimation of Radio Channel Parameters, Models and Algorithms," Ph.D. dissertation, Technische Universität Ilmenau, Germany, 2005.

[76] J. Chen, R. Whiton, X. Li, and F. Tufvesson, "High-resolution channel sounding and parameter estimation in multi-site cellular networks," in *2023 Joint European Conference on Networks and Communications & 6G Summit (EuCNC/6G Summit)*. IEEE, 2023, pp. 90–95.

[77] X. Zhu, W. Qu, T. Qiu, L. Zhao, M. Atiquzzaman, and D. O. Wu, "Indoor intelligent fingerprint-based localization: Principles, approaches and challenges," *IEEE Communications Surveys & Tutorials*, vol. 22, no. 4, pp. 2634–2657, 2020.

[78] R. Liu, J. Wang, and B. Zhang, "High Definition Map for Automated Driving: Overview and Analysis," *The Journal of Navigation*, vol. 73, no. 2, pp. 324–341, 2020.

[79] K. Jo, C. Kim, and M. Sunwoo, "Simultaneous localization and map change update for the high definition map-based autonomous driving car," *Sensors*, vol. 18, no. 9, p. 3145, 2018.

[80] Z. Guo, Y. Huang, X. Hu, H. Wei, and B. Zhao, "A survey on deep learning based approaches for scene understanding in autonomous driving," *Electronics*, vol. 10, no. 4, p. 471, 2021.

[81] Y. Mao, Z. Xiao, C.-T. Lin *et al.*, "Decentralized training of 3D lane detection with automatic labeling using HD maps," in *2023 IEEE 97th Vehicular Technology Conference (VTC2023-Spring)*. IEEE, 2023, pp. 1–7.

[82] F. Yin, Z. Lin, Q. Kong *et al.*, "Fedloc: Federated learning framework for data-driven cooperative localization and location data processing," *IEEE Open Journal of Signal Processing*, vol. 1, pp. 187–215, 2020.

[83] T. Sattler, W. Maddern, C. Toft *et al.*, "Benchmarking 6DOF outdoor visual localization in changing conditions," in *Proceedings of the IEEE conference on computer vision and pattern recognition*, 2018, pp. 8601–8610.

Paper V

Paper V

Reproduced, with permission, from: IEEE

R. Whiton, J. Chen, and F. Tufvesson, "Flexible Density-based Multipath Component Clustering Utilizing Ground Truth Pose," *2023 IEEE 98th Vehicular Technology Conference: (VTC2023-Fall), Hong Kong, Hong Kong*, pp. 1-6, Oct. 2023, doi: 10.1109/VTC2023-Fall60731.2023.10333453..

Flexible Density-based Multipath Component Clustering Utilizing Ground Truth Pose

Russ Whiton[*‡], Junshi Chen[†‡], Fredrik Tufvesson[‡]

[*]Volvo Car Corporation, SE-405 31 Gothenburg, Sweden

[†]Terranet AB, Lund, Sweden

[‡]Dept. of Electrical and Information Technology, Lund University, Lund, Sweden

Email: {russell.whiton, junshi.chen, fredrik.tufvesson}@eit.lth.se

Abstract

Accurate statistical characterization of electromagnetic propagation is necessary for the design and deployment of radio systems. State-of-the-art channel models such as the Enhanced COST 2100 Channel Model utilize the concept of clusters of multipath components, and characterize channels by their inter- and intra-cluster statistics. Automatic clustering algorithms have been proposed in literature, but the subjective nature of the problem precludes any from being deemed objectively correct. In this paper, a new algorithm is proposed, based on density-reachability and ground truth receiver pose, with the explicit focus of extracting clusters for the purpose of channel characterization. Measurements of downlink signals from a commercial LTE base station by a passenger vehicle driving in an urban environment with a massive antenna array on the roof are used to evaluate the repeatability and intuitiveness of the proposed clustering algorithm.

I. INTRODUCTION

Radio systems have made enormous leaps in capabilities in recent decades, and are intricately woven into the fabric of modern industrial society. The International Telecommunication Union (ITU) suggests that increased data traffic volume, diversified service requirements, higher demands on Quality-of-Service (QoS) and cost pressure will necessitate innovative solutions for future development [1]. Maximizing spectral efficiency can be antithetical to achieving Ultrareliable and Low-Latency Communication (URLLC), for example [2], and all parameters of future systems require close scrutiny to meet the ITU vision for this evolution.

One fundamental building block for designing radio systems to meet these diverse requirements is a deep understanding of electromagnetic wave propagation. Physical models for wave propagation have been developed explicitly for this purpose, and typically models are employed in which the channel is characterized as a number of discrete Multipath

Components (MPCs) originating at the transmitter and impinging upon the receiver [3]. Sometimes the concept of *dense multipath* [4] is also included in the model, in which one or more exponential functions in the time domain are also jointly considered. The modeling of these MPCs is typically done either with site-specific channel models (including ray models) where the complete wave trajectories are determined analytically, or alternatively the parameters of MPCs are treated stochastically [5]. Stochastic modeling has enjoyed widespread attention, especially Geometry-based Stochastic Channel Models (GSCMs), because GSCMs can be generalized broadly and are of utility for many aspects of system design and verification. Since the advent of Third Generation (3G) cellular systems, GSCMs have evolved from an MPC-based understanding of propagation to a *cluster*-based understanding, in which MPCs sharing similar properties are grouped together [6].

However, the cluster-based understanding of radio channels necessarily entails ambiguity about the definition of a cluster, and it would be difficult or impossible to define a single objective metric for this purpose. Early work in MPC clustering relied on visual analysis of the delay-domain arrival of MPCs, but subsequent work has resulted in numerous proposals for automatic clustering algorithms operating in other domains. The algorithms also differ in their applicability across frequencies and measurement environments, the number of parameters required for tuning, and whether they are intended to work in real-time or in post-processing. There still appears to be a need for an intuitive and flexible algorithm for MPC clustering which is scalable to large data sets.

In this paper, a novel automatic clustering algorithm is proposed for rapid and repeatable clustering of large channel measurement data sets for propagation modeling, utilizing precise estimates of receiver position and orientation. The proposed model uses DBSCAN [7] in *odometry space* (defined in Sec. II), and is evaluated on test data received by a passenger vehicle-mounted measurement system operating in an urban environment, receiving 2.66 GHz downlink signals from a commercial Long-Term Evolution (LTE) base station paired with a high-end ground truth positioning system. The clustering algorithm has the following salient features:

- Simultaneous consideration of the entire measurement series when performing clustering, eliminating any need for inner/outer filters for cluster birth/death processes operating across a time series.
- Cluster definitions directly influenced by physical movement of the receiver, so-called Visibility Regions (VRs).
- Applicability across frequencies and geometries.
- Consideration of second-order and higher reflections.
- Simple parameter tuning with intuitive physical interpretation, and quick map-based visualization of results.

The paper is organized as follows: Section II provides background on clustering algorithms and describes the proposed algorithm; Section III discusses the measurement

system and data collection campaign; Section IV provides the results of the measurements; and finally Section V offers conclusions and suggestions for future work.

Notes on mathematical representation:

- Vectors are indicated in lower-case bold font $\boldsymbol{x}$ or $\boldsymbol{\omega}$
- $\|\boldsymbol{x}\|$ indicates the L2-norm of vector $\boldsymbol{x}$
- $\{x_{a,b}\}$ is the set of $x_{a,b}$ for all valid combinations of a and b

II. MULTIPATH COMPONENT CLUSTERING

A. Waves and Clusters

In the field of propagation modeling, the double-directional channel response is typically modeled as the superposition of L waves (planar or spherical) originating at the transmitter and arriving at the receiver. The waves are parameterized by their delays τ_l, the angles-of-departure Ω_l^{TX} and arrival Ω_l^{RX} (which can be further subdivided into azimuthal angles-of-arrival/departure ϕ_l^{RX} and ϕ_l^{TX}, and elevation-of-arrival/departure θ_l^{RX} and θ_l^{TX}), the complex-valued path loss α_l and Doppler shift[1] ψ_l:

$$h(t, \tau, \Omega^{TX}, \Omega^{RX}, \psi) = \sum_{l=1}^{L} h(t, \alpha_l, \tau_l, \Omega_l^{TX}, \Omega_l^{RX}, \psi_l). \tag{1}$$

In a seminal work on electromagnetic propagation modeling, the authors observed that MPCs tend to arrive in clusters of similar delay and uniformly distributed random phase [8], use of this observation allows for more precise modeling of the channel rather than treating the arrival of individual MPCs as a Poisson process. Clusters of MPCs with similar propagation parameters (including delays, angles and Doppler frequencies) are distinguishable from other clusters with different propagation parameters because the objects that the electromagnetic waves interact with typically give rise to several paths simultaneously with similar geometries [9]. Understanding the nature of clusters continues to be an active area of research, with the Enhanced COST 2100 channel model setting a new state-of-the-art in sophistication [5] and reformulating the channel in terms of C clusters, each with L_c MPCs. The channel has an overall path-loss G, and each cluster has its own visibility gain V_c, shadow fading S_c and cluster attenuation G_c. This cluster-based formulation of the channel response is expressed as a double summation over clusters and the MPCs within each cluster:

$$h(t, \tau, \Omega^{TX}, \Omega^{RX}, \psi) = \frac{1}{G} \sum_{c=1}^{C} V_c \sqrt{\frac{S_c}{G_c}} \sum_{l=1}^{L_c} h(t, \alpha_{l,c}, \tau_{l,c}, \Omega_{l,c}^{TX}, \Omega_{l,c}^{RX}, \psi_{l,c}). \tag{2}$$

---

[1]Polarization is omitted in this work, as in [4], for brevity, but could also be considered for clustering if desired.

Clusters can be classified as local clusters, single clusters, or twin clusters depending on the geometry. Fig. 1 illustrates two clusters for a mobile receiver traversing a short figure-eight trajectory. One single cluster and one twin cluster are visible, and the MPCs for the final snapshot of the trajectory are illustrated.
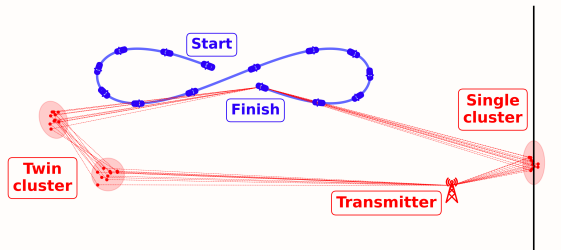

Fig. 1: An example clustering scenario. A vehicle drives a short trajectory and receives signals from two clusters, one of which has a single reflection and another stemming from a double reflection. Rays are illustrated for the last snapshot.

B. Automatic Clustering Algorithms

Pioneering work on MPC clusters identified inter- and intra-cluster parameters in the delay domain through visual inspection of a limited data set [8]. The Random-Cluster Model was presented in [3], which compared hierarchical tree clustering and KPowermeans. Kernel-Power-Density was suggested in [10], and a modified DBSCAN algorithm was proposed in [11], with the latter mapping clusters to physical points in space on a single-bounce cluster assumption, i.e., no twin clusters are considered. The motivations for all these novel automatic clustering algorithms have emphasized the ambiguity and fallibility of visual clustering, the need for scalability and repeatability, and the value of minimizing user-specified parameters.

Some shortcomings are apparent with the existing clustering algorithms. Visual identification of MPCs in the delay or even angle-delay domain quickly becomes difficult not only with increasing numbers of MPCs and clusters, but also with movement and rotation of the measurement apparatus (for Ω^{RX}) or a mobile transmitter (for Ω^{TX}). This can be partially mitigated through joint clustering and tracking, in which measurements are processed sequentially to keep track of clusters, MPCs and dense multipath [12], but this makes tuning difficult in that it requires cluster birth/death processes with their heuristics for data association. Fig. 2 shows simulated measurement data for the scenario of Fig. 1. Examining the entire measurement series together without regard for the time evolution (left side) results in ambiguity regarding the number of clusters and their shape. Joint clustering and tracking using the time series (right side) should permit effective differentiation in

this case. Either a sliding window or filtering is typically used to increase stationarity, but window size also impacts performance. For the purpose of propagation modeling, as opposed to real-time operation, it is desirable to define clusters based on the complete data set simultaneously, rather than sequentially processing the measurements.
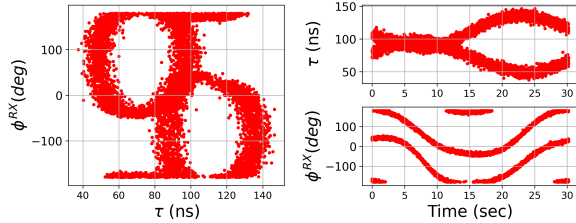

Fig. 2: (Left) Clustering in the Angle-of-Arrival-Delay Domain for the full measurement series in Fig. 1. Drawing a clear boundary between the two clusters in this view is difficult. (Right) Time series view of the same measurements intended for joint clustering and tracking. Cluster identification in the time series of the angular domain is more obvious.

In the COST 2100 Channel Model, it is implicit that motion in space (and *not* change in time) causes channel statistics to change, and clusters are understood to correspond with ellipsoids at fixed points in space associated with movement in and out of VRs [9]. In the Random Cluster Model, clusters are treated as "moving" with time (apparent in the time series of Fig. 2). Transmitter or receiver rotation should not impact the view of the cluster[2], but rather physical movement is what impacts visibility.

C. A New MPC Clustering Algorithm

With these limitations in mind, in this subsection a novel MPC clustering algorithm is proposed based on density-reachability using DBSCAN [7]. DBSCAN is a clustering algorithm that elegantly captures arbitrarily-shaped clusters with only two tuning parameters and a distance criterion. The first tuning parameter, ϵ, is a heuristic for deciding "reachability" between two points in one or more dimensions y^p and y^q according to the distance criterion $d(y^p, y^q)$, and the second tuning parameter N_{min} governs the number of reachable points for classification of "core points" around which the clusters are subsequently defined. DBSCAN and its extensions are thoroughly described in other literature, e.g., [13], so the algorithm details are not restated in this paper.

Some of the compelling strengths of DBSCAN are not fully realized with previous application for MPC clustering [11]. The algorithm scales well for large data sets, but channel estimation algorithms rarely estimate more than tens of MPCs for a single snapshot,

---

[2]The antenna radiation patterns will of course impact the complex channel gain.

particularly subspace-based channel estimation methods. An additional unrealized strength of DBSCAN is that the clustering domain can also be formulated in a highly abstract manner, meaning that *a strict interpretation of MPC physical location is unnecessary*. Twin clusters can be captured with higher abstraction, as well as single-bounce clusters or Line-of-Sight (LOS) clusters. In this subsection a method is described in which MPCs are first mapped into *vehicle space*, the coordinate system of the vehicle, then rotated and shifted into a world coordinate system *projected space* (but not their true location, with the exception of the LOS MPCs), and finally receiver movement is added as an arbitrary dimension (a dimension tailored to conform with the concept of VRs) for extension into *odometry space* before clustering is performed with DBSCAN.

The complete 6-dimensional pose of the receiver for snapshot index t is expressed in terms of three-dimensional position, in meters, defined in an East-North-Up (ENU) frame[3] $\boldsymbol{p}_t = [e_t, n_t, u_t]^T$ as well as three-dimensional orientation in terms of yaw, pitch and roll angles in radians $\boldsymbol{\omega}_t = [\gamma_t, \lambda_t, \eta_t]^T$. For each snapshot t, a variable number of MPCs L_t are estimated per Equation (1). The angles-of-arrival and component delays of these individual MPCs $\theta_{l,t}^{RX}$, $\phi_{l,t}^{RX}$, $\tau_{l,t}$, are first translated from spherical form into vector form and scaled by their total path lengths into *vehicle space*[4] denoted $\boldsymbol{\psi}_{l,t}$:

$$\boldsymbol{\psi}_{l,t} = \begin{bmatrix} \psi_{l,t}^{forw} \\ \psi_{l,t}^{left} \\ \psi_{l,t}^{abov} \end{bmatrix} = \tau_l \begin{bmatrix} sin(\theta_{l,t})cos(\phi_{l,t}) \\ sin(\theta_{l,t})sin(\phi_{l,t}) \\ cos(\theta_{l,t}) \end{bmatrix} . \tag{3}$$

Individual MPCs in vehicle space are subsequently rotated and translated into the ENU frame by using both the orientation $\boldsymbol{\omega}_t$ and position $\boldsymbol{p}_t$ of the receiver at the relevant epoch. These projections are denoted *projection space* and represented by $\boldsymbol{\zeta}_{l,t}$:

$$\boldsymbol{\zeta}_{l,t} = \begin{bmatrix} \zeta_{l,t}^e \\ \zeta_{l,t}^n \\ \zeta_{l,t}^u \end{bmatrix} = \begin{bmatrix} \psi_{l,t}^{forw} \\ \psi_{l,t}^{left} \\ \psi_{l,t}^{abov} \end{bmatrix} \begin{bmatrix} 1 & 0 & 0 \\ 0 & cos(\eta_t) & sin(\eta_t) \\ 0 & -sin(\eta_t) & cos(\eta_t) \end{bmatrix}$$
$$\begin{bmatrix} cos(\lambda_t) & 0 & -sin(\lambda_t) \\ 0 & 1 & 0 \\ sin(\lambda_t) & 0 & cos(\lambda_t) \end{bmatrix} \begin{bmatrix} cos(\gamma_t) & sin(\gamma_t) & 0 \\ -sin(\gamma_t) & cos(\gamma_t) & 0 \\ 0 & 0 & 1 \end{bmatrix} - \begin{bmatrix} e_t \\ n_t \\ u_t \end{bmatrix} . \tag{4}$$

Vector representations of MPCs for the scenario depicted in Fig. 1 are illustrated in Fig. 3. In the vehicular coordinate system, the evolution of MPCs $\boldsymbol{\psi}_l$ clearly follows the heading change of the vehicle, and while the two clusters are distinguishable by inspection, the

---

[3]Position can be expressed equivalently in any arbitrarily defined reference frame.

[4]The vehicular system used is Forward-Left-Above, per the ISO8855 standard.
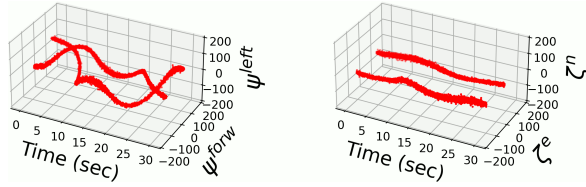
Fig. 3: (Left) Representation of MPCs $\boldsymbol{\psi_l}$ in vehicle space for the scenario in Fig. 1. (Right) Time evolution of MPCs in an external reference frame (projection space) using vehicle pose including $\boldsymbol{p}_t$ and $\boldsymbol{\omega}_t$, which constrains apparent motion of cluster locations.

apparent movement in the vehicular frame may appear to be a series of unlikely innovations for a filter tracking the cluster locations. In the ENU frame, cluster movement is smaller in absolute terms.

A physical interpretation of vehicular space for the clusters in Fig. 1 is illustrated in Fig. 4. In the vehicular coordinate system, the clusters appear to wander and joint clustering and tracking would entail using the time series to track the moving cluster center locations and deciding whether to expand or contract the number of clusters. Fig. 5 shows the same scenario in projected space. Depending on the order (LOS, single or twin cluster) and type of the reflector, aggregated MPCs with similar parameters will define either concentrated clouds or arcs as the receiver moves through VRs.

The final step in MPC representation is to append to each MPC the associated odometry value of the measurement apparatus χ_t for extension into odometry space. In this manner, arcs that project to the same location in projection space will be separated when clustering,
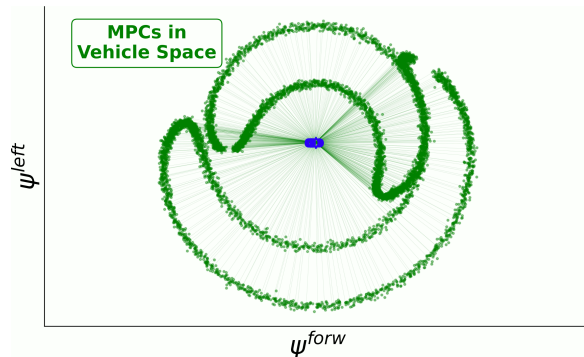

Fig. 4: MPCs from the scenario in Fig. 1 in vehicle space. Vehicle movement results in an apparent movement of the cluster locations.
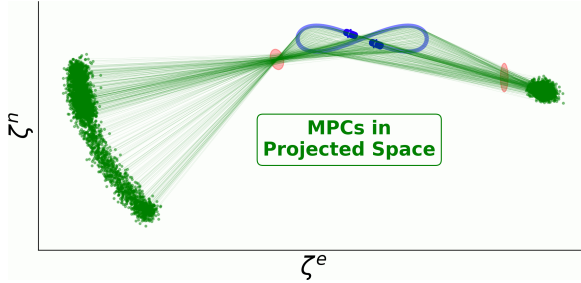
Fig. 5: MPCs from Fig. 1 shown in projection space. Projected MPCs in the external coordinate system do not correspond with the physical locations, except for the LOS path.
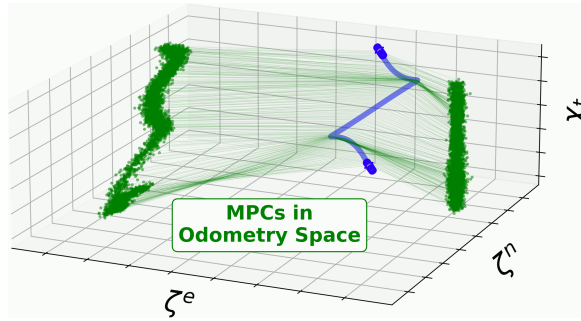

Fig. 6: MPCs from Fig. 1 in odometry space, the domain in which DBSCAN is applied. Overlapping arcs in physical space will not be clustered together if no neighborhood can be established with consideration for the ϵ parameter in physical space, i.e., with sufficient receiver movement.

which improves scalability to large data sets where the projection space might become crowded. This is shown in Fig. 6. When exiting a VR, additional movement will create separation in the odometry dimension. Multiple passes through the same VR, separated by movement outside the VR, will generate new clusters:

$$\chi_t = \int_0^t \left\| \frac{d}{dt} \boldsymbol{p}_t \right\| = \int_0^t \left\| \begin{bmatrix} \frac{\partial}{\partial t} e_t \\ \frac{\partial}{\partial t} n_t \\ \frac{\partial}{\partial t} u_t \end{bmatrix} \right\|. \tag{5}$$

The final representation of each MPC in odometry space consists of the three-dimensional

projected points[5] and the associated odometry value, i.e., $\boldsymbol{y}_{l,t} = [\chi_t, \zeta^e_{l,t}, \zeta^n_{l,t}, \zeta^u_{l,t}]^T$. The odometry space version of the MPCs for the twin cluster of Fig. 1 is shown in Fig. 6.

DBSCAN is applied directly to the points in odometry space. For the measurements described in Sec. III, $N_{min} = 15$, $\epsilon = 8$ and the distance criterion is Euclidian distance in odometry space, i.e., $d(\boldsymbol{y}^p, \boldsymbol{y}^q) = \|\boldsymbol{y}^p - \boldsymbol{y}^q\|$. For three-dimensional projections, visualization in odometry space can be accomplished through compression in one position dimension, as Fig. 6 does for the vertical spatial dimension (altitude). More concisely, given the entire set of all odometry space MPCs $\{\boldsymbol{y}_{l,t}\}$ for all T snapshots, DBSCAN assigns a label p to each member of the set:

$$DBSCAN : \{\boldsymbol{y}_{l,t}\} \rightarrow \{\boldsymbol{y}_{l,t,p}\}. \tag{6}$$

The number of clusters P is not pre-defined, and points classified as noise (not density-reachable from a core point) are assigned a label of -1. The algorithm steps are summarized in Fig. 7.
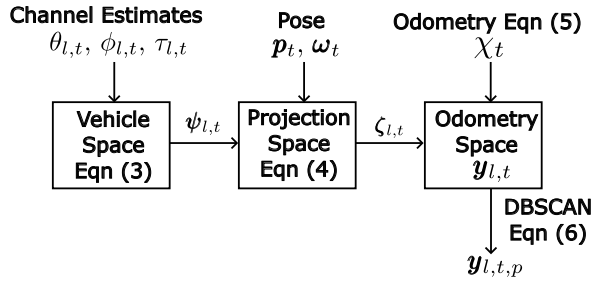

Fig. 7: Flow chart describing the novel clustering algorithm. MPCs are transformed into the odometry space domain before clustering is applied with DBSCAN.

[5]Projection could be done in a similar fashion using angles-of-departure either as an alternative or simultaneously, but the measurement system described in Sec. III is not fully double-directional.
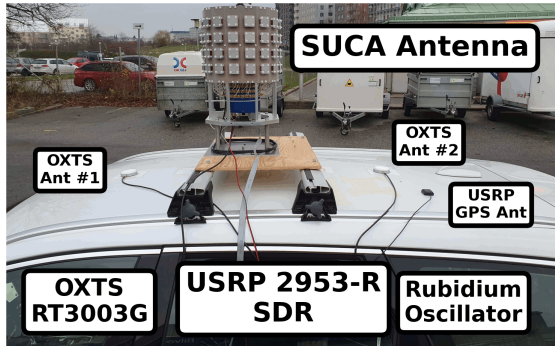
III. LTE Measurements

Fig. 8: System components for measurements. The SDR controls the antenna switching and has the same external time synchronization as the OXTS 3003G Ground Truth System.

To verify the clustering concept on measured data, a passenger vehicle was equipped with a massive 128-port Stacked Uniform Circular Array (SUCA), connected to and controlled by a Software-Defined Radio (SDR), which was programmed to receive Cell-Specific Reference Symbols (CRS) from commercial LTE base stations operating at 2.66 GHz. For a detailed description of the test system and signal processing, readers are referred to [14]. Channel estimates for MPCs were generated in post-processing on a snapshot-by-snapshot basis at 75 ms intervals by employing the SAGE algorithm [15]. Angles-of-arrival, delays and signal power are estimated, but CRS are transmitted on only one antenna port at a time, precluding estimation of angles of departure.

The vehicle was driven through an urban canyon environment, with four to five story buildings, as shown in Fig. 9, initially with LOS and then losing it for the remainder of the test drive. The route is split into two sections for illustration and analysis. The transition from LOS to non-LOS occurs during Segment A (which has a duration of approximately 215 meters), and then four laps, two in each direction, define Segment B (approximately 370 meters per lap), to examine repeatability of the proposed clustering algorithm. The measurements were made around mid-day, and the presence of other vehicles including city buses entailed variable start and stop locations. The Northern and Southern sections of Section B are one-way streets which also necessitated different speeds and start/stop intervals from lap to lap.
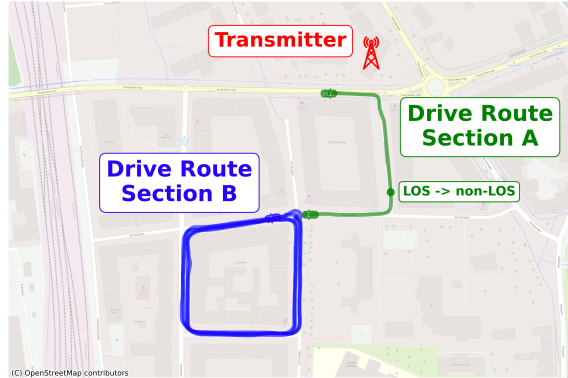
Fig. 9: Drive route in downtown Lund, Sweden (approximate location 55.71°N, 13.19°E). The route is split into Segment A for illustrating MPCs in projection space and Segment B for analyzing repeatability of the proposed clustering algorithm.

IV. RESULTS

The clusters from Section A of the drive route are shown in projection space and overlaid on a map in Fig. 10. MPC angles of arrival are clearly governed by the geometry of the surrounding buildings and clustered accordingly. Points to the East intersect a building with segments of wall spaced about 20 meters apart, which are the plausible source of the reflections giving rise to these clusters. Multiple projected points seem to correspond with objects in the vicinity of the transmitter. After the transition to non-LOS, the large buildings farther to the South and East appear to be the dominant source of clustered MPCs. When the vehicle starts to enter the urban canyon at the end of the route, the clusters are large and split into Northern and Southern segments. This indicates close proximity to the cluster ellipsoids in the street canyon.

Statistics regarding the number of snapshots, MPCs, and clusters together with VR durations from the four laps of Section B of the Drive Route are shown in Table I. The four laps have a variable number of 75-ms snapshots because starts, stops and exact locations were governed by other traffic and two laps (1 and 4) were driven counter-clockwise while the others (2 and 3) were driven clockwise. A similar percentage of estimated MPCs is clustered in all passes. If it were desirable to increase the percentage of clustered components, the tuning parameter N_{min} could be decreased in order to relax the requirement on the number of proximate MPCs in odometry space necessary for cluster formation, and the parameter ϵ can be increased for more liberal definitions of ϵ-neighborhoods. Ultimately, the percentage of clustered MPCs and the number of clusters are functions not only of

TABLE I: Clustering Statistics - Section B

Parameter	Lap 1	Lap 2	Lap 3	Lap 4
Number of Snapshots T	5049	5377	5051	4953
Number of MPCs	18602	22917	24587	24293
Number of Clusters P	70	72	61	53
% of MPCs Clustered	66	62	68	66
Median Cluster VR (m)	11.9	12.3	12.9	10.8
Max Cluster VR (m)	62	61	70	62

the measurement apparatus resolution in time and space, but are also a function of speed and snapshot interval duration. A slowly-moving vehicle, or a faster snapshot interval will result in proportionally more MPCs for potential clustering, because more snapshots will aggregate while moving through each VR. The number of clusters is relatively consistent from lap to lap, as are the median VR lengths. The maximum VR for all laps is associated with a reflecting object to the East, visible for the entire Northern section of the route before rounding the corner. Cumulative distribution functions of VR lengths for each lap are shown in Fig. 11.
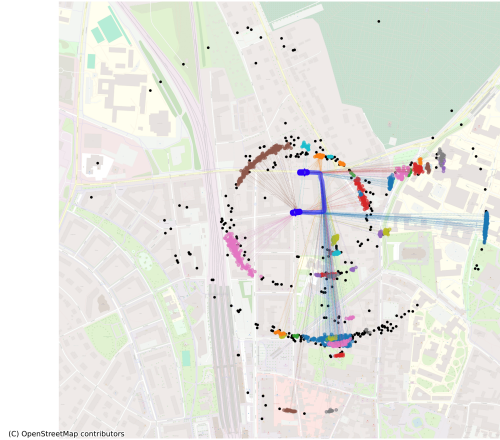
Fig. 10: Clusters in projection space, overlaid on a map. MPCs belonging to the same cluster are shown in the same color (some colors are re-used) and discarded MPCs (noise, for DBSCAN) are illustrated as black with no connecting segments. Not all MPCs are shown to reduce visual clutter.
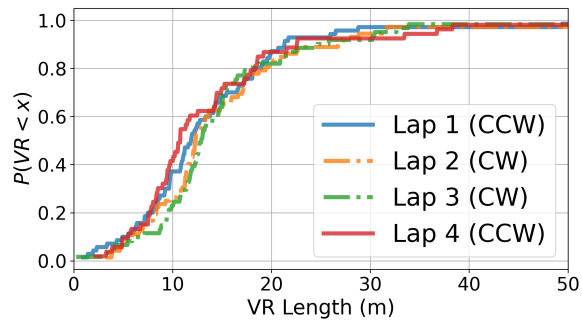

Fig. 11: Cumulative distribution function of VR lengths for the four laps, two clockwise (CW) and two counter-clockwise (CCW).

V. CONCLUSION

The algorithm is shown to produce similar cluster statistics with multiple passes over the same test route (in opposing directions) even in a complicated propagation environment with irregular surfaces, limited signal bandwidth, and in non-LOS conditions with no tuning parameters required other than a distance metric ϵ and a minimum number of adjacent points N_{min} for determining core points, which can be quickly and intuitively analyzed by examining channel estimation results in projection space or odometry space.

Future work could introduce heuristics for cluster combination and classification. Measurements with a system enabling estimation of angles-of-departure would add additional dimensions in which to perform clustering. Additionally, integration of "dense multipath" into the clustering framework could offer additional insight, as well as the integration of Doppler shifts and polarization.

ACKNOWLEDGEMENT

REFERENCES

[1] M. Series, "IMT vision–framework and overall objectives of the future development of IMT for 2020 and beyond," *Recommendation ITU*, vol. 2083, no. 0, 2015.

[2] M. Bennis, M. Debbah, and H. V. Poor, "Ultrareliable and low-latency wireless communication: Tail, risk, and scale," *Proceedings of the IEEE*, vol. 106, no. 10, pp. 1834–1853, 2018.

[3] N. Czink, "The random-cluster model - a stochastic MIMO channel model for broadband wireless communication systems of the 3rd generation and beyond," Ph.D. dissertation, Vienna University of Technology, 12 2007.

[4] S. Jiang, W. Wang *et al.*, "A survey of dense multipath and its impact on wireless systems," *IEEE Open Journal of Antennas and Propagation*, 2022.

[5] K. Haneda, R. Rudd *et al.*, "Radio propagation modeling methods and tools," in *Inclusive Radio Communications for 5G and Beyond*. Elsevier, 2021, pp. 7–48.

[6] H. Tataria, K. Haneda *et al.*, "Standardization of propagation models for terrestrial cellular systems: A historical perspective," *International Journal of Wireless Information Networks*, vol. 28, pp. 20–44, 2021.

[7] M. Ester, H.-P. Kriegel *et al.*, "A density-based algorithm for discovering clusters in large spatial databases with noise," ser. KDD'96. AAAI Press, 1996, p. 226–231.

[8] A. A. Saleh and R. Valenzuela, "A statistical model for indoor multipath propagation," *IEEE Journal on selected areas in communications*, vol. 5, no. 2, pp. 128–137, 1987.

[9] L. Liu, C. Oestges *et al.*, "The COST 2100 MIMO channel model," *IEEE Wireless Communications*, vol. 19, no. 6, pp. 92–99, 2012.

[10] R. He, Q. Li *et al.*, "A kernel-power-density-based algorithm for channel multipath components clustering," *IEEE Transactions on Wireless Communications*, vol. 16, no. 11, pp. 7138–7151, 2017.

[11] Y. Ge, F. Wen *et al.*, "5G SLAM using the clustering and assignment approach with diffuse multipath," *Sensors*, vol. 20, no. 16, p. 4656, 2020.

[12] M. Zhu, G. Eriksson, and F. Tufvesson, "The COST 2100 channel model: Parameterization and validation based on outdoor MIMO measurements at 300 MHz," *IEEE transactions on wireless communications*, vol. 12, no. 2, pp. 888–897, 2013.

[13] K. Khan, S. U. Rehman *et al.*, "DBSCAN: Past, present and future," in *The fifth international conference on the applications of digital information and web technologies (ICADIWT 2014)*. IEEE, 2014, pp. 232–238.

[14] J. Chen, R. Whiton *et al.*, "High-resolution channel sounding and parameter estimation in multi-site cellular networks," in *2023 Joint European Conference on Networks and Communications & 6G Summit (EuCNC/6G Summit)*, 2023, pp. 90–95.

[15] B. H. Fleury, M. Tschudin *et al.*, "Channel parameter estimation in mobile radio environments using the SAGE algorithm," *IEEE Journal on selected areas in communications*, vol. 17, no. 3, pp. 434–450, 1999.